DURBAN UNIVERSITY OF TECHNOLOGY
INYUVESI YASETHEKWINI YEZOBUCHWEPHESHE

Design and Optimization of an Adsorption Method for the Removal of Textile Azo Dyes from Aqueous Solutions using *Plantago lanceolata*

Submitted in fulfilment of the requirements of the Degree of Master of Applied Science in Chemistry in the Faculty of Applied Sciences at the Durban University of Technology, Durban, South Africa

Thabisile Penelope Kaunda

2022

Supervisor: Professor R.M. Gengan

Co-Supervisor: Dr T. Singh

DECLARATION

I, Thabisile Penelope Kaunda hereby declare that this dissertation titled "Design and Optimization of an Adsorption Method for the Removal of Textile Azo Dyes from Aqueous Solutions using "*Plantago Lanceolata*", submitted to the Durban University of Technology, in fulfillment of the requirements for the award of the Degree of Master of Applied Science in the Faculty of Applied Sciences, is the result of my own work and that all sources used or quoted have been indicated and acknowledged by means of complete references.

Signed: _____ 31 January 2022

Thabisile Penelope Kaunda Date

Signed: _____ 29 January 2022

Promoter: Prof R.M. Gengan Date

Signed: _____ 30 January 2022

Co-supervisor: Dr T. Singh Date

Department of Chemistry

Durban University of Technology

DEDICATION

This dissertation is dedicated to my entire family, especially my sons **Sbongokuhle Andile Kaunda** and **Sbongakonke Bandile Kaunda** who have been so understanding and supporting throughout my academic journey. My parents **Ella Nosipho Zindela**, and **Themba Clifford Zindela**, my late grandmother **Nozipho Veronica Kaunda** and my uncle **Thomas Mxolisi Kaunda** for their continuous support, unconditional love and for always being there for me throughout my upbringing. Every challenges I have encountered they have been my cheerleaders and always wishing the best for me and my siblings. God bless you for all your love and efforts.

ACKNOWLEDGEMENTS

First and foremost, I would like to thank the Lord, God Almighty for all this would have not been possible without His grace and mercies, and His abundant blessings throughout my entire life and the wisdom granted upon me for the completion of this study.

My warm and heartfelt gratitude goes to my supervisor **Prof Robert Moonsamy Gengan** for his guidance during this study, his tremendous mentorship, being the father at most times. His wisdom, encouragement, understanding, allowing me to grow in Chemistry and as a person, always believing in me by seeing the best in me. For always availing himself to discuss ideas and editing of this thesis.

I thank **Dr Thishana Singh**, my co-supervisor from the University of Kwa-Zulu Natal, School of Physics and Chemistry for that critic's eye in ensuring this research was success.

I would like to thank all the DUT staff and laboratory personnel that played a vital role in assisting me during this study. My colleagues **Dr Muthu Thangaraj**, **Dr Talent Raymond Makhanya**, **Dr Myalowenkosi Innocent Sabela**, **Ms Nikisha Rajkoomar**, **Dr Arul Murugasen**, **Mr Zamokwakhe Miya** and **Mr Jimmy Chetty** for their valuable assistance.

I would like to thank my entire family **oKaunda, Mbimbi.** All my uncles, aunts and relatives for their continued support and prayers. All my siblings and cousins, especially **Ziyanda Magadla** for taking care of my kids while I was pursuing this degree, **Siphindile Kaunda** and **Philile Zindela** for their love and support. **Bina Kaunda, Isaac Kaunda, Mxolisi Kaunda**, **Ella and Themba Zindela**. The **12 Apostle and the prophets congregation** for prayers and being with me throughout all the challenges I faced during this time.

I would like to thank **Nation Research Foundation** (NRF), and The **Health and Welfare Sector Education and Training Authority** (HWSETA) for the funding at different aspects of this study.

Special thanks to **Zuzile Gama**, **Silindile Ngcobo**, **Ncomeka Mgxadeni**, **Senzekile Majola**, my love, my sons and all my friends that supported me throughout.

ABSTRACT

Water is an essential commodity for human survival; however, this resource is predicted to be scarce within the 21st Century due to pollution and industrialization. Textile industries are among the many polluters of water, and hence methods to remediate textile waste-water need attention. In this study, a common garden weed *Plantago Lanceolata* was used for the preparation of novel activated carbon materials as an adsorbent for the degradation of textile azo dyes Reactive Blue 222 (RB), Reactive Red 195 (RR), and Reactive Yellow 145 (RY). The activated carbon was modified with four different chemical activators to produce phosphoric acid-based activated carbon (H_3PO_4-AC), sulfuric acid-based activated carbon (H_2SO_4-AC), potassium hydroxide-based activated carbon (KOH-AC), and sodium hydroxide-based activated carbon (NaOH-AC). These materials were characterized by Fourier- transfer infrared spectroscopy (FTIR), scanning electron microscope with energy dispersive X-ray (SEM/EDX), high resolution transmitting electron microscope (HRTEM), and a thermogravimetric analyzer with differential scanning calorimeter (TGA/DSC). The initial concentration of the adsorbate, adsorbent dosage concentration, contact time, temperature, and pH were optimized. The four materials adsorption capacity was studied, and H_3PO_4-AC produced the best results of adsorption capacity 98,98% - 100%, with optimum agitation time of 70 minutes, the optimum dosage of 0.8 g/60 mL of adsorbent, and pH of 6. The experimental data were fitted using Langmuir (type 1-4), Freundlich, Temkin, and Dubinin-Radushkevich isotherms. The data from this study best fitted the Langmuir isotherm type 1: RB (q_m -15.58 mg g^{1}), RR (q_m – 11.24 mg g^{1}) and RY (q_m - 11.24 mg g^{1}). Furthermore, the reaction rate followed the pseudo-second-order kinetic model while the intraparticle diffusion model had no impact. Its thermodynamic parameters indicated the reaction as spontaneous and exothermic. Furthermore, a nanocomposite was prepared from H_3PO_4-AC and iron oxide to produce an iron oxide/activated carbon nanocomposite. FTIR, SEM/EDX, HRTEM, and TGA/DSC fully characterized this novel material. The iron oxide/H_3PO4-AC nanocomposite produced slightly better results compared to H_3PO4-AC: RB (99.60% - 100%), RR (99.59 – 100%) and RY (99.48% – 100%). The experimental data fitted Langmuir isotherm type 1, and the reaction followed the pseudo-second-order kinetic reaction model.

CONFERENCES

A poster titled "Chemical Activation of Garden Weed Plantago Lanceolata and its Adsorption Capacity for Textile Dyes" was presented at the Durban University of Technology, Faculty Research Day on the 8th of November 2019, held in the Durban International Convention Centre, Durban, South Africa.

LIST OF TABLES

LIST OF FIGURES

LIST OF APPENDICES

ABBREVIATIONS

COD	- chemical oxygen demand
TDS	- total dissolved solids
TSS	- total suspended solids
BOD	- biochemical oxygen demand
C.I	- chemical index
^{o}C	- degrees Celsius
C_O	- initial concentration
mg g^{-1}	- milligrams per gram
L mg^{-1}	- litre per milligram
mg L^{-1}	- milligrams per litre
g L^{-1}	- grams per litre
g	- grams
mol^2/KJ^2	- mole squared per kilo joule squared
t	- time
min	- minute
s	- second
hr	- hour
EDX	- Energy Dispersive X-ray
TEM	- Transmission electron microscope
HRTEM	- High resolution transmission electron microscope
SEM	- Scanning electron microscope
TGA	- Thermogravimetric analysis
DSC	- Differential scanning calorimetry
nm	- nanometer
rpm	- revolutions per minute

FTIR	- Fourier transfer infrared spectroscopy
ATR	- attenuated total reflection
mol	- mole (number of moles)
cm	- centimeter
m	- meter
mm	- millimeters
mL	- milliliter
L	- litre
AC	- activated carbon
np	- nanoparticle
ppm	- parts per million
H_3PO_4-AC	- phosphoric acid treated activated carbon
H_2SO_4-AC	- sulfuric acid treated activated carbon
KOH-AC	- potassium hydroxide treated activated carbon
NaOH-AC	- sodium hydroxide treated activated carbon
M	- molarity (moles per litre)
RB	- Reactive blue 222 dye
RR	- Reactive red 195 dye
RY	- Reactive yellow 145 dye
D-R	- Dubinin Radushkevich isotherm
IPD	- Intraparticle diffusion
T	- temperature
LOD	- Limit of detection
LOQ	- Limit of quantification
Wt.	- weight
%	- percentage

UV/Vis	- Ultra violet /visible spectrophotometer
Iron oxide/H3PO4-AC carbon nanocomposite	- iron oxide/phosphoric acid treated activated

TABLE OF CONTENTS

CHAPTER ONE: INTRODUCTION

1.1 General Introduction

Environmental pollution is a worldwide phenomenon in different forms such as air, soil, and water and is an increasing concern in most countries. The source of water pollution is primarily from industries, agricultural sectors, and domestic waste that discharge contaminated organic compounds, pesticides, and pharmaceutical residues as effluent (Natarajan, Bajaj and Tayade 2018). These poor practices limit clean water production from natural sources (Konicki *et al.* 2017). Globally, contaminants in wastewater have become the focus of significant studies due to the adverse effects caused by untreated and poorly treated effluent of organic and inorganic pollutants such as dyes, bleaching agents and detergents (El Zawahry and Kamel 2004). Since these pollutants are released as effluent into rivers, lakes, and streams (Shen and Gondal 2017), they negatively impact the environment and living organisms. Thus, they pose a severe threat to humans, animals and plants.

Although several pollutants exist, some are becoming ubiquitous. Dyes are viewed with significant trepidation due to their mutagenic and carcinogenic properties (Ngulube *et al.* 2017). There are several classes of dyes; however, the azo dye presents a severe hazard since it may also affect humans and animals' liver, digestive, and nervous systems (El-Zawahry *et al.* 2016). Furthermore, the reductive cleavage of anionic azo dyes produces toxic aromatic amines released as effluent. These aromatic amines are stable and difficult to biodegrade (Aksu and Tezer 2005). The visible colour in dye bodies inhibits light penetration into the soil, thus hindering photosynthetic activities. Additionally, soil fertility is affected in the surrounding area where the chemical effluent is released. Poor soil fertility is a significant concern to environmentalists and farmers, especially in developing countries, affecting food quality and health safety (Garg *et al.* 2004; Lata, Garg and Gupta 2007).

Numerous methods for treating chemical effluent are used in wastewater treatment plants. These include flocculation, precipitation, coagulation, membrane filtration, electro-flotation, ozonation, irradiation, ion exchange, Fenton's reagent and adsorption (Garg *et al.* 2004; Chuah *et al.* 2005; Lata, Garg and Gupta 2007). Nanotechnology has also been the focus of many studies for dye removal from wastewater (Oliveira *et al.* 2002). In addition, adsorption has gained prominence in wastewater treatment,

especially for removing dyes and toxic metals. Currently, activated carbon is the most widely used material since it has excellent adsorption capacity due to its high surface area (Gopinathan, Bhowal and Garlapati 2017). However, it is an expensive material which makes it unaffordable to most developing countries (Ramesh, Lee and Wong 2005). Therefore, investigations of adsorbents that can be derived from cheaper materials are attracting more scientists' attention globally (Konduru and Ramakrishna 1997).

1.2 Aim of the Study

This investigation aimed to develop and optimize a method for removing three organic textile azo dyes from synthetic effluent by means of adsorption using activated carbons derived from a common garden weed named *Plantago Lanceolata.*

1.3 The Objectives of the Study were to:

1.3.1 Prepare four different types of activated carbon using *Plantago Lanceolata*.

1.3.2 Characterize the activated carbon to determine its morphology and crystalline structure.

1.3.3 Investigate the efficiency of removing textile azo dyes in synthetic effluent by varying the pH of the dye bath, concentration, temperature, adsorbent dosage and adsorbent contact time using a batch method system.

1.3.4 Prepare the activated carbon and iron oxide magnetic nanocomposite using *Plantago Lanceolata*.

1.3.5 Investigate the adsorption process of this composite using parameters such as adsorbent dosage, adsorbent contact time and concentration of the dye bath.

1.3.6 Assess desorption of the textile dyes.

1.3.7 Evaluate the thermodynamics, equilibrium and kinetic process.

1.4 Structure of the Dissertation

This dissertation is composed of five chapters.

Chapter One introduces the negative impact that untreated and poorly treated effluent/ wastewater has on the environment, plants and humans. Next, a discussion of the current conventional methods for treating water dye bodies and a brief insight on the new materials is presented. After that, the purpose of the study, research objectives, and the effect of adsorption is discussed.

Chapter Two presents the literature survey on the study undertaken, including the different methodologies used to remove pollutants in water. The different types of dyes, structure, and properties are presented, emphasizing the textile azo dyes. Adsorption details of the materials that have thus far been investigated are described. The potential use of natural resources such as natural waste/ plant material is also discussed. Finally, the use of nanotechnology for the removal of dyes in the effluent is explained.

Chapter Three will detail the experimental procedures and materials used in this study. This chapter will also include all the equations used for thermodynamic study, all the tested adsorption isotherms, and the reaction kinetics.

Chapter Four is divided into two parts.

The first part will comprise an outline of the adsorption studies using four different types of activated carbon (modified by phosphoric acid, sodium hydroxide, potassium hydroxide and sulfuric acid) prepared from the common garden weed *Plantago Lanceolata*. Next, the results are presented, analyzed using various methodologies, and interpreted. Finally, the characterization of all four types of activated carbon produced is analyzed and discussed.

The second part of this chapter briefly introduces the removal of dyes using nanotechnology. Data for the activated carbon-magnetic oxide composites for the removal of textile azo dyes is presented, analyzed, interpreted, and followed by a discussion and characterization of the composites produced using *Plantago Lanceolata* as a precursor material.

Chapter Five summarizes the findings obtained in this study, discusses the possibility of further investigations that may have arisen from the results, and provides recommendations for future work in this area.

1.5 Reference

Aksu, Z. and Tezer, S. 2005. Biosorption of reactive dyes on the green alga *Chlorella Vulgaris*. *Process Biochemistry*, 40 (3): 1347-1361.

Chuah, T. G., Jumasiah, A., Azni, I., Katayon, S. and Thomas Choong, S. Y. 2005. Rice husk as a potentially low-cost biosorbent for heavy metal and dye removal: an overview. *Desalination*, 175 (3): 305-316.

El-Zawahry, M. M., Abdelghaffar, F., Abdelghaffar, R. A. and Hassabo, A. G. 2016. Equilibrium and kinetic models on the adsorption of Reactive Black 5 from aqueous solution using *Eichhornia crassipes*/chitosan composite. *Carbohydrate Polymers*, 136: 507-515.

El Zawahry, M. M. and Kamel, M. M. 2004. Removal of azo and anthraquinone dyes from aqueous solutions by *Eichhornia Crassipes*. *Water Research*, 38 (13): 2967-2972.

Garg, V. K., Amita, M., Kumar, R. and Gupta, R. 2004. Basic dye (methylene blue) removal from simulated wastewater by adsorption using Indian Rosewood sawdust: a timber industry waste. *Dyes and Pigments*, 63 (3): 243-250.

Gopinathan, R., Bhowal, A. and Garlapati, C. 2017. Thermodynamic study of some basic dyes adsorption from aqueous solutions on activated carbon and new correlations. *The Journal of Chemical Thermodynamics*, 107: 182-188.

Konduru R and Ramakrishna, T. V. 1997. Dye removal using low cost adsorbents. *Water Science and Technology*, 36 (2-3): 189-196.

Konicki, W., Aleksandrzak, M., Moszyński, D. and Mijowska, E. 2017. Adsorption of anionic azo-dyes from aqueous solutions onto graphene oxide: Equilibrium, kinetic and thermodynamic studies. *Journal of Colloid and Interface Science*, 496: 188-200.

Lata, H., Garg, V. K. and Gupta, R. K. 2007. Removal of a basic dye from aqueous solution by adsorption using Parthenium hysterophorus: An agricultural waste. *Dyes and Pigments*, 74 (3): 653-658.

Natarajan, S., Bajaj, H. C. and Tayade, R. J. 2018. Recent advances based on the synergetic effect of adsorption for removal of dyes from wastewater using photocatalytic process. *Journal of Environmental Sciences*, 65: 201-222.

Ngulube, T., Gumbo, J. R., Masindi, V. and Maity, A. 2017. An update on synthetic dyes adsorption onto clay based minerals: A state-of-art review. *Journal of Environmental Management*, 191: 35-57.

Oliveira, L. C. A., Rios, R. V. R. A., Fabris, J. D., Garg, V., Sapag, K. and Lago, R. M. 2002. Activated carbon/iron oxide magnetic composites for the adsorption of contaminants in water. *Carbon*, 40 (12): 2177-2183.

Ramesh, A., Lee, D. J. and Wong, J. W. C. 2005. Thermodynamic parameters for adsorption equilibrium of heavy metals and dyes from wastewater with low-cost adsorbents. *Journal of Colloid and Interface Science*, 291 (2): 588-592.

Shen, K. and Gondal, M. A. 2017. Removal of hazardous Rhodamine dye from water by adsorption onto exhausted coffee ground. *Journal of Saudi Chemical Society*, 21: S120-S127.

CHAPTER TWO: LITERATURE SURVEY

2.1 Pollution by Textile Industries

The disposal of effluents containing synthetic dyes is a global concern as this type of water pollution contaminates our natural water resources (Konicki *et al.* 2017). Approximately 100 000 dyes are available commercially, with more than 7×10^5 tonnes of dyes being released annually from different industries such as food, textile, paper, cosmetics, plastics, rubber and dye manufacturing industries (Yagub et al. 2014). The textile industries are responsible for 67% of dye production, while approximately 15% are discharged as effluent (Lata, Garg and Gupta 2007).

Wastewater dye effluents exhibit high chemical oxygen demand (COD), total dissolved solids (TDS), total suspended solids (TSS), low biochemical oxygen demand (BOD), high temperature, high pH variation range, heavy metals and intense pigmentation (Aslam *et al.* 2004; Hossain, Sarker and Khan 2018). Hence, this leads to variations in the environment's physical, chemical, and biological properties, leading to adverse effects on biodiversity and human health (Sultana *et al.* 2009).

2.2 Types of Dyes

Dyes are divided into two major categories, namely: natural and synthetic. Dyes obtained from natural sources were widely used centuries ago but are currently limited for industries (Adrosko 2012). Natural dyes are usually extracted from insects, roots, plants and leaves (de Ferri *et al.* 2018). Their chromophores are often derivatives of their sources, for example, flavonoids extracted from different plant species and anthraquinones obtained from plants and insects (Ferreira *et al.* 2004). Although these dyes are now obsolete, they were pretty distinct. Also, impurities from the tree sources gave the dyes unique colours (Adrosko 2012). Extracting the dye from a natural source and applying it to cloth is time-consuming. Also, it is not easy to store these dyes (Adrosko 2012).

Synthetic dyes are currently used in the textile industry as they have excellent characteristics (Hemmati *et al.* 2017). They are distinguished by their bright colours, resistance to fading from exposure to chemicals and high temperatures, and their water-fastness application of fabrics, through simple techniques that require low electricity usage, is advantageous (Aksu and Tezer 2005). Synthetic dyes bind

strongly to fabric due to their highly steric structures. However, they pose a challenge to degrade their colour in the effluent (Ghoreishi and Haghighi 2003). This is primarily due to chromophores such as anthraquinone, azine, azo, nitro, nitroso, phthalocyanine, quinoline, sulfur, and thiazine xanthene, which exchange net charges with the aqueous solution resulting in strong bonds. Synthetic dyes are classified into three broad categories: anionic, cationic, and non-ionic (Aksu and Tezer 2005). Furthermore, there are different types of dyes available commercially in each category: azo, acidic, basic, direct, reactive, and many others (Allen and Koumanova 2005). Of these types, the azo dyes are the largest category and diversified. (Azin and Moghimi 2018).

2.2.1 Acid Dyes

These dyes are applied under acidic conditions in the pH range of 3.0 – 7.0, usually with formic or acetic acid depending on the acidity strength of the individual dye (Nunn 1979). The structure of an acid dye (Figure 2.1) usually includes metal complexes and sulfonated groups, which enhances water solubility as its significant property. The other good properties include, excellent wet-fastness and lightfastness ranging from blue scale of 5.0-6.0 (Benkhaya, El Harfi and El Harfi 2017). The chromophores may be pre-metalized azo, azine, nitro, anthraquinone, triphenylmethane, nitroso and xanthene groups (Benkhaya, El Harfi and El Harfi 2017). Acid dyes are usually applied to nylon, wool, silk and modified acrylics. This makes them suitable for use different industries such as textiles, leather, cosmetics, paper, ink-jet, food and printing industries (Hunger 2007). However, their bonding on wool substrates is weaker when compared to other substrates since the interaction of the sulfonate groups with the ammonium groups on the wool fibre is weak (Benkhaya, El Harfi and El Harfi 2017).

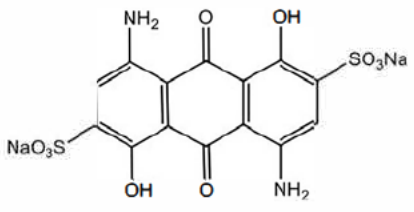

(a)

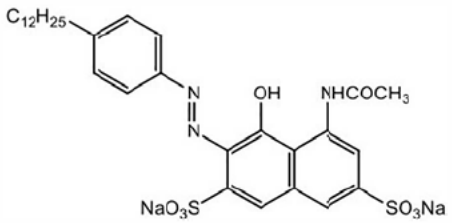

(b)

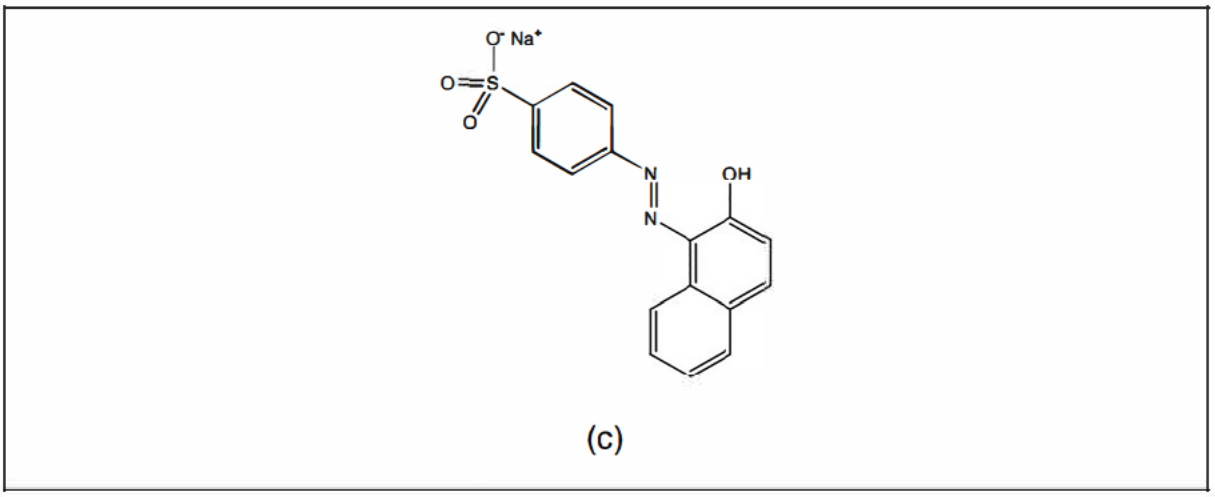

(c)

Figure 2.1 Structure of (a) C.I Acid blue 45 (b) C.I Acid red 138 (c) C.I Acid orange 7

2.2.2 Azoic Dyes

Azoic dyes are used extensively in cosmetics, food, leather, paper, paint, textile, and pharmaceutical (Benkhaya, El Harfi and El Harfi 2017). The azo dyes display $N=N-$chromophore attached to aromatics substituents, resulting in complex structures that contribute to various colours. They usually contain the sulfonate group (Rajaguru *et al.* 2002). The dyes are further classified as monoazo (one azo), diazo (two azo), triazo (three azo) and polyazo groups (Hunger 2007; Benkhaya, El Harfi and El Harfi 2017). Furthermore, azoic dyes containing only aromatic substituents are carbocyclic or heterocyclic azo dyes, usually indoles, pyridines, and pyrazolones (Hunger 2007). Their wide application in the textile industry is due to the different shades and intensities that the dye can possess. This colour property is because of the conjugated systems (McMullan *et al.* 2001; Robinson *et al.* 2001). Azoic dyes bind easily to cellulose fibre, cotton and polyester through a simple coupling reaction and diazonium salt (Hunger 2007).

2.2.3 Basic Dyes

Basic dyes (Figure 2.2) release cations in aqueous solutions. They bind electrostatically onto the substrate's negative charges that have been applied by the acidic dye baths (Benkhaya, El Harfi and El Harfi 2017). These dyes bind strongly to acrylic, paper and nylon surfaces, but their application is in silk, wool, and modified polyester fabrics in the textile industries. Basic dyes are usually used with retarding devices as their movement is inferior in solutions of extreme temperature (Clark 2011).

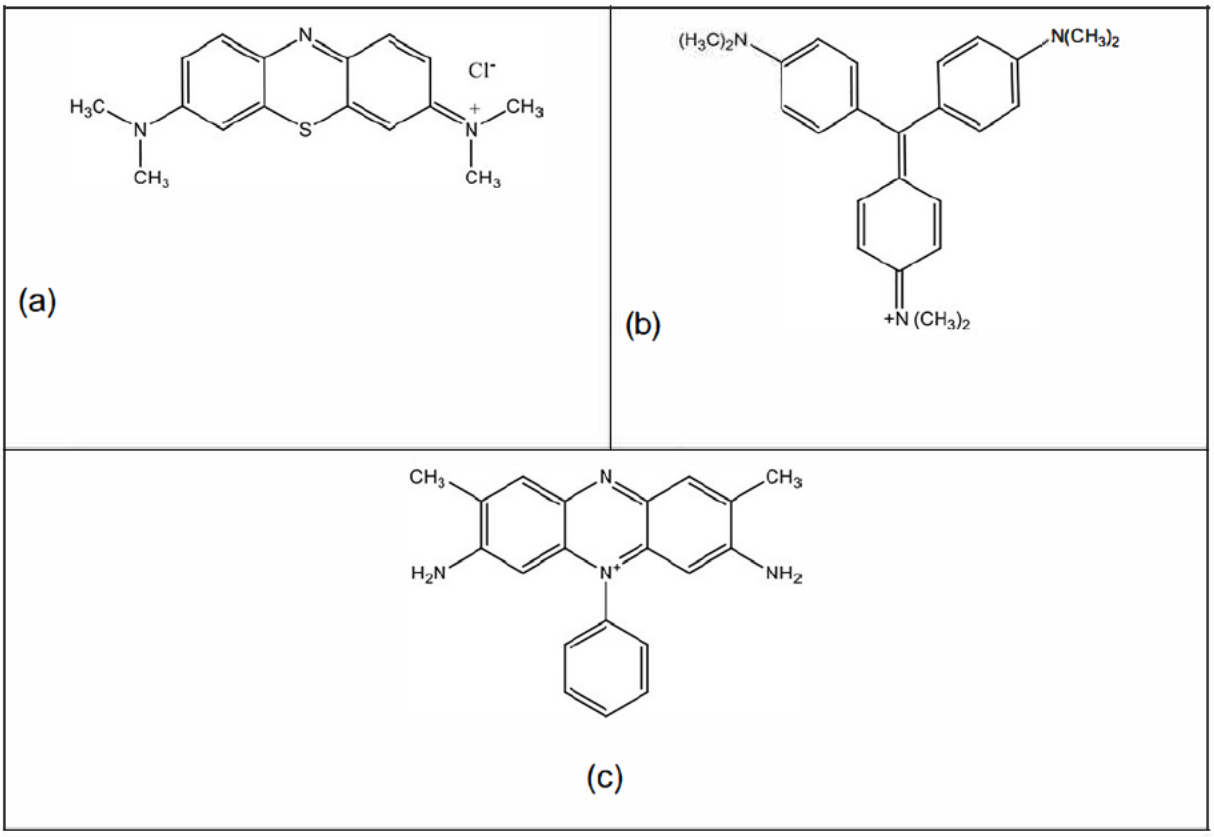

Figure 2.2 Structure of basic dyes: (a) Methylene blue (b) Crystal violet (c) Safranin

2.2.4 Direct Dyes

Direct dyes are anionic and water-soluble (Figure 2.3). They are characterized by their application, chromophore, or colour fastness properties. They are usually polyazo with substituents such as oxazines and phthalocyanines (Hunger 2007; Benkhaya, El Harfi and El Harfi 2017). Direct dyes have wide application in the textile and printing industries, primarily for dyeing cellulose, cotton, leather, nylon and paper due to their excellent properties. The anions from the dye attach firmly to the cellulose substrate through diffusion in an aqueous solution (Aspland 1997; Hunger 2007). Although direct dyes containing the azo chromophore are popular in the textile industry, their wash-fastness is less impressive than the azo group's reactive dyes. Hence, their commercial use is unfavorable (Benkhaya, El Harfi and El Harfi 2017).

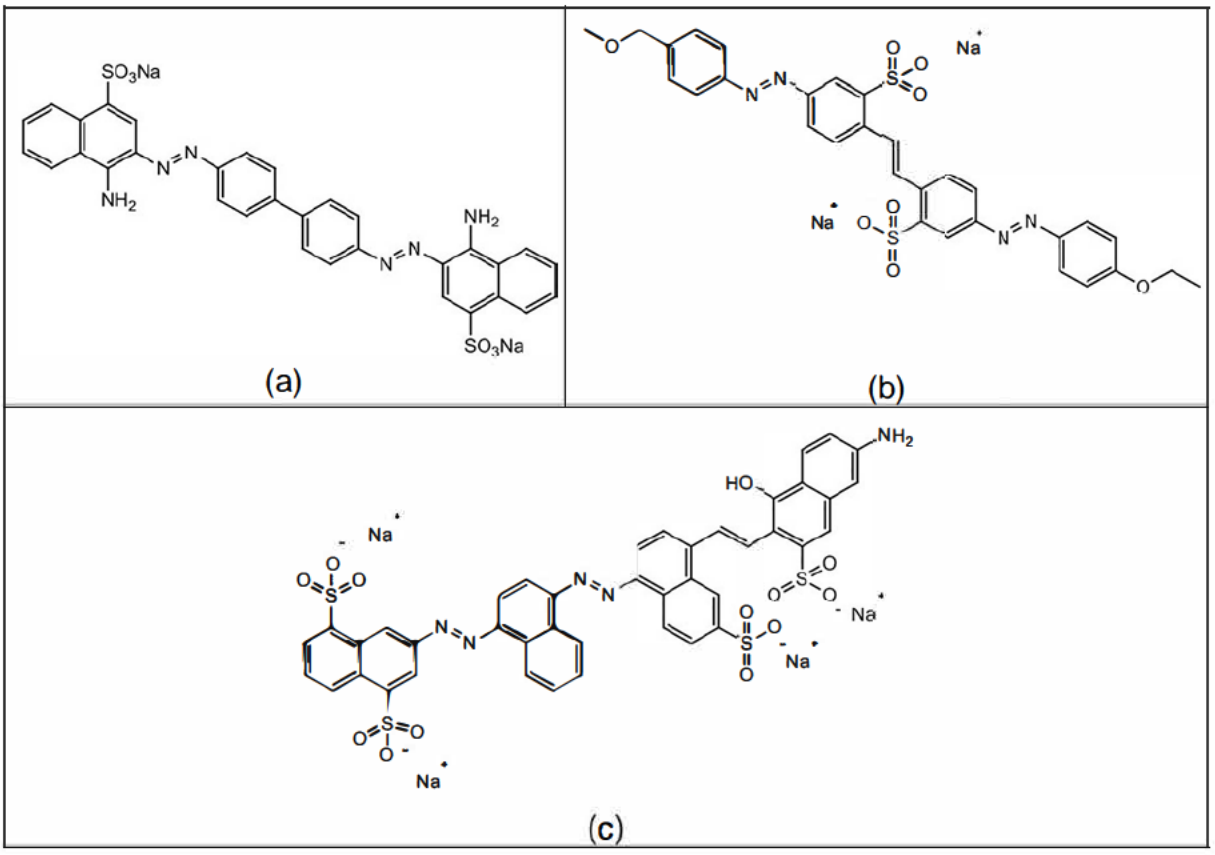

Figure 2.3 Structure of: (a) C.I Direct red 28 (b) C.I Direct yellow 12 (c) C.I Direct blue 71

2.2.5 Disperse Dyes

Disperse dyes (Figure 2.4) are characterized by their non-ionic nature and insolubility or partial solubility in water. They are applied to polyesters but rarely on acrylic fibres, cellulose acetate and nylon. Their wash-fastness is very poor on most substrates and requires large amounts of water for application in aqueous dispersion, ultimately resulting in a large volume of effluent waste (Hunger 2007; Clark 2011; Benkhaya, El Harfi and El Harfi 2017). Because of their relatively low molecular mass, temperatures between 80ºC-90ºC are required for the dyeing application. The azo disperse dyes strongly impact the material and are more economical than the anthraquinone and other disperse dyes. However, the azo dispersed dyes have relatively low stability during the dyeing process (Koh 2011). Furthermore, during the dyeing process, when using disperse dyes, a monolayer on the substrate must be produced, and the excess dye has to be removed as it limits the wet-fastness and wash-fastness properties since this results in a light fabric (Murray and Mortimer 1971; Aspland 1992a).

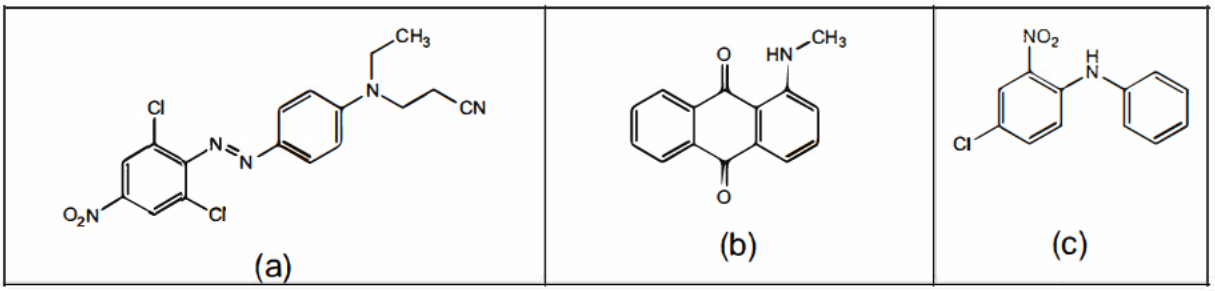

Figure 2.4 Structure of: (a) C.I Disperse orange 37 (b) C.I Disperse red 9 (c) C.I Disperse yellow 26

2.2.6 Reactive Dyes

Reactive dyes (Figure 2.5) form strong covalent bonds through sulfonate functional group with the cellulosic substrate, usually cotton. There is also limited use in wool, silk and nylon substrates (Hunger 2007). Their chromophores are azo, anthraquinone, phthalocyanine, triphenylmethane and oxazine. Their tinctorial strength is within the surface, resulting in a brighter and broader spectrum of shades (Zollinger 2003; Farouk and Gaffer 2013). The reactive dyes possess excellent characteristics such as high wet-fastness, excellent wash fastness, easy application onto the substrate, good light fastness, resistance to fading quickly even with the use of chlorine, and the broadest range of bright colours (Aspland 1992b; Hunger 2007; Benkhaya, El Harfi and El Harfi 2017).

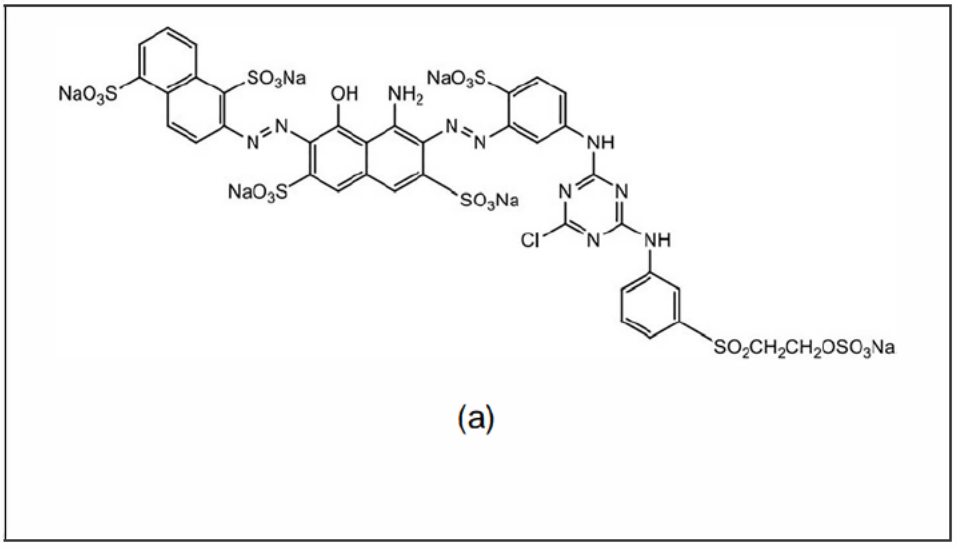

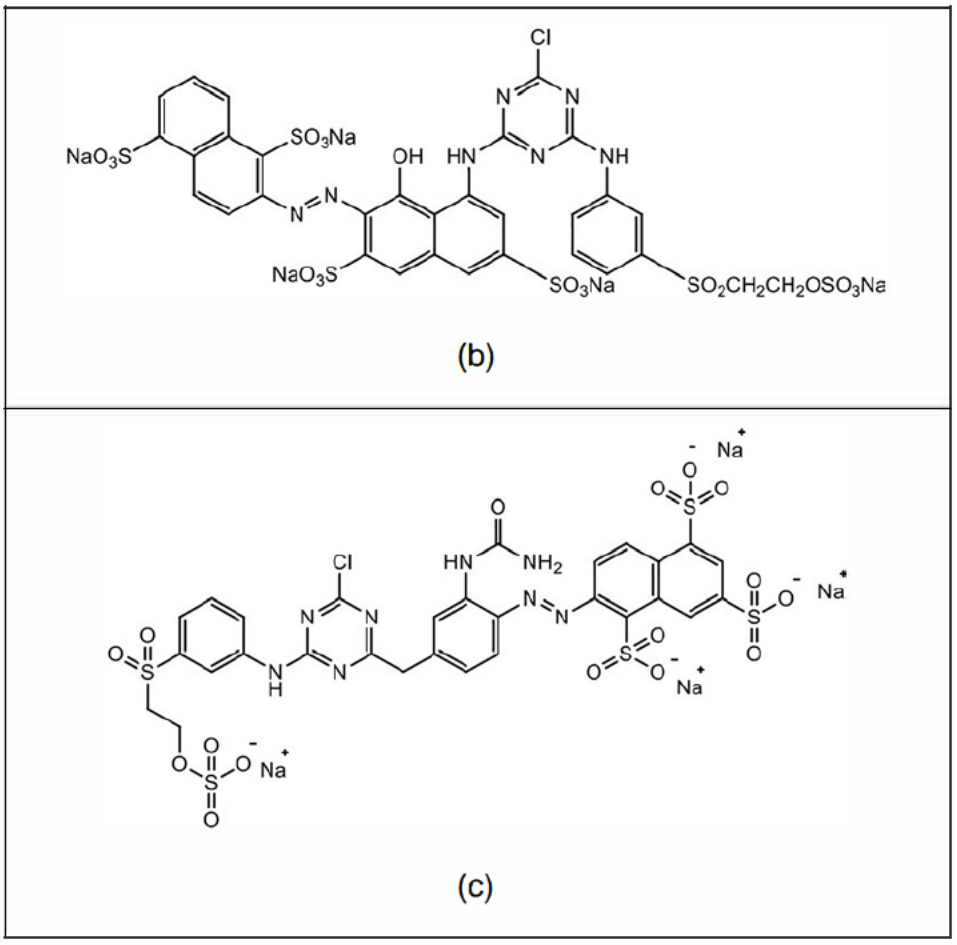

Figure 2.5 Structure of: (a) C.I Reactive blue 222 (b) C.I Reactive red 195 (c) C.I Reactive yellow 145

2.3 Remediation of Textile Dyes from Wastewater

Synthetic dyes have complex molecular structures and pose a considerable threat to the environment when disposed of without proper treatment. They are aromatic compounds that are stable and difficult to biodegrade. They are synthesized to withstand high temperatures and degradation by detergents (Aksu and Tezer 2005). Conventional remediation technologies include biological, chemical, electrical and physical processes (Natarajan, Bajaj and Tayade 2018). Solid-liquid separation plays a significant role in physical remediation compared to other methods. Chemical methods depend primarily on the type of dyes that requires removal from water, while electrochemical processes are used mainly to sterilize the sludge (Cheremisinoff 2001). Some of the methods used include Fenton's process (Lahkimi et al. 2007), flocculation/coagulation (Sadri Moghaddam, Alavi Moghaddam and Arami 2010),

precipitation, membrane filtration (Rozzi, Antonelli and Arcari 1999), electro-flotation (Essadki *et al.* 2008), ozonation (Ghuge and Saroha 2018), irradiation, ion exchange (Karcher, Kornmüller and Jekel 2002), activated carbon (El Qada, Allen and Walker 2008), silica gel (ALzaydien 2009), photo-catalysis (Daneshvar, Salari and Khataee 2004) and microbial decolourization (Banat *et al.* 1996).

The different types of conventional methodologies currently used in the textile industry to treat dye effluent are shown in Figure 2.6 (Slokar and Majcen Le Marechal 1998; Kharub 2012). These decolourization technologies have been used for decades and are very efficient; however, some significant disadvantages have been identified. In the physical process, microfiltration methods are excellent for removing small molecular weight dyes but ineffective in removing high molecular weight dyes and soluble dyes such as reactive, direct, basic, and acid dyes (Akbari, Remigy and Aptel 2002). As a result, adsorption, a physical process, has gained prominence in wastewater treatment, especially for removing dyes and toxic metals. Currently, activated carbon is the most widely used material since it has excellent adsorption capacity due to its large surface area. However, it is expensive, non-selective, and unaffordable in developing countries (Babel and Kurniawan 2003; Ramesh, Lee and Wong 2005; Gopinathan, Bhowal and Garlapati 2017).

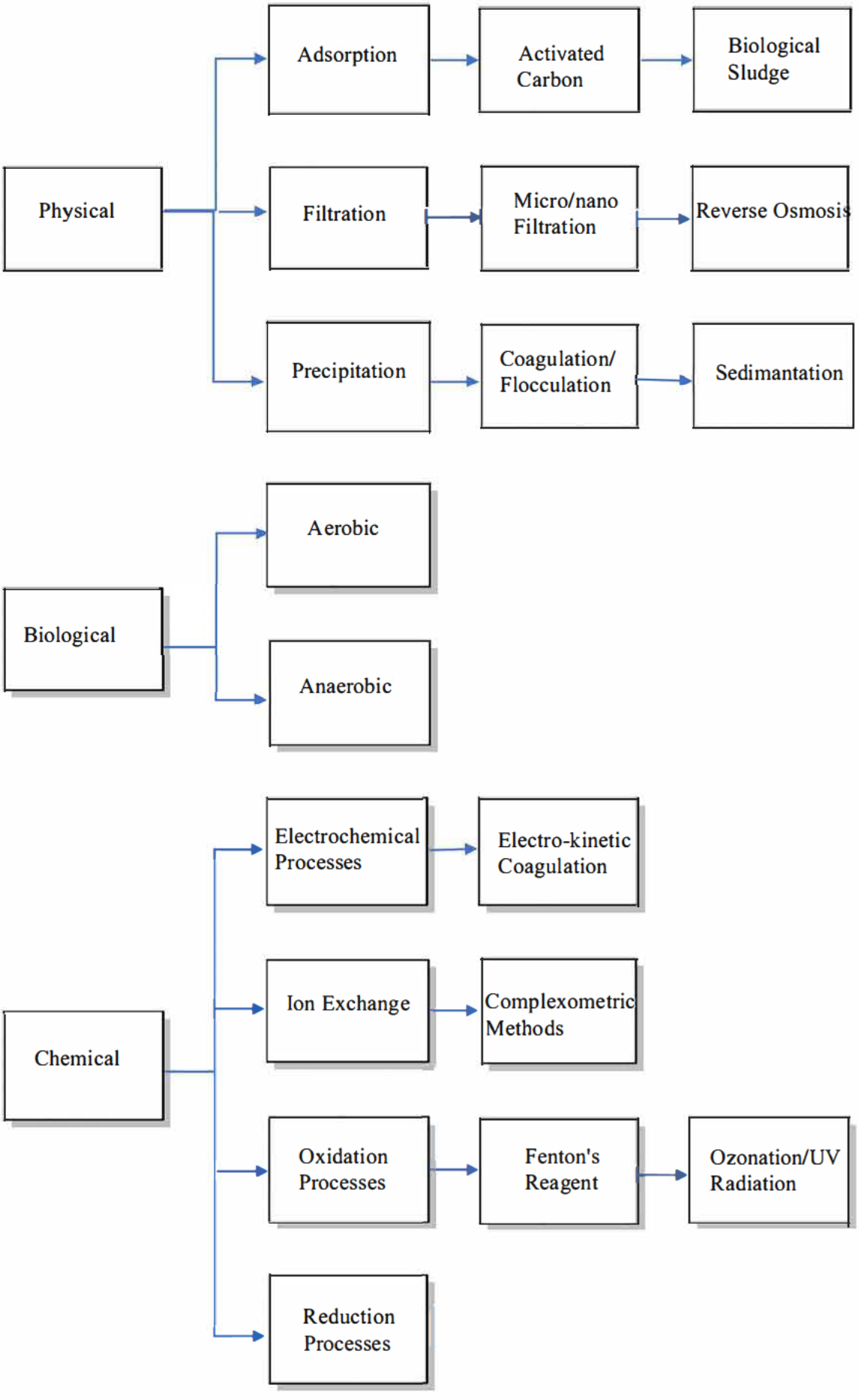
Physical
Adsorption
Activated Carbon
Biological Sludge
Filtration
Micro/nano Filtration
Reverse Osmosis
Precipitation
Coagulation/ Flocculation
Sedimantation
Biological
Aerobic
Anaerobic
Chemical
Electrochemical Processes
Electro-kinetic Coagulation
Ion Exchange
Complexometric Methods
Oxidation Processes
Fenton's Reagent
Ozonation/UV Radiation
Reduction Processes

Figure 2.6 Current conventional technologies used in wastewater treatment

Therefore studies of adsorbents derived from cheaper materials have attracted much attention globally (Ramakrishna 1997). Furthermore, promising technologies have been developed on a laboratory scale and are due for trials in some industries. These include various adsorption techniques, electrolysis and flotation (Vandevivere, Bianchi and Verstraete 1998). Some of the advantages and the shortcomings of the current methods are listed in Table 2.1.

Table 2.1 Advantages and Limitations of the current conventional technologies used in the remediation of dye effluent

METHOD	ADVANTAGES	LIMITATIONS
Activated carbon	Highly effective for various dyes	High cost
Biological treatment	Feasible in removing some dyes	Technology not established
Coagulation/ Flocculation	Economically friendly	High sludge production
Electrochemical processes	No hazardous by-products	High energy consumption
Fenton's reagent	Effective color removal	A large amount of sludge
Ion exchange	No loss of adsorbent	Ineffective for some dyes
Membrane filtration	Decolourization of all dyes	Produce concentrated sludge
Oxidation	Effective in dye removal	High cost of electricity and formation of by-products
NaOCl	Initiates azo bond cleavage	Release of toxic aromatic amines
Photo-catalysis	No sludge produced	By-products are formed
Silica gel	Effective for cationic dyes	Side reaction in effluent

2.4 Application of Adsorption in Wastewater Treatment

Materials for removing textile dye by physicochemical and biological methodologies (Annadurai, Juang and Lee 2002) are presented in Table 2.1. Scientists worldwide are investigating new methods using alternate cheaper materials that can be used for wastewater treatment (Vikrant *et al.* 2018). Among the methods considered, adsorption has still shown prominence in removing organic and inorganic pollutants in water (Annadurai, Juang and Lee 2002; Lata, Garg and Gupta 2007). Adsorption is a safe method for water purification since it is an economically friendly method with no hazardous by-products (Hemmati *et al.* 2017). Activated carbon has already produced excellent results for removing pollutants such as dyes due to its vast adsorption surface area (Annadurai, Juang and Lee 2002; Ramesh, Lee and Wong 2005). In many research studies, various natural materials (Table 2.2) that are cheap have been tested as adsorbents for their efficiency and effectiveness (ALzaydien 2009).

Table 2.2 Types of natural materials used as starting material for adsorption in wastewater treatment

Agricultural waste	**Sea materials**	**Soil and ore minerals**
Rice husk, coconut shells, sugarcane bagasse	Chitosan	Clay
Sawdust, fruit and vegetable waste, petroleum waste	Seaweed and algae	Red mud
Wood bark, scrap tyres, fly ash	Peat	Zeolites

2.5 The Different Types of Adsorption

The relationship of the adsorbate molecules and the adsorbent surface is best described by applying adsorption isotherms from experimental data. This phenomenon best describes how the adsorbate (dye) molecules will attach themselves to the substrate (activated carbon) when equilibrium is reached. Isotherm parameters such as the Langmuir, Freundlich, and Temkin are used in the data analysis. The determination of the most fitting model is significant since the predicted

isotherm model can be used to design and determine the effectiveness of the adsorbents used by providing information of mass of the adsorbate that can be accommodated by the adsorbent sites at constant temperature (Hamdaoui 2006; Hameed, Ahmad and Latiff 2007). It is also vital to establish the adsorption mechanisms by conducting a kinetic study to determine the order of the reaction whether it is chemisorption of physiosorption, while the thermodynamic parameters are used to determine the spontaneity of the reaction (ALzaydien 2009; Konicki *et al.* 2017).

2.5.1 Adsorption Isotherms

Specific parameters such as the effect of dye concentration, temperature, solution pH, adsorbent dosage, and adsorbent contact time must be optimized to design the possible new adsorption method. The Langmuir isotherm (Langmuir 1918) has been one of the ancient isotherms used to describe the adsorption mechanism of gaseous/liquid molecules onto a solid substrate. The Langmuir isotherm type 1 is the most common. It assumes a monolayer coverage, no interaction between adsorbate particles, and equivalent active sites available for adsorption (Adkins 2006). The description of the Langmuir isotherm (Ghosal and Gupta 2017) is :

$$A + Vs \leftrightarrow [Vs - A] \qquad 2.1$$

Where *A* = is the adsorbate

Vs = is the vacant site within the adsorbent

Vs-A = is the adsorbate particle attached on the vacant site of the adsorbent surface

The equilibrium constant is represented by:

$$K = \frac{[Vs - A]}{[A][Vs]} \qquad 2.2$$

The equilibrium constant, *K*, is then used to define the molarity of the adsorbent and adsorbate in terms of the activity coefficient, μ.

$$K = \frac{\mu_{VS-A}}{\mu_A \mu_{VS}} \quad 2.3$$

The molar activity coefficient μ, for the liquid-solid interface, is expressed in concentrations, C_e Langmuir isotherm monolayer coverage is denoted as follows:

$$\frac{d\theta}{dt_{ads}} = K_{ads} C_e \ (1 \quad \theta) \quad 2.4$$

$$\frac{d\theta}{dt_{des}} = K_{des}\theta \quad 2.5$$

Where θ = represents the fraction of the adsorption and desorption

$$\theta = \frac{q_e}{q_m} \quad 2.6$$

q_e = is the mass adsorbed in the surface of the substrate

q_m = is the monolayer capacity of mass adsorbed on the surface of the substrate

At equilibrium, the Langmuir isotherm is produced when equation 2.4 is equal to equation 2.5 (Azizian, Eris and Wilson 2018):

$$\theta_e = \frac{K_L C_e}{1 + K_L C_e} \quad 2.7$$

$K_L = K_{ads}/K_{des}$

Substitution of equations 2.6 to 2.7 gives the linear form of the Langmuir isotherm expression:

$$q_e = \frac{q_m K_L C_e}{1 + K_L C_e} \quad 2.8$$

q_e = denotes the amount of adsorbate adsorbed at equilibrium (mg g^{-1})

q_m = denotes the Langmuir capacity of adsorbate adsorbed (mg g^{-1})

K_L = is the Langmuir constant for adsorption studies at equilibrium (L mg^{-1})

C_e = is the amount of adsorbate concentration adsorbed at equilibrium (mg L^{-1})

A plot of C_e/q_e as a function of C_e is used to determine q_m and K_L from the slope and y-intercept, respectively.

The Freundlich isotherm (Freundlich 1926) is also a popular isotherm involving adsorption of gases and liquid interfaces. The equation is:

$$\log q_e = \frac{1}{n}\log C_e + \log K_f \qquad 2.9$$

q_e = is the amount of adsorbate adsorbed on the surface of the adsorbent (mg.g^{-1})

n = is the intensity of the Freundlich adsorption capacity

C_e = is the concentration of the adsorbate adsorbed at equilibrium (mg L^{-1})

K_f = is the Freundlich isotherm constant (mg g^{-1}) (L $mg^{-1})^{1/n}$

The *log* q_e as a function of *log* C_e yields a straight line. n and K_f can be computed from the slope and y-intercept, respectively.

Dubinin-Radushkevich Isotherm is one of the extensions of the Langmuir isotherms. It shows the location where the adsorption occurs, whether it is the macropores, mesopores, or micropores (Dubinin and Stoeckli 1980). The linear equation is represented as:

$$\ln q_e = \ln q_s - K_{ad}\,\epsilon^2 \qquad 2.10$$

q_e = is the amount of dye particles adsorbed by the substrate at equilibrium (mg g^{-1})

q_s = is the saturation isotherm capacity (mg g^{-1})

K_{ad} = represents the Dubinin-Radushkevich constant (mol^2/KJ^2)

ϵ = denotes the Polanyi potential

A plot of *log* q_e as the function of ϵ^2 will yield a straight line with K_{ad} and q_s determined from the slope and y-intercept, respectively.

The Temkin isotherm depicts the interaction of the adsorbate versus the adsorbent as a function of temperature. The heat of adsorption is said to decrease linearly with the attachment of the adsorbate particles to the adsorbent surface. It is represented as follows:

$$q_e = \frac{RT}{b_T} \ln A_T + \frac{RT}{b_T} \ln C_e \qquad 2.11$$

q_e = the amount of reactive dye adsorbed by the activated carbon at equilibrium (mg g^{-1})

B = the heat absorption constant of the Temkin isotherm model

R = is the universal gas constant (8.314 J.$mol^{-1}K^{1}$)

T = is the temperature of the reaction (K)

B_T = represents the Temkin isothermal constant

A_T = determines the Temkin isotherm binding constant at equilibrium (L g^{-1})

C_e = is the concentration of the reactive dye after the interaction with adsorbent at equilibrium.

A plot of q_e as the function of *ln* C_e determines *B* and A_T from the slope and y-intercept, respectively.

2.5.2 Adsorption Kinetics

Determination of the adsorption processes is crucial in designing an adsorption method. Therefore, kinetics is taken into consideration to determine the order of the reaction, the rate-limiting steps and the reaction mechanisms. Hence, the use of the pseudo-first-order kinetics (Lagergren 1898), the pseudo-second-order (Ho and McKay 1999), and the intraparticle diffusion (Weber and Morris 1963) are used.

The linear equation represents Lagergren's pseudo 1st order kinetics:

$$\log(q_m - q_t) = \log q_e - \frac{K_{L1}}{2.303} t \qquad 2.12$$

Where K_{L1} = is the Lagergren pseudo kinetic constant for first-order reaction (min^{-1})

q_e = is the amount of reactive dyes adsorbed at equilibrium (mg g^{-1})

q_t = is the amount of reactive dyes adsorbed at any given time (mg g^{-1})

The plot of *log* $(q_m - q_t)$ as a function of time, t is plotted to obtain K_{L1} and q_e from the slope and y-intercept, respectively.

Ho and McKay's pseudo 2nd order kinetics is presented by this linear equation:

$$\frac{t}{q_t} = \frac{1}{K_{H2} q_e^2} + \frac{t}{q_e} \qquad 2.13$$

K_{H2} = is the Ho and McKay's pseudo-second-order kinetic constant (g mg^{-1} min^{-1})

t = is the time (min)

q_t = is the amount of adsorbate adsorbed at any time (mg g^{-1})

q_e = is the amount of adsorbate adsorbed at equilibrium

The plot of t/q_t as the function of time, t gives q_e and K_{H2} from the slope and the y-intercept, respectively.

The Intraparticle diffusion linear expression is:

$$q_t = K_{IPD} t^{0.5} + I \qquad 2.14$$

K_{IPD} = representing the intraparticle rate diffusion constant (mg/g.$min^{-0.5}$)

I = is the mass transfer constant

q_t = is the amount of reactive dyes adsorbed at any time, t (mg g^{-1})

t = time (min)

2.5.3 Activated Carbon

While activated carbon is the most widely used material, it is expensive, non-selective and unaffordable in most developing countries. (Babel and Kurniawan 2003; Ramesh, Lee and Wong 2005; Gopinathan, Bhowal and Garlapati 2017). Therefore, studies of adsorbents derived from cheaper materials have gained more scientists' interest globally (Konduru and Ramakrishna 1997). The precursor sorbent material should be inexpensive, readily available, eco-friendly, have good adsorption capacity, must be re-usable and locally available with high carbon and oxygen content. It should have high thermal stability and abrasion with a small pore diameter for greater surface area for adsorption (Ali, Asim and Khan 2012; Panić *et al.* 2013). Furthermore, to ensure excellent adsorption capacity, the precursor material is required to have mesoporous crystallinity with high porosity (Ayati *et al.* 2016). These characteristics promote strong interaction between the adsorbate (dye) molecule and the surface of the adsorbent (Vikrant *et al.* 2018). The binding by physical forces to the surface of the activated carbon and detachment using a mild solvent, thus promoting the adsorption-desorption mechanism, is presented in Fig 2.7.

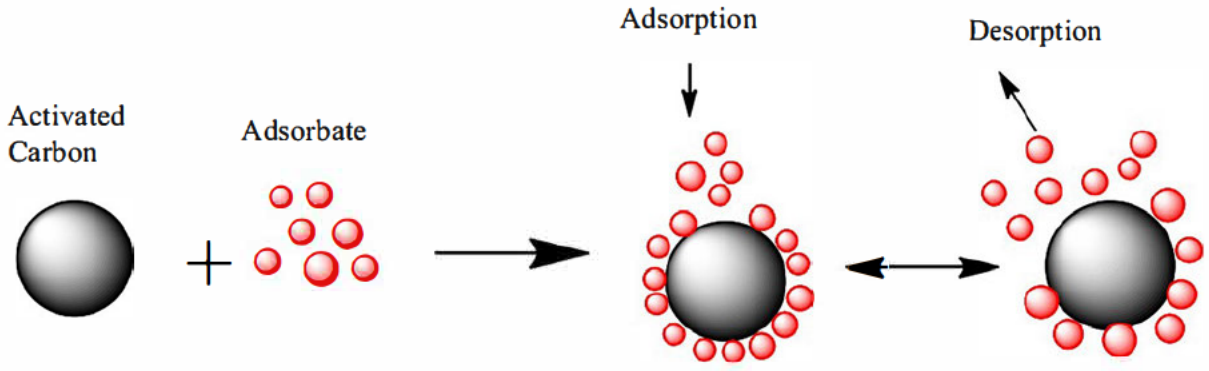

Figure 2.7 Illustration of Adsorption/desorption process onto activated carbon

2.6 Low-cost Material Used as Precursors for Adsorption Studies in Wastewater Treatment

Studies of natural materials and waste materials have shown good dye removal efficiency (Gupta and Suhas 2009). The use of low-cost adsorbent is favourable with high selectivity, easy operation, good adsorption capacity with no hazard exerted onto the organism. However, it is dependent on specific parameters, adsorbent characteristics and experimental conditions (Crini 2006). The precursor may require chemical or physical modification to ensure proper morphological conditions for optimum adsorption (Ali, Asim and Khan 2012). The synthesis of an amphoteric adsorbent to remove all ionic dyes simultaneously was reported (Azha *et al.* 2018). Table 2.3 shows some of the low-cost materials reported for the adsorption of dyes in dye effluent.

Table 2.3 Some low-cost adsorbents currently reported for the adsorption of dyes in effluent

Adsorbent Type	**Low-cost Material**	**Adsorbate**	**References**
Fruit & vegetable waste	Banana peel, orange peel	Congo Red, Methylene Blue, Methylene Orange, Methylene Violet	(Annadurai, Juang and Lee 2002)
	Pear peels, broccoli stems, white sapote seeds	Acid Blue 74, Crystal Violet, Direct Blue 80, Methylene Blue	(Peláez-Cid *et al.* 2016)
Household waste	Exhausted coffee ground	Rhodamine B, Rhodamine 6G	(Shen and Gondal 2017)
	Spent tea leaves	Malachite Green	(Akar, Altinişik and Seki 2013)
	Hair, cotton, bark	Methylene Blue, Safranin	(McKay, Porter and Prasad 1999)
Agricultural waste	*Parthenium hysterophorus*	Methylene Blue	(Lata, Garg and Gupta 2007)
	Cannabis Savita L.	Acid Blue 9	(Yang *et al.* 2011)
	Rice husk	Malachite Green, Acid Yellow 36	(Chuah *et al.* 2005)
Biomass	Sawdust	Methylene Blue	(Garg *et al.* 2004)
	Sugarcane bagasse	Methyl Orange	(Amin 2008)
	Pinus sylvestris Linneo	Reactive Red 195	(Aksakal and Ucun 2010)
	Pinus radiata (cone)	Methylene Blue	(Sen 2011)
Industrial waste	Coal	Reactive Red 194, Reactive Yellow 145	(Gül, Özcan and Erbatur 2007)
Metals	Graphene oxide	Acid Orange 8, Direct Red 23	(Konicki *et al.* 2017)

Sea waste	Chitosan	Methylene Blue, Methylene Orange	(León *et al.* 2018)
	Cerastoderma lamarcki shell	Acid Black 1	(Najafi Saleh *et al.* 2018)
	Camellia Oleifera seed shell	Methylene Blue	(Guo *et al.* 2018)
Microbial organisms	*Murcor circinelloides*	Congo Red	(Azin and Moghimi 2018)
	Thermomuco indicae-seudaticae	Azure B, Congo Red, Trypan Blue, Remazol Brilliant Blue R	(Taha *et al.* 2014)
Clay	Fouchana Tunisian clay	Real effluent mixture of acid, reactive, direct dyes and direct and indigo dyes	(Errais, Duplay and Darragi 2010)
	Jordanian Tripoli	Methylene blue	(ALzaydien 2009)
Composites	Bentonite clay, acrylic and polyethylene diamine	Brilliant Green, Acid Red 1	(Azha *et al.* 2018)
	Eichhonia crasipes/ chitosan	Reactive Black 5	(El-Zawahry *et al.* 2016)
	Bentonite/ proline polymer	Reactive Blue 222, Reactive Red 195, Reactive Yellow 145	(Raghunath *et al.* 2016)

2.7 The Importance of Plant-Based Adsorbents

Adsorbents from natural sources are being investigated for the adsorption of heavy metals and dyes. Plant-based adsorbents contain a high quantity of cellulose with good adsorption capacity (Inthorn *et al.* 2004). Plant-based materials are fully biodegradable with no hazardous by-products that will affect water quality and aquatic life (Yin 2010). The adsorbents prepared from plant precursors should be abundant in nature, economically friendly, produces no sludge, and be recyclable (Bhatnagar, Sillanpää and Witek-Krowiak 2015; Postai *et al.* 2016). However, chemical modification is essential to enhance adsorption capacity. Chemicals for cellulose surface modification may include organic acids, bases, oxidizing agents and minerals (Hokkanen, Bhatnagar and Sillanpää 2016).

Table 2.4 Plants based adsorbents, their chemical modifying agents versus the removal efficiency

Adsorbent	**Adsorbate**	**Chemical Modifying agent**	**Removal Efficiency**	**References**
Parthenium hysterophorus	Methylene blue	H_3PO_4	97	(Lata, Garg and Gupta 2007)
Parthenium hysterophorus	Rhodamine B	H_2SO_4	99	(Lata, Garg and Gupta 2008)
Vegetable residues	Acid blue 74, Direct Blue 80, Crystal Violet, Methylene Blue	H_3PO_4	93-99	(Peláez-Cid *et al.* 2016)
Cannabis sativa L.	Acid Blue 9	H_3PO_4	_	(Yang *et al.* 2011)
Bamboo hydrochar	Methylene Blue	NaOH	-	(Qian *et al.* 2018)
Weeds	Methylene Blue	HNO_3	-	(Güzel *et al.* 2017)
Banana trunk	Methylene Blue	H_3PO_4	99.5-99.9	(Danish *et al.* 2018)
Watermelon Seeds	Reactive Yellow 145	C_6H_{14}	87	(Benkaddour *et al.* 2018)
Sugarcane Bagasse Pith	Reactive Orange	$H_3PO_4 + ZnCl_2$	58-100	(Amin 2008)
Groundnut Shell	Malachite Green	$ZnCl_2$	94.5	(Malik, Ramteke and Wate 2007)

2.8 Plantago Lanceolate

Plantago Lanceolate L. species, commonly known as ribwort or narrow leaf plantain, is the most common garden weed in South Africa. It is of abundance worldwide in most agricultural soil and grassland. *Plantago Lanceolate* can withstand drought, antimicrobial attacks and pests (Stewart 1996). They are used as traditional remedies in some countries, including China (Chau and Wu 2006). However, this common garden weed has not been reported in any literature on wastewater treatment and adsorption. This work features the use of this common weed as the potential low-cost adsorbent in removing some selected textile azo dyes. Currently, this plant is purposeless and only contributes to land pollution. This species multiplies throughout the world regardless of the types of soil. It has biologically active compounds that supplement the animals that graze on them. *Plantago Lanceolate* is a plant that is cellulose-based, hence the study of its potential as a cost-effective adsorbent.

Figure 2.8 *Plantago Lanceolate* garden weed

2.9 Method for characterization of the adsorbent

Table 2.5 A summary of the characterization techniques

CHARACTERISATION TECHNIQUE	INFORMATION
EDX	It gives details of all the elements present on the adsorbent and how they are distributed on the surface.
FTIR	It determines the active functional groups and their positions
HRTEM	It determines the lattice crystal structure and its defects within the derived activated carbon
SEM	It assists in studying the surface morphology of the activated carbon produced
TGA/DSC	Is used in determination of the nature of activated carbon produced through studying it thermal processing steps and mass loss

2.10 The Use of Nanoparticles in Adsorption

Nanomaterials are becoming popular in different industries such as medicals for drug delivery, medical diagnostics, gene therapy, and antimicrobial activities. The large surface area to volume ratio of nanoparticles makes them valuable. The nanomaterials used for wastewater treatments are divided into three classes: carbonaceous nanomaterials, dendrimers, and metal-based zeolites (Tiwari, Behari and Sen 2008). Characterization of these nanostructures is essential as they provide information on the shape and size, hence the nanomaterial properties. These materials should be > 100 nm (Kaegi *et al.* 2011). In addition, the stability of the nanoparticles is crucial for their performance. Carbonaceous and metals oxides nanoparticles such as Fe_2O_3, ZnO, TiO_2 display good stability (Zhang *et al.* 2008). Iron oxide has found popularity in wastewater treatment because of its tremendous magnetism (Darwesh, Matter and

Eida 2019) property which allows regeneration of the biosorbent, therefore minimizing the cost.

2.11 Iron Oxide Nanoparticles

Iron oxide nanoparticles have received tremendous attention from different spheres of research. These particles are well known for their larger surface-area-to-volume ratio, catalytic properties, and great interfacial energy (Zia-ur-Rehman *et al.* 2018). Because of their unique properties, applications in medicine, water treatment, magnetic resonance imaging, catalysis, and data storage are typical (Nizamuddin *et al.* 2019). Moreover, these nanoparticles are excellent adsorbents in air purification and wastewater treatment. This is due to their structural porosity, massive surface area and magnetic capability (Nizamuddin *et al.* 2019). The iron oxide nanoparticles can be obtained in different shapes such as flowers, cubes, rods, spheres. However, their size and properties depend on the synthetic method (Truskewycz, Shukla and Ball 2016).

There are different types of iron oxide nanoparticles (Zia-ur-Rehman *et al.* 2018) that are used in nanotechnology:

Magnetite (Fe_3O_4)

This molecule consists of 32 oxygen ions packed towards the centre with divalent and trivalent stoichiometry, forming a cubic spinal structure.

Maghemite (γ-Fe_2O_3)

The structure of these molecules resembles magnetite in crystallinity and its oxygen packaging in a cubic form. Maghemite usually results from the oxidation of Fe_3O_4.

Hematite (α-Fe_2O_3)

It is the most stable iron oxide nanoparticle used universally to synthesize maghemite and magnetite. It consists of a cubic crystal formation of octahedral ion formation.

2.11.1 Properties and Application of Iron Oxide Nanoparticles

The iron oxide nanoparticles are known for their superparamagnetic nature, promoting easy separation and biocompatibility. Their excellent surface-area-to-volume ratio, highly selective reactivity, and dispersity of sizes as small as 10-20 nm make them valuable. Furthermore, compared to other types of nanoparticles, these are cheap. Most properties are dependent on the nanomaterials' shape and size (Xu *et al.* 2012; Nizamuddin *et al.* 2019). Moreover, because of their attractive properties, they find use in broad applications such as bio-sensing applications, contrast agents for MRI, magnetic inks for jet printing, adsorption research of different pollutants, including removal of inorganic and organic toxins in water (Laurent *et al.* 2008).

2.11.2 Synthesis of Magnetic Iron Oxide Nanoparticles

Various methods are used to synthesize magnetic iron oxides that result in different shapes and sizes. The most widely used methods are synthesis by co-precipitation and surface modification techniques. Other methods include sol-gel, sonolysis, hydrothermal reactions, biosynthesis, direct and reverse emulsification (Laurent *et al.* 2008; Zia-ur-Rehman *et al.* 2018). The co-precipitation technique is prominent because of its fast and straightforward synthesis method, producing many nanoparticles of different shapes and sizes. However, its drawback is that it is challenging to acquire or control the desired size of the particles. Hence the use of chelating agents is required (Laurent *et al.* 2008). Furthermore, because of the tendency of the nanoparticles to aggregate, surface modification techniques are necessary to enhance the monodisperse and stability of the nanoparticles (Zia-ur-Rehman *et al.* 2018). Figure 2.9 depicts the synthesis of various shapes of iron oxide nanoparticles such as nanospheres, nanocubes, nanorods, and nanohexagons formed under certain conditions.

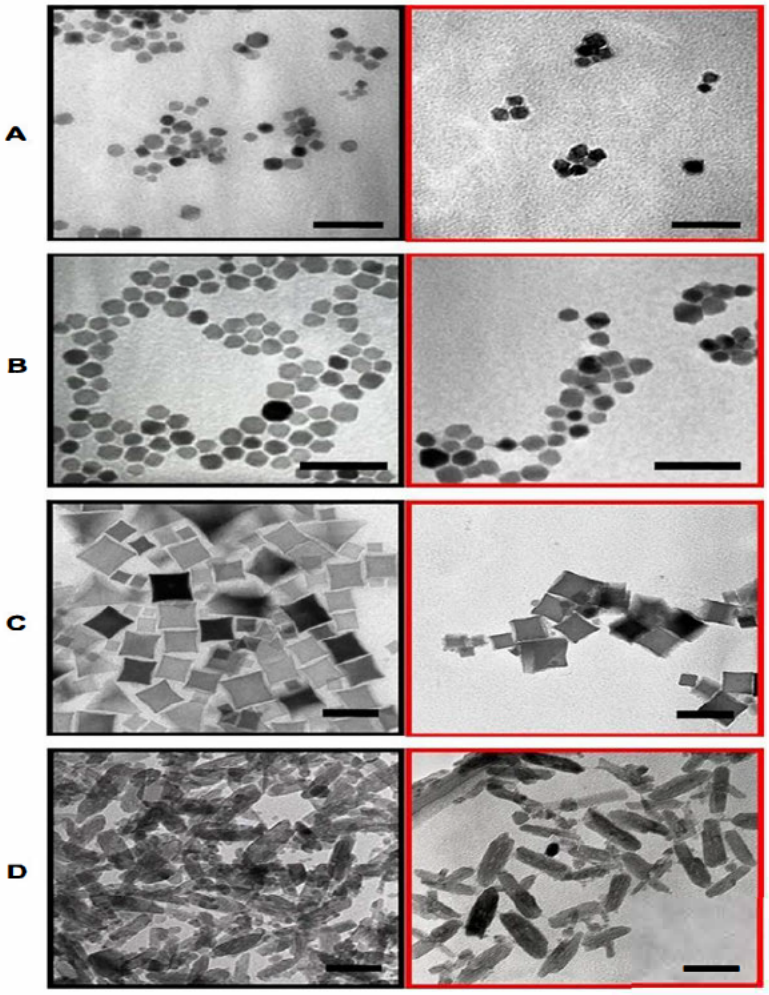

Figure 2.9 Some of the iron oxide nanoparticles with different shapes (A)nanospheres (B)nanohexagons (C)nanocubes (D)nanorods (de Montferrand et al. 2013).

2.11.3 Green Synthesis of Magnetic Iron Oxide Particles

Recently, researchers have opted for green synthesis instead of conventional chemical and physical methods. This method is eco-friendly, has low cost, provides biocompatibility, high adsorption capacity, sensitivity and simple preparation techniques (Saikatendu *et. al*) .As a result, the use of plant extracts and other natural sources is gaining prominence in water remediation and other applications (Zia-ur-Rehman *et al.* 2018). The preparation of the green iron oxide nanoparticles is usually due to the use of plant extracts instead of an inorganic base used in conventional methods, with the aid of a strong base to aid precipitation of metal oxides. Table 2.6 illustrates some of the examples of the green pre-cursor materials used for the synthesis of iron oxide nanoparticles, and their adsorption capacity of different pollutants in water. All though the green synthesized iron oxide nanoparticles have found prominence in the removal of heavy metals in wastewater, however,

photocatalytic degradation is also noted in recent studies (Saikatendu *et. al*). As the use of iron oxide nanoparticles gains prominence in the medical sectors as well as in the preparation of biosensors, an easier and faster greener methods are established. With the green co-precipitation method, a high energy ultrasound can be used to synthesize the iron oxide particles in a minute (Perez-Beltran *et. al*).

Table 2.6 Some green synthesis of iron oxide nanoparticles on the removal of pollutants in wastewater

NATURAL SOURCE	**POLLUTANT**	**References**
Clay	Pb, Cd, As	(Pawar *et al.* 2018)
Coconut shell	phenol	(Hao *et al.* 2018)
Macrocystis pyrifera	Reactive Black 5	(García *et al.* 2018)
Sargassum horneri	Acridine orange, crystal violet, safranin O, methylene blue	(Angelova *et al.* 2016)

2.11.4 The Stability of Ferromagnetic Nanoparticles

The small size of nanoparticles provides a large surface area for the active site; however, magnetic particles stability is compromised, making it prone to aggregation. This inhibits magnetism, reactivity and reduces the surface area-to-volume ratio (Nizamuddin *et al.* 2019). Hence, anchoring the iron oxide nanoparticles to uphold their stability and vectorization is necessary as observed in Figure 2.10. This is due to Van der Waals and electrostatic forces. A surface coating is required during the manufacturing stage of the Ferro-nanoparticles to prevent clustering and instability. It has been reported that specific polymers and activated carbon, with suitable functional groups, were used for stabilizing nanoparticles by anchoring them. Amine, hydroxyl and phosphoric acid groups are suitable to support modifications for the stability of these particles (Xu *et al.* 2012).

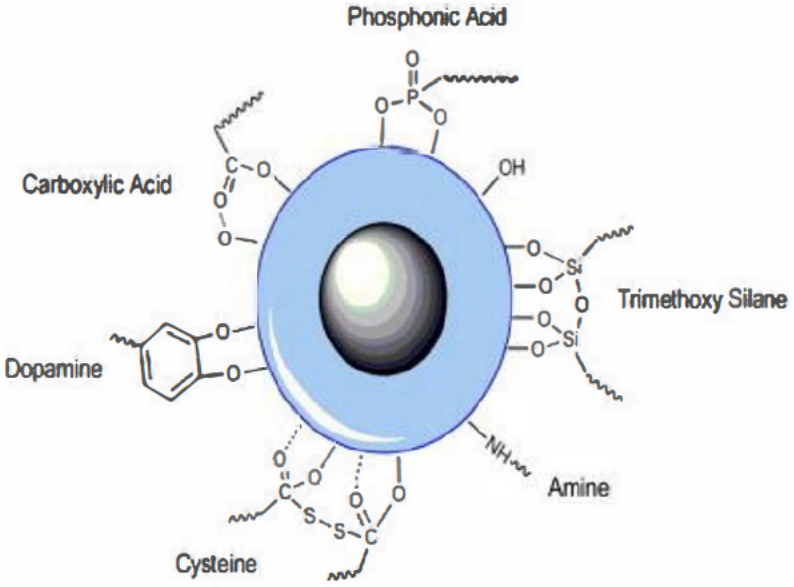

Figure 2.10 Illustration of typical standard anchor moieties of polymer and functional groups at the surface of iron oxide nanoparticles (Dias et al. 2011)

2.11.5 The Use of Activated Carbon/Iron Oxide Nanocomposites for Wastewater Treatment

Activated carbon incorporating magnetic iron nanoparticles improves adsorption capacity because the high surface area of activated carbon and porosity of the nanomaterial is not significantly compromised (Qu *et al.* 2008). As a result, the activated carbon/iron oxide nanocomposite can be easily separated using a magnetic field. This promotes recyclability and regeneration, as there is no loss of the adsorbent, and after that, desorption can be easily performed (Do *et al.* 2011). The use of activated carbon/iron oxide nanocomposites derived from waste material has been found effective for the removal of chromium (VI) irons for water remediation. The efficiency of the activated carbon increased from 83.3 mg g^{1} to 500.0 mg g^{1}, on an activated carbon/iron oxide nanoparticle (Kaur *et. al*). Other examples are the activated carbon/iron oxide nanomaterial are observed in Table 2.7.

Table 2.7: Wastewater remediation of pollutants using an activated carbon/iron oxide nanocomposite as an adsorbent.

Pollutant Removed	**Removal Capacity mg g^{-1}**	**Reference**
Cr (VI) ions	500	Kaur *et. al*
Oil spills	-	Raj *et. al*
Arsenic (V)	27.78	Yurum *et. al*
Pb and Congo Red	144 and 122	Kumar *et.al*

2.12 References

Adrosko, R. J. 2012. *Natural dyes and home dyeing*. Courier Corporation, 1-149.

Akar, E., Altinişik, A. and Seki, Y. 2013. Using of activated carbon produced from spent tea leaves for the removal of malachite green from aqueous solution. *Ecological Engineering*, 52: 19-27.

Akbari, A., Remigy, J. C. and Aptel, P. 2002. Treatment of textile dye effluent using a polyamide-based nanofiltration membrane. *Chemical Engineering and Processing: Process Intensification*, 41 (7): 601-609.

Aksakal, O. and Ucun, H. 2010. Equilibrium, kinetic and thermodynamic studies of the biosorption of textile dye (Reactive Red 195) onto Pinus sylvestris L. *Journal of Hazardous Materials*, 181 (1): 666-672.

Aksu, Z. and Tezer, S. 2005. Biosorption of reactive dyes on the green alga Chlorella vulgaris. *Process Biochemistry*, 40 (3): 1347-1361.

Ali, I., Asim, M. and Khan, T. A. 2012. Low cost adsorbents for the removal of organic pollutants from wastewater. *Journal of Environmental Management*, 113: 170-183.

Allen, S. and Koumanova, B. 2005. Decolourisation of water/wastewater using adsorption. *Journal of the University of Chemical Technology and Metallurgy*, 40 (3): 175-192.

ALzaydien, A. S. 2009. Adsorption of methylene blue from aqueous solution onto a low-cost natural Jordanian Tripoli. *American Journal of Applied Sciences*, 6 (6): 1047.

Amin, N. K. 2008. Removal of reactive dye from aqueous solutions by adsorption onto activated carbons prepared from sugarcane bagasse pith. *Desalination*, 223 (1): 152-161.

Angelova, R., Baldikova, E., Pospiskova, K., Maderova, Z., Safarikova, M. and Safarik, I. 2016. Magnetically modified Sargassum horneri biomass as an adsorbent for organic dye removal. *Journal of Cleaner Production*, 137: 189-194.

Annadurai, G., Juang, R.-S. and Lee, D.-J. 2002. Use of cellulose-based wastes for adsorption of dyes from aqueous solutions. *Journal of Hazardous Materials*, 92 (3): 263-274.

Aslam, M. M., Baig, M., Hassan, I., Qazi, I. A., Malik, M. and Saeed, H. 2004. Textile wastewater characterization and reduction of its COD and BOD by oxidation. *EJEAF Che*, 3 (6): 804-811.

Aspland, J. 1992a. Disperse dyes and their application to polyester. *Textile Chemist and Colorist*, 24: 18-18.

Aspland, J. 1992b. Reactive dyes and their application. *Textile Chemist and Colorist*, 24 (5): 31-36.

Aspland, J. R. 1997. *Textile dyeing and coloration*. AATCC.

Ayati, A., Shahrak, M. N., Tanhaei, B. and Sillanpää, M. 2016. Emerging adsorptive removal of azo dye by metal–organic frameworks. *Chemosphere*, 160: 30-44.

Azha, S. F., Shamsudin, M. S., Shahadat, M. and Ismail, S. 2018. Low cost zwitterionic adsorbent coating for treatment of anionic and cationic dyes. *Journal of Industrial and Engineering Chemistry*, 67: 187-198.

Azin, E. and Moghimi, H. 2018. Efficient mycosorption of anionic azo dyes by Mucor circinelloides: Surface functional groups and removal mechanism study. *Journal of Environmental Chemical Engineering*, 6 (4): 4114-4123.

Azizian, S., Eris, S. and Wilson, L. D. 2018. Re-evaluation of the century-old Langmuir isotherm for modeling adsorption phenomena in solution. *Chemical Physics*, 513: 99-104.

Babel, S. and Kurniawan, T. A. 2003. Low-cost adsorbents for heavy metals uptake from contaminated water: a review. *Journal of Hazardous Materials*, 97 (1): 219-243.

Banat, I. M., Nigam, P., Singh, D. and Marchant, R. 1996. Microbial decolorization of textile-dyecontaining effluents: A review. *Bioresource Technology*, 58 (3): 217-227.

Benkaddour, S., Slimani, R., Hiyane, H., El Ouahabi, I., Hachoumi, I., El Antri, S. and Lazar, S. 2018. Removal of reactive yellow 145 by adsorption onto treated watermelon seeds: Kinetic and isotherm studies. *Sustainable Chemistry and Pharmacy*, 10: 16-21.

Benkhaya, S., El Harfi, S. and El Harfi, A. 2017. Classifications, properties and applications of textile dyes: A review. *Applied Journal of Environmental Engineering Science*, 3: 311-320.

Bhatnagar, A., Sillanpää, M. and Witek-Krowiak, A. 2015. Agricultural waste peels as versatile biomass for water purification – A review. *Chemical Engineering Journal*, 270: 244-271.

Chau, C. F. and Wu, S. H. 2006. The development of regulations of Chinese herbal medicines for both medicinal and food uses. *Trends in Food Science & Technology*, 17 (6): 313-323.

Cheremisinoff, N. P. 2001. *Handbook of water and wastewater treatment technologies*. Butterworth-Heinemann.

Chuah, T. G., Jumasiah, A., Azni, I., Katayon, S. and Thomas Choong, S. Y. 2005. Rice husk as a potentially low-cost biosorbent for heavy metal and dye removal: an overview. *Desalination*, 175 (3): 305-316.

Perez-Beltran, C.H., Garcia-Guzman, J.J., Ferreira, B., Estevez-Hernandez, O., Lopez-Iglesias, D., Cubillana-Aguilera, L., Link, W., Stanica, N., Rosa da Costa, A., Palacios-Santander, J.M. One-minute and green synthesis of magnetic iron oxide nanoparticles assisted by design of experiments and high energy ultrasound: application to biosensing and immunoprecipitation. *Journal of Materials Science and Engineering:C, 123.*

Clark, M. 2011. *Handbook of textile and industrial dyeing: principles, processes and types of dyes*. Elsevier.

Crini, G. 2006. Non-conventional low-cost adsorbents for dye removal: A review. *Bioresource Technology*, 97 (9): 1061-1085.

Daneshvar, N., Salari, D. and Khataee, A. R. 2004. Photocatalytic degradation of azo dye acid red 14 in water on ZnO as an alternative catalyst to TiO2. *Journal of Photochemistry and Photobiology A: Chemistry*, 162 (2): 317-322.

Danish, M., Ahmad, T., Majeed, S., Ahmad, M., Ziyang, L., Pin, Z. and Shakeel Iqubal, S. M. 2018. Use of banana trunk waste as activated carbon in scavenging methylene blue dye: Kinetic, thermodynamic, and isotherm studies. *Bioresource Technology Reports*, 3: 127-137.

Darwesh, O. M., Matter, I. A. and Eida, M. F. 2019. Development of peroxidase enzyme immobilized magnetic nanoparticles for bioremediation of textile wastewater dye. *Journal of Environmental Chemical Engineering*, 7 (1): 102805.

de Ferri, L., Tripodi, R., Martignon, A., Ferrari, E. S., Lagrutta-Diaz, A. C., Vallotto, D. and Pojana, G. 2018. Non-invasive study of natural dyes on historical textiles from the

collection of Michelangelo Guggenheim. *Spectrochimica Acta Part A: Molecular and Biomolecular Spectroscopy*, 204: 548-567.

de Montferrand, C., Hu, L., Milosevic, I., Russier, V., Bonnin, D., Motte, L., Brioude, A. and Lalatonne, Y. 2013. Iron oxide nanoparticles with sizes, shapes and compositions resulting in different magnetization signatures as potential labels for multiparametric detection. *Acta Biomaterialia*, 9 (4): 6150-6157.

Dias, A. M. G. C., Hussain, A., Marcos, A. S. and Roque, A. C. A. 2011. A biotechnological perspective on the application of iron oxide magnetic colloids modified with polysaccharides. *Biotechnology Advances*, 29 (1): 142-155.

Do, M. H., Phan, N. H., Nguyen, T. D., Pham, T. T. S., Nguyen, V. K., Vu, T. T. T. and Nguyen, T. K. P. 2011. Activated carbon/Fe3O4 nanoparticle composite: Fabrication, methyl orange removal and regeneration by hydrogen peroxide. *Chemosphere*, 85 (8): 1269-1276.

Dubinin, M. M. and Stoeckli, H. F. 1980. Homogeneous and heterogeneous micropore structures in carbonaceous adsorbents. *Journal of Colloid and Interface Science*, 75 (1): 34-42.

El-Zawahry, M. M., Abdelghaffar, F., Abdelghaffar, R. A. and Hassabo, A. G. 2016. Equilibrium and kinetic models on the adsorption of Reactive Black 5 from aqueous solution using Eichhornia crassipes/chitosan composite. *Carbohydrate Polymers*, 136: 507-515.

El Qada, E. N., Allen, S. J. and Walker, G. M. 2008. Adsorption of basic dyes from aqueous solution onto activated carbons. *Chemical Engineering Journal*, 135 (3): 174-184.

Errais, E., Duplay, J. and Darragi, F. 2010. Textile dye removal by natural clay – case study of Fouchana Tunisian clay. *Environmental Technology*, 31 (4): 373-380.

Essadki, A. H., Bennajah, M., Gourich, B., Vial, C., Azzi, M. and Delmas, H. 2008. Electrocoagulation/electroflotation in an external-loop airlift reactor—Application to the decolorization of textile dye wastewater: A case study. *Chemical Engineering and Processing: Process Intensification*, 47 (8): 1211-1223.

Farouk, R. and Gaffer, H. E. 2013. Simultaneous dyeing and antibacterial finishing for cotton cellulose using a new reactive dye. *Carbohydrate Polymers*, 97 (1): 138-142.

Ferreira, E. S., Hulme, A. N., McNab, H. and Quye, A. 2004. The natural constituents of historical textile dyes. *Chemical Society Reviews*, 33 (6): 329-336.

Freundlich, H. 1926. Colloid and capillary-Translated from the third German edition by H. *Stafford Hartfield. Methuen and Co, Ltd, London*,

García, F. E., Plaza-Cazón, J., Montesinos, V. N., Donati, E. R. and Litter, M. I. 2018. Combined strategy for removal of Reactive Black 5 by biomass sorption on Macrocystis pyrifera and zerovalent iron nanoparticles. *Journal of Environmental Management*, 207: 70-79.

Garg, V. K., Amita, M., Kumar, R. and Gupta, R. 2004. Basic dye (methylene blue) removal from simulated wastewater by adsorption using Indian Rosewood sawdust: a timber industry waste. *Dyes and Pigments*, 63 (3): 243-250.

Ghoreishi, S. M. and Haghighi, R. 2003. Chemical catalytic reaction and biological oxidation for treatment of non-biodegradable textile effluent. *Chemical Engineering Journal*, 95 (1): 163-169.

Ghosal, P. S. and Gupta, A. K. 2017. Determination of thermodynamic parameters from Langmuir isotherm constant-revisited. *Journal of Molecular Liquids*, 225: 137-146.

Ghuge, S. P. and Saroha, A. K. 2018. Catalytic ozonation of dye industry effluent using mesoporous bimetallic Ru-Cu/SBA-15 catalyst. *Process Safety and Environmental Protection*, 118: 125-132.

Gopinathan, R., Bhowal, A. and Garlapati, C. 2017. Thermodynamic study of some basic dyes adsorption from aqueous solutions on activated carbon and new correlations. *The Journal of Chemical Thermodynamics*, 107: 182-188.

Gül, Ş., Özcan, Ö. and Erbatur, O. 2007. Ozonation of C.I. Reactive Red 194 and C.I. Reactive Yellow 145 in aqueous solution in the presence of granular activated carbon. *Dyes and Pigments*, 75 (2): 426-431.

Guo, H., Bi, C., Zeng, C., Ma, W., Yan, L., Li, K. and Wei, K. 2018. Camellia oleifera seed shell carbon as an efficient renewable bio-adsorbent for the adsorption removal of hexavalent chromium and methylene blue from aqueous solution. *Journal of Molecular Liquids*, 249: 629-636.

Gupta, V. K. and Suhas. 2009. Application of low-cost adsorbents for dye removal – A review. *Journal of Environmental Management*, 90 (8): 2313-2342.

Güzel, F., Sayğılı, H., Akkaya Sayğılı, G., Koyuncu, F. and Yılmaz, C. 2017. Optimal oxidation with nitric acid of biochar derived from pyrolysis of weeds and its application

in removal of hazardous dye methylene blue from aqueous solution. *Journal of Cleaner Production*, 144: 260-265.

Kaur, J.,Kaur, M., Ubhi, M.K., Kaur, N., Greneche, J. 2020. Composition optimization of activated carbon-iron oxide nanocomposite for effective removal of Cr(VI) ions. *Journal of Materials Chemistry and Physics*, 258 (124002).

Kumar, N., Narayanasamy, S., and Priyan, V. 2022. Toxicological assessment and adsorptive removal of lead (Pb) and Congo red (CR) from water by synthesized iron oxide/activated carbon (Fe_3O_4/AC) nanocomposite.*Journal of Chemisphere (294)133758.*

Hamdaoui, O. 2006. Batch study of liquid-phase adsorption of methylene blue using cedar sawdust and crushed brick. *Journal of Hazardous Materials*, 135 (1): 264-273.

Hameed, B. H., Ahmad, A. L. and Latiff, K. N. A. 2007. Adsorption of basic dye (methylene blue) onto activated carbon prepared from rattan sawdust. *Dyes and Pigments*, 75 (1): 143-149.

Hao, Z., Wang, C., Yan, Z., Jiang, H. and Xu, H. 2018. Magnetic particles modification of coconut shell-derived activated carbon and biochar for effective removal of phenol from water. *Chemosphere*, 211: 962-969.

Hemmati, M., Asghari, A., Ghaedi, M. and Rajabi, M. 2017. Chemometric assisted sonochemical dyes adsorption in ternary solutions onto Cu nanowires loaded on activated carbon. *Journal of the Taiwan Institute of Chemical Engineers*, 76: 115-125.

Ho, Y. S. and McKay, G. 1999. Pseudo-second order model for sorption processes. *Process Biochemistry*, 34 (5): 451-465.

Hokkanen, S., Bhatnagar, A. and Sillanpää, M. 2016. A review on modification methods to cellulose-based adsorbents to improve adsorption capacity. *Water Research*, 91: 156-173.

Hossain, L., Sarker, S. K. and Khan, M. S. 2018. Evaluation of present and future wastewater impacts of textile dyeing industries in Bangladesh. *Environmental Development*, 26: 23-33.

Hunger, K. 2007. *Industrial dyes: chemistry, properties, applications*. John Wiley & Sons.

Inthorn, D., Singhtho, S., Thiravetyan, P. and Khan, E. 2004. Decolorization of basic, direct and reactive dyes by pre-treated narrow-leaved cattail (Typha angustifolia Linn.). *Bioresource Technology*, 94 (3): 299-306.

Kaegi, R., Voegelin, A., Sinnet, B., Zuleeg, S., Hagendorfer, H., Burkhardt, M. and Siegrist, H. 2011. Behavior of metallic silver nanoparticles in a pilot wastewater treatment plant. *Environmental Science & Technology*, 45 (9): 3902-3908.

Karcher, S., Kornmüller, A. and Jekel, M. 2002. Anion exchange resins for removal of reactive dyes from textile wastewaters. *Water Research*, 36 (19): 4717-4724.

Kharub, M. 2012. Use of various technologies, methods and adsorbents for the removal of dye.*Journal of environmental reearch and development* 6 (3A) 879-883.

Koh, J. 2011. Dyeing with disperse dyes. In: *Textile Dyeing*. InTech.

Konduru R. Ramakrishna, T. V. 1997. Dye removal using low cost adsorbents. *Water Science & Technology*, 36 (2-3): 189-196.

Konicki, W., Aleksandrzak, M., Moszyński, D. and Mijowska, E. 2017. Adsorption of anionic azo-dyes from aqueous solutions onto graphene oxide: Equilibrium, kinetic and thermodynamic studies. *Journal of Colloid and Interface Science*, 496: 188-200.

Lagergren, S. 1898. About the theory of so-called adsorption of soluble substances. *Sven. Vetenskapsakad. Handingarl*, 24: 1-39.

Lahkimi, A., Oturan, M. A., Oturan, N. and Chaouch, M. 2007. Removal of textile dyes from water by the electro-Fenton process. *Environmental Chemistry Letters*, 5 (1): 35-39.

Langmuir, I. 1918. The adsorption of gases on plane surfaces of glass, mica and platinum. *Journal of the American Chemical Society*, 40 (9): 1361-1403.

Lata, H., Garg, V. K. and Gupta, R. K. 2007. Removal of a basic dye from aqueous solution by adsorption using Parthenium hysterophorus: An agricultural waste. *Dyes and Pigments*, 74 (3): 653-658.

Lata, H., Garg, V. K. and Gupta, R. K. 2008. Adsorptive removal of basic dye by chemically activated Parthenium biomass: equilibrium and kinetic modeling. *Desalination*, 219 (1): 250-261.

Laurent, S., Forge, D., Port, M., Roch, A., Robic, C., Vander Elst, L. and Muller, R. N. 2008. Magnetic iron oxide nanoparticles: synthesis, stabilization, vectorization, physicochemical characterizations, and biological applications. *Chemical Reviews*, 108 (6): 2064-2110.

León, O., Muñoz-Bonilla, A., Soto, D., Pérez, D., Rangel, M., Colina, M. and Fernández-García, M. 2018. Removal of anionic and cationic dyes with bioadsorbent oxidized chitosans. *Carbohydrate Polymers*, 194: 375-383.

Malik, R., Ramteke, D. S. and Wate, S. R. 2007. Adsorption of malachite green on groundnut shell waste based powdered activated carbon. *Waste Management*, 27 (9): 1129-1138.

McKay, G., Porter, J. F. and Prasad, G. R. 1999. The removal of dye colours from aqueous solutions by adsorption on low-cost materials. *Water, Air, and Soil Pollution*, 114 (3): 423-438.

McMullan, G., Meehan, C., Conneely, A., Kirby, N., Robinson, T., Nigam, P., Banat, I., Marchant, R. and Smyth, W. 2001. Microbial decolourisation and degradation of textile dyes. *Applied Microbiology and Biotechnology*, 56 (1-2): 81-87.

Murray, A. and Mortimer, K. 1971. Carrier dyeing. *Review of Progress in Coloration and Related Topics*, 2 (1): 67-72.

Najafi Saleh, H., Dehghani, M. H., Nabizadeh, R., Mahvi, A. H., yaghmaeian, k., Hossein, F., Ghaderpoori, M., Yousefi, M. and Mohammadi, A. 2018. Data on the acid black 1 dye adsorbtion from aqueous solutions by low-cost adsorbent- Cerastoderma lamarcki shell collected from the northern coast of Caspian Sea. *Data in Brief*, 17: 774-780.

Natarajan, S., Bajaj, H. C. and Tayade, R. J. 2018. Recent advances based on the synergetic effect of adsorption for removal of dyes from waste water using photocatalytic process. *Journal of Environmental Sciences*, 65: 201-222.

Nizamuddin, S., Siddiqui, M. T. H., Mubarak, N. M., Baloch, H. A., Abdullah, E. C., Mazari, S. A., Griffin, G. J., Srinivasan, M. P. and Tanksale, A. 2019. Chapter 17 - Iron oxide nanomaterials for the removal of heavy metals and dyes from wastewater. In: Thomas, S., Pasquini, D., Leu, S.-Y. and Gopakumar, D. A. eds. *Nanoscale Materials in Water Purification*. Elsevier, 447-472. Available: http://www.sciencedirect.com/science/article/pii/B9780128139264000239 (Accessed

Nunn, D. 1979. *The dyeing of synthetic-polymer and acetate fibres*. Dyers Co. Publications Trust.

Panić, V. V., Šešlija, S. I., Nešić, A. R. and Veličković, S. J. 2013. Adsorption of azo dyes on polymer materials. *Hemijska Industrija*, 67 (6): 881-900.

Pawar, R. R., Lalhmunsiama, Kim, M., Kim, J.-G., Hong, S.-M., Sawant, S. Y. and Lee, S. M. 2018. Efficient removal of hazardous lead, cadmium, and arsenic from aqueous environment by iron oxide modified clay-activated carbon composite beads. *Applied Clay Science*, 162: 339-350.

Peláez-Cid, A.-A., Herrera-González, A.-M., Salazar-Villanueva, M. and Bautista-Hernández, A. 2016. Elimination of textile dyes using activated carbons prepared from vegetable residues and their characterization. *Journal of Environmental Management*, 181: 269-278.

Peter Adkins, J. D. P. 2006. *Physical Chemistry*. 8 ed. United States and Canada: W.H. Freeman and Company.

Postai, D. L., Demarchi, C. A., Zanatta, F., Melo, D. C. C. and Rodrigues, C. A. 2016. Adsorption of rhodamine B and methylene blue dyes using waste of seeds of Aleurites Moluccana, a low cost adsorbent. *Alexandria Engineering Journal*, 55 (2): 1713-1723.

Qian, W.-C., Luo, X.-P., Wang, X., Guo, M. and Li, B. 2018. Removal of methylene blue from aqueous solution by modified bamboo hydrochar. *Ecotoxicology and Environmental Safety*, 157: 300-306.

Qu, S., Huang, F., Yu, S., Chen, G. and Kong, J. 2008. Magnetic removal of dyes from aqueous solution using multi-walled carbon nanotubes filled with Fe2O3 particles. *Journal of Hazardous Materials*, 160 (2): 643-647.

Raghunath, S., Anand, K., Gengan, R. M., Nayunigari, M. K. and Maity, A. 2016. Sorption isotherms, kinetic and optimization process of amino acid proline based polymer nanocomposite for the removal of selected textile dyes from industrial wastewater. *Journal of Photochemistry and Photobiology B: Biology*, 165: 189-201.

Rajaguru, P., Vidya, L., Baskarasethupathi, B., Kumar, P. A., Palanivel, M. and Kalaiselvi, K. 2002. Genotoxicity evaluation of polluted ground water in human peripheral blood lymphocytes using the comet assay. *Mutation Research/Genetic Toxicology and Environmental Mutagenesis*, 517 (1): 29-37.

Ramesh, A., Lee, D. J. and Wong, J. W. C. 2005. Thermodynamic parameters for adsorption equilibrium of heavy metals and dyes from wastewater with low-cost adsorbents. *Journal of Colloid and Interface Science*, 291 (2): 588-592.

Robinson, T., McMullan, G., Marchant, R. and Nigam, P. 2001. Remediation of dyes in textile effluent: a critical review on current treatment technologies with a proposed alternative. *Bioresource Technology*, 77 (3): 247-255.

Rozzi, A., Antonelli, M. and Arcari, M. 1999. Membrane treatment of secondary textile effluents for direct reuse. *Water Science and Technology*, 40 (4): 409-416.

Sadri Moghaddam, S., Alavi Moghaddam, M. R. and Arami, M. 2010. Coagulation/flocculation process for dye removal using sludge from water treatment plant: Optimization through response surface methodology. *Journal of Hazardous Materials*, 175 (1): 651-657.

Saikatendu Deb Roy, Krishna Chandra Das and Siddhartha Sankar Dhar. 2021. Conventional to green synthesis of magnetic oxide nanoparticles; its application as a catalyst, photocatalyst and toxicity: A short review. *Inorganic Chemistry Communications,* 134:1-22.

Sen, T. K. 2011. Equilibrium, kinetics and mechanism of removal of methylene blue from aqueous solution by adsorption onto pine cone biomass of *Pinus radiata*. *Water, Air, and Soil Pollution*, 218 (1-4): 499-515.

Shen, K. and Gondal, M. A. 2017. Removal of hazardous Rhodamine dye from water by adsorption onto exhausted coffee ground. *Journal of Saudi Chemical Society*, 21: S120-S127.

Slokar, Y. M. and Majcen Le Marechal, A. 1998. Methods of decoloration of textile wastewaters. *Dyes and Pigments*, 37 (4): 335-356.

Stewart, A. 1996. Plantain (Plantago lanceolata)-a potential pasture species. In: Proceedings of *Proceedings of the Conference-New Zealand Grassland Association*. 77-86.

Sultana, M. S., Islam, M. S., Saha, R. and Al-Mansur, M. 2009. Impact of the effluents of textile dyeing industries on the surface water quality inside DND embankment, Narayanganj. *Bangladesh Journal of Scientific and Industrial Research*, 44 (1): 65-80.

Taha, M., Adetutu, E. M., Shahsavari, E., Smith, A. T. and Ball, A. S. 2014. Azo and anthraquinone dye mixture decolourization at elevated temperature and concentration by a newly isolated thermophilic fungus, Thermomucor indicae-seudaticae. *Journal of Environmental Chemical Engineering*, 2 (1): 415-423.

Truskewycz, A., Shukla, R. and Ball, A. S. 2016. Iron nanoparticles synthesized using green tea extracts for the fenton-like degradation of concentrated dye mixtures at

elevated temperatures. *Journal of Environmental Chemical Engineering*, 4 (4, Part A): 4409-4417.

Raj, K.G. and Joy, P.A. 2015. Coconut shell based activated carbon-iron oxide magnetic nanocomposite for fast and efficient removal of oil spills. *Journal of Environmnental Chemical Engineering,* 3: 2068-2075.

Vandevivere, P. C., Bianchi, R. and Verstraete, W. 1998. Treatment and reuse of wastewater from the textile wet-processing industry: Review of emerging technologies. *Journal of Chemical Technology & Biotechnology: International Research in Process, Environmental and Clean Technology*, 72 (4): 289-302.

Vikrant, K., Giri, B. S., Raza, N., Roy, K., Kim, K.-H., Rai, B. N. and Singh, R. S. 2018. Recent advancements in bioremediation of dye: Current status and challenges. *Bioresource Technology*, 253: 355-367.

Weber, W. J. and Morris, J. C. 1963. Kinetics of adsorption on carbon from solution. *Journal of the Sanitary Engineering Division*, 89 (2): 31-60.

Xu, P., Zeng, G. M., Huang, D. L., Feng, C. L., Hu, S., Zhao, M. H., Lai, C., Wei, Z., Huang, C., Xie, G. X. and Liu, Z. F. 2012. Use of iron oxide nanomaterials in wastewater treatment: A review. *Science of The Total Environment*, 424: 1-10.

Yagub, M. T., Sen, T. K., Afroze, S. and Ang, H. M. 2014. Dye and its removal from aqueous solution by adsorption: A review. *Advances in Colloid and Interface Science*, 209: 172-184.

Yang, R., Liu, G., Xu, X., Li, M., Zhang, J. and Hao, X. 2011. Surface texture, chemistry and adsorption properties of acid blue 9 of hemp (Cannabis sativa L.) bast-based activated carbon fibers prepared by phosphoric acid activation. *Biomass and Bioenergy*, 35 (1): 437-445.

Yin, C.-Y. 2010. Emerging usage of plant-based coagulants for water and wastewater treatment. *Process Biochemistry*, 45 (9): 1437-1444.

Yurum, A., Kocabas-Atakli, Z.O., Sezen, M., Semiat, R., and Yurum, Y. 2014. Fast desorption of porous iron oxide on activated carbon by microwave heating and arsenic (V) removal from water. *Chemical Engineering Journal,* 242: 321-332.

Zhang, Y., Chen, Y., Westerhoff, P., Hristovski, K. and Crittenden, J. C. 2008. Stability of commercial metal oxide nanoparticles in water. *Water Research*, 42 (8): 2204-2212.

Zia-ur-Rehman, M., Naeem, A., Khalid, H., Rizwan, M., Ali, S. and Azhar, M. 2018. Chapter 10 - Responses of Plants to Iron Oxide Nanoparticles. In: Tripathi, D. K., Ahmad, P., Sharma, S., Chauhan, D. K. and Dubey, N. K. eds. *Nanomaterials in Plants, Algae, and Microorganisms*. Academic Press, 221-238. Available: http://www.sciencedirect.com/science/article/pii/B9780128114872000104 (Accessed

Zollinger, H. 2003. *Color chemistry: syntheses, properties, and applications of organic dyes and pigments*. John Wiley & Sons.

CHAPTER 3: EXPERIMENTAL

3.1 Materials

Plantago Lanceolate L. (identified in appendix 1) was collected at the Durban University of Technology (Durban) and identified at the KwaZulu-Natal Herbarium (South African National Biodiversity Institute). Sodium hydroxide and potassium hydroxide pellets were purchased from RADCHEM Laboratory Supplies. Sulfuric acid (98%), ferrous sulphate heptahydrate (99%), iron chloride anhydrous powder (97%), and hydrochloric acid were purchased from Sigma Aldrich. Phosphoric acid (85%) was purchased from Fluka Biochemika. All the reagents used were of analytical grade. The dyes used: Reactive Blue 222, Reactive Red 195 and Reactive Yellow 145 were purchased from Colchem Chemicals and Dyes South Africa. Double deionized was used for the preparation of solutions and was obtained from a MilliQ Millipore system. Whatman filter paper no 1 was used for all filtrations. All the glassware was thoroughly washed using double deionized water. For the pH studies, the adjustments were made using either 0.1 M HCl or 0.1 M NaOH solutions. All the analyses were performed in triplicate, and the mean was used for the calculations.

3.2 Instrumentation

The Perkin Elmer Spectrum 100 FT-IR Spectrometer, CPU 32 main with a Universal ATR (attenuated total reflection) was used. The samples were analyzed in the scanning range of 4000 cm^{1} to 380 cm^{1}, with a resolution of 1 cm^{1} using a germanium crystal. The ZEISS EVO 15 Environmental Scanning Electron Microscope analyzer coupled with the Energy Dispersive X-ray was used for the surface morphology analysis. HR-TEM JOEL JEM 2000EXII transmission electron microscope was used to determine the diffraction and lattice fringe images. A METTLER TOLEDO TGA system and a Differential Scanning Calorimetry model 1 SF/1346 with STARe system software was used for thermogravimetric analysis. A Shimadzu UV 1800 UV/Visible Spectrophotometer was used to determine the absorbance readings, with a pair of 1 cm path length quartz cuvettes. All the samples were scanned in the region of 800–200 nm, at a scanning rate of 0.5 nm/s. The SPL 15 MP Labcon Platform Shaker was used for agitating the conical flasks at a speed of 150 rpm. The Hettich Universal II Centrifuge was used at a speed at 4000 rpm. The Metrohm 691 pH meter was used for the pH measurements.

3.3 Methods

3.3.1 Preparation of Phosphoric Acid Treated *Plantago Lanceolata* Activated Carbon (H_3PO_4-AC)

The leaves were washed with tap water to remove dust, mud and insects and dried overnight in an oven at 105°C. Thereafter it was crushed into a fine powder using a mortar and pestle; total yield mass was 154 g. 25.0 g of the powder was immersed into a solution of 42% H_3PO_4 in a 1:2 ratios (w/v). The excess liquid was decanted, and the material was then transferred into a muffle furnace, set at 120°C for 24 hrs then at 500°C for 3 hours. The carbon that was obtained was washed 3 times with double deionized water to remove the excess acid and then dried overnight in a hot air oven at 110°C. The dried H_3PO_4-AC was sieved to collect the fine particles of less than 1.5 mm in diameter. The fine powder was stored in a labelled air- tight glass container for further analysis. A scheme for the preparation of activated carbon is presented in Fig 3.1.

3.3.2 Preparation of Sulfuric Acid Treated *Plantago Lanceolata* Activated Carbon (H_2SO_4-AC)

The method used (Singh *et al.* 2008) for adsorbent preparation with sulfuric acid as a modifier, was carried out with minor changes. The carbon powder (25.0 g) was treated with 98% sulfuric acid in a ratio of 1:2 biomass: acid (w/w).). The excess liquid was decanted, and the material was then transferred into a muffle furnace, set at 120°C for 24 hrs then at 500°C for 3 hours. The carbon that was obtained was washed 3 times with double deionized water then left to soak in a solution of 1% sodium bicarbonate, overnight, to remove the excess acid. The activated carbon was washed several times with deionized water and dried at 110°C. The dried H_2SO_4-AC was sieved to collect the fine particles of less than 1.5 mm in diameter. The fine powder was stored in an air-tight glass container.

3.3.3 Preparation of Potassium Hydroxide Treated *Plantago Lanceolata* Activated Carbon (KOH-AC)

The method followed (Sabela *et al.* 2016) for the preparation of KOH-AC was carried out with minor changes The carbon powder 25.0 g was soaked, overnight at room temperature, in a 10% KOH solution in the ratio 1:2 (w/v) . The excess liquid was decanted, and the material was then transferred into a muffle furnace set at 300ºC-500ºC which was gradually increased for 2 hours, to carbonize the material. until the. The activated carbon was washed with 0.1 M HCl then 3 times with double deionized water to remove the excess base. The carbon was dried overnight in a hot air oven at 110ºC and sieved in a ground sieve with filters to collect particles less than 1.5 mm in diameter. The carbon was stored in an air-tight labelled glass container until further use.

3.3.4 Preparation of Sodium Hydroxide Treated *Plantago Lanceolata* Activated Carbon (NaOH-AC)

The carbon powder 25.0 g was soaked in 10% NaOH solution in the ratio 1:2 (w/v). The excess liquid was decanted, and the material was transferred into a muffle furnace set at 300ºC-500ºC. The activated carbon was washed with 0.1 M HCl and then rinsed several times with deionized water to remove the excess base. It was then dried in a hot air oven at 110ºC. The carbon was dried overnight in a hot air oven at 110ºC and sieved using a ground sieve with filters to collect particles less than 1.5 mm in diameter. The carbon was stored in an air-tight labelled glass container until further use.

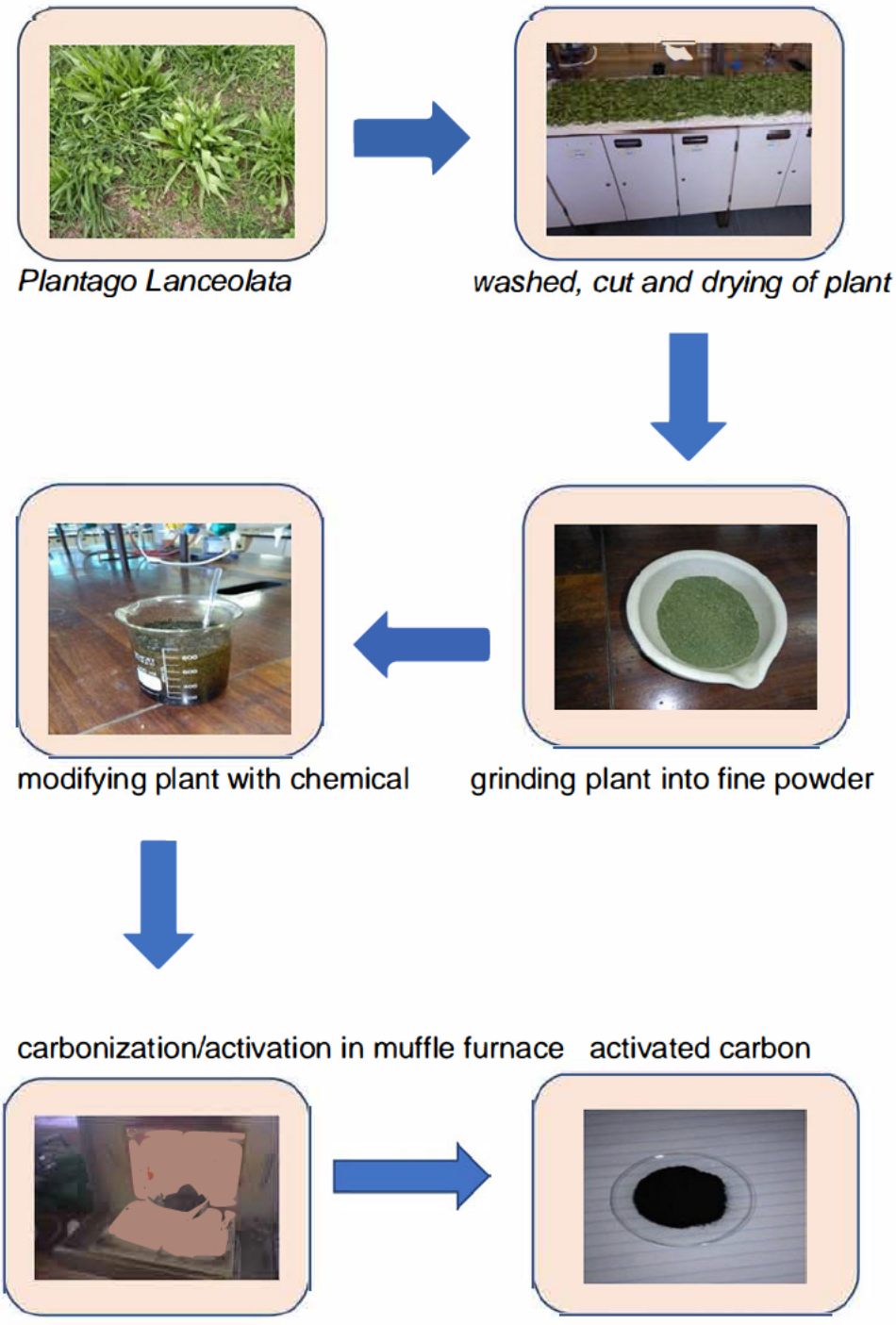

Figure 3.1 A scheme showing the preparation of the activated carbon from weed

3.3.5 Preparation of Iron Oxide Based Activated Carbon Composite

A mass of 12.12 g of H_3PO_4-AC was added to a 400 mL aqueous solution containing $FeCl_3$ anhydrous (7.8 g) and $FeSO_4.7H_2O$ (3.9 g) to produce a composite of ratio 3:1. This aqueous mixture was slowly precipitated using 100mL of 5 $mol.L^{-1}$ NaOH solution at a fixed oil bath temperature of 70ºC under reflux conditions following the method proposed by Oliveira (Oliveira *et al.* 2004). The mixture was refluxed for 2 hrs, cooled

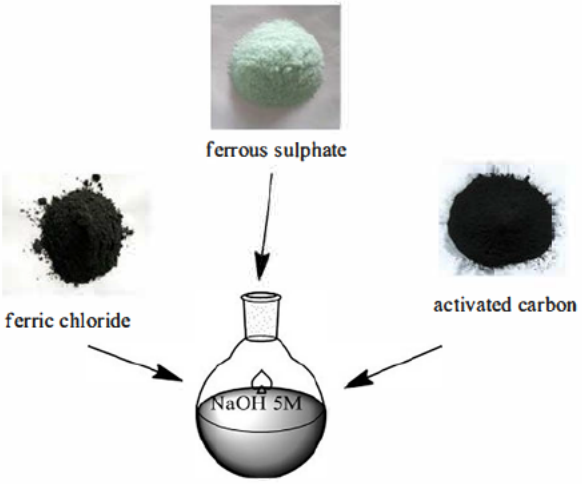

Figure 3.2 Preparation of the iron oxide/H_3PO_4-AC magnetic nanocomposite

and dried for 2 hrs in an oven set at 50ºC. The iron oxide based activated carbon composite was and placed in a glass air-tight container for further analysis and characterizations.

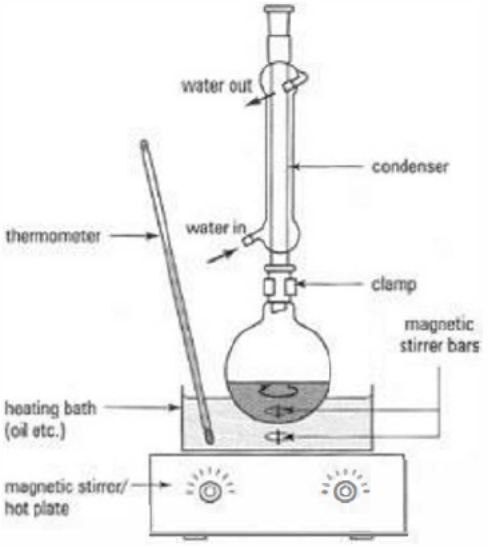

Figure 3.3 Illustration of the reflux system for the preparation of the iron oxide/ H_3PO_4-AC magnetic composite

3.3.6 Preparation of Stock Solutions and Dye standards

A stock solution of 400 mg L^{-1} was prepared by weighing out 0.2 g of each dye (RB, RR and RY) into a clean weighing boat. This was transferred into a 500 mL volumetric flask, using a glass funnel, and made up to mark with double deionized water. The working standards were then prepared by taking aliquots using bulb pipettes (5 mL, 10 mL, 15 mL, 20 mL, 25 mL and 30 mL) to make up the 20 mg L^{-1}, 40 mg L^{-1}, 60 mg L^{-1}, 80 mg L^{-1}, 100 mg L^{-1} and 120 mg L^{-1} standards, respectively, in 6 different 100 mL clean and dry volumetric flasks.

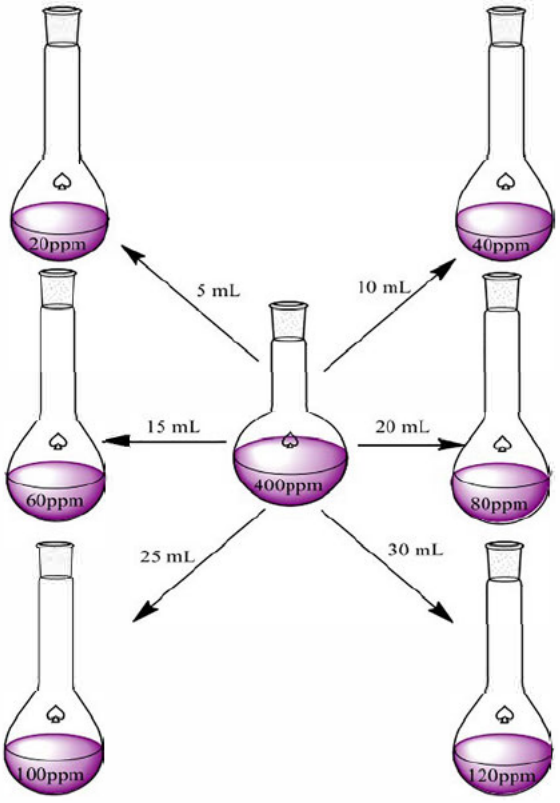

Figure 3.4 Preparation of the mixed dyes working standards from the stock solution

3.4 Adsorption Studies

3.4.1 Batch method experiments

A fixed quantity of adsorbent 0,5 g (unless stated otherwise) such as H_3PO_4-AC, H_2SO_4-AC, KOH-AC and NaOH-AC was weighed separately and transferred into 100 mL stoppered conical flasks containing 60 mL (unless stated otherwise) of the mixed dye solutions. The mixed dye solutions (RB, RR and RY) of known concentration were also added, and the flasks were placed in a shaker incubator at 150 rpm for fixed time

intervals (30 minutes). All the analyses were performed at room temperature (±25 °C) unless stated otherwise. The samples were then transferred into centrifuge tubes and centrifuged at 4000 rpm for 30 minutes. After the tubes were removed, the supernatant was transferred into quartz cuvettes for analysis using the UV/Visible spectrophotometer. Optimization of the method included five parameters: the effects of dye concentration, adsorbent dosage concentration, pH of the adsorbates, adsorbent contact time and solution temperature. The calibration plot was obtained along with the maximum wavelength for all the dyes viz. RB (611 nm), RR (540 nm) and RY (420 nm). Beer Lambert's law (BV and HYDRAULICS 1962) was applied for the determination of the adsorbed concentration. The adsorption removal capacity of the ternary reactive dye system was computed using equation 3.1 (Hameed, Ahmad and Latiff 2007).

$q_e = (C_o\text{-}C_e)\,\frac{V}{W}$	3.1

q_e (mg g^{-1}) refers to the amount of reactive azo dyes mixture adsorbed at equilibrium, C_o and C_e (mg L^{-1}) is the initial and equilibrium concentration respectively, V (L) is the volume of the dye used and W (g) is the mass weighed of activated carbon.

The percentage of dye removed was calculated using equation (3.2):

$\%\ \text{Dye adsorbed} = \frac{\text{Co-Cf}}{\text{Co}} \times 100$	3.2

where Co, C_f (mg L^{-1}) are the initial and final concentration. All the analyses were performed in triplicate and the mean values were used in the calculation.

3.5 The Adsorption of Textile Dyes on Activated

Four adsorbents were used in the initial dye bath concentration studies using a dye mixture of reactive blue 222, reactive red 195 and reactive yellow 145. The factors optimized were dye concentration, pH, adsorbent dosage, adsorbent contact time and temperature. The adsorbent with the highest adsorption capacity for the removal of dyes was then used for further studies.

3.5.1 Comparison of Different Activated Carbon Adsorbents and their Effect on Textile Dye Removal

The effect of the initial dye concentration on adsorption onto H_3PO_4-AC, KOH-AC, H_2SO_4-AC and NaOH-AC was conducted. A batch method was used by weighing 0.5 g (accurate masses are stipulated in Table 3.1) of each of the prepared activated carbon into conical flasks containing 30 mL of the mixed dye standards of: 20 mg L^{-1}, 40 mg L^{-1}, 60 mg L^{-1}, 80 mg L^{-1}, 100 mg L^{-1} and 120 mg L^{-1}, separately. These solutions were agitated for 30 minutes in a thermostat shaker at 150 rpm at 25ºC. Thereafter, the dye solutions were transferred into centrifuge tubes and centrifuged at 4000 rpm for 30 minutes. The supernatant was collected and the maximum absorbance for each solution was recorded using the UV- visible spectrophotometer.

Table 3.1 Mass of adsorbents for the determination of suitable adsorbents

ADSORBENT USED	**CONCENTRATION (mg L^{-1})**	**MASS OF ACTIVATED CARBON WEIGHED (g)**
H_3PO_4-AC	20	0.5008
	40	0.5085
	60	0.5024
	80	0.5008
	100	0.5023
	120	0.5031
KOH-AC	20	0.5003
	40	0.5082
	60	0.5040
	80	0.5001
	100	0.5033
	120	0.5007
H_2SO_4-AC	20	0.5073
	40	0.5031
	60	0.5207
	80	0.5057
	100	0.5010
	120	0.5206

NaOH-AC	20	0.5014
	40	0.5091
	60	0.5100
	80	0.5096
	100	0.5003
	120	0.5012

3.5.2 Effect of Initial Dye Concentration and Adsorbent Contact Time on Textile Dye Removal

The rate of adsorption on the initial dye concentration using the mixed dye standards (20 mg L^{-1}, 40 mg L^{-1}, 60 mg L^{-1}, 80 mg L^{-1}, 100 mg L^{-1} and 120 mg L^{-1}) was determined. Dye standards (50 mL) containing 0.5 g of H_3PO_4-AC which are shown in Table 3.2, were agitated in a thermostat shaker at 25ºC, at 150 rpm for 90 minutes. An initial aliquot sample was removed at 10 minutes of the reaction time. Thereafter, aliquot samples were taken at 15-minute intervals. The samples were centrifuged for 30 minutes at 4000 rpm and the supernatant was analysed using the UV-visible spectrophotometer.

Table 3.2 Mass of H_3PO_4-AC adsorbent used for the effect of concentration studies

Concentration (mg L^{-1})	**Mass (g)**
20	0.5006
40	0.5014
60	0.5042
80	0.5009
100	0.5030
120	0.5086

3.5.3 The Effect of Initial solution pH on Textile Dye Removal

The investigation on the effect of solution pH was carried out by placing 50 mL of 100 mg L^{-1} mixed dye standard into 7 conical flasks. The pH of the dye solutions was adjusted using 0.1 M HCl or 0.1 M NaOH standardised solutions to obtain the desired pH's (2, 4, 6, 7, 8, 10, and 12). An adsorbent mass of 0.5 g (Table 3.3) of H_3PO_4-AC

was used. The study was carried out at 25ºC using a controlled thermostat shaker at 150 rpm for 30 minutes. The dyes were centrifuged at 4000 rpm for 30 minutes and the supernatant was analysed using a UV-visible spectrophotometer.

Table 3.3 Mass of H_3PO_4-AC adsorbent used for the effect of pH studies

pH	Adsorbent (g)
2.29	0.5001
4.02	0.5035
6.00	0.5007
7.15	0.5132
8.76	0.5073
10.25	0.5006
12.01	0.5020

3.5.4 Effect of Adsorbent Dosage on Textile Dye Removal

The adsorption of the mixed reactive dye having a concentration of 120 mg L^{-1} (highest standard) was determined by accurately weighing the H_3PO_4-AC adsorbent (Table 3.4) which was 0.4 g, 0.5 g, 0.6 g, 0.8 g, 1.0 g and 1.2 g respectively, into 50.00 mL of the dye solution into separate conical flasks. A thermostat shaker (25ºC) was used to agitate the samples for 30 minutes at 150 rpm. The samples were then centrifuged at 4000 rpm for 30 minutes. The samples were filtered, filtrates collected and analysed using the UV-visible spectrophotometer.

Table 3.4 Mass of H_3PO_4-AC adsorbent used for the equilibrium studies

Concentration (mg L^{-1})	Volume (mL)	Mass (g)
120	50.00	0.4104
120	50.00	0.5023
120	50.00	0.6202
120	50.00	0.8017
120	50.00	1.0039
120	50.00	1.2062

3.5.5 Effect of Temperature on Textile Dye Removal

The effect of temperature on the initial dye bath was determined for the adsorption process using H_3PO_4-AC. A temperature was set and equilibrated according to the desired temperature (20ºC, 30ºC and 40ºC) before the reaction began. The dye standard (50 mL of 100 mg L^{-1}) was introduced into separate conical flasks; The mass of the adsorbent seen in Table 3.5 (~0.5 g) was used for the reaction. The solutions were agitated in a thermostat shaker for 30 minutes at 150 rpm, and then centrifuged at 4000 rpm for 30 minutes. The samples were filtered, and the filtrates were analysed using the UV-visible spectrophotometer.

Table 3.5 Mass of adsorbents for the thermodynamic studies

Concentration (mg L^{-1})	**Temperature (ºC)**	**Mass (g)**
100	20	0.5024
100	30	0.5018
100	40	0.5022

3.5.6 Effect of Initial Dye Concentration in the Remediation of Textile Dyes

A 400 mg L^{-1} mixed dye (RB, RR and RY) stock solution was used to prepare working standards (20, 40, 60, 80,100 and 120 mg L^{-1}) in 250 mL volumetric flasks. 60 mL of each working standard was transferred into stoppered 250 mL conical flasks containing 0.5 g of the iron oxide/H_3PO_4-AC composite (Table 3.6). The reaction mixture was agitated in a thermostat shaker at 25ºC, 150 rpm for 90 minutes. An initial sample aliquot 10 mL. Thereafter, aliquot samples were taken at 15-minute intervals. The samples were centrifuged for 30 minutes at 4000 rpm and the supernatant was analysed using the UV-visible spectrophotometer.

Table 3.6 Mass of iron oxide/H_3PO_4-AC adsorbent used for the effect of concentration study

Concentration (mg L^{-1})	**Mass (g)**
20	0.5120
40	0.5126
60	0.5002
8	0.5051
100	0.5079
120	0.5082

3.5.7 Effect of Adsorbent Dosage in the Remediation of Textile Dyes

The adsorption of the mixed reactive dye standard (concentration 120 mg L^{1}) was determined by accurately weighing the iron oxide/H_3PO_4-AC adsorbent namely, 0.5 g, 0.6 g, 0.7 g, 0.8 g, 1.0 g and 1.3 g separately, into 50.00 mL of the dye solution in separate conical flasks. The same procedure described in 3.5.4 was followed for agitation and centrifuge separation. The samples were filtered, filtrates were collected and analysed using the UV-visible spectrophotometer.

3.5.8 Desorption Studies

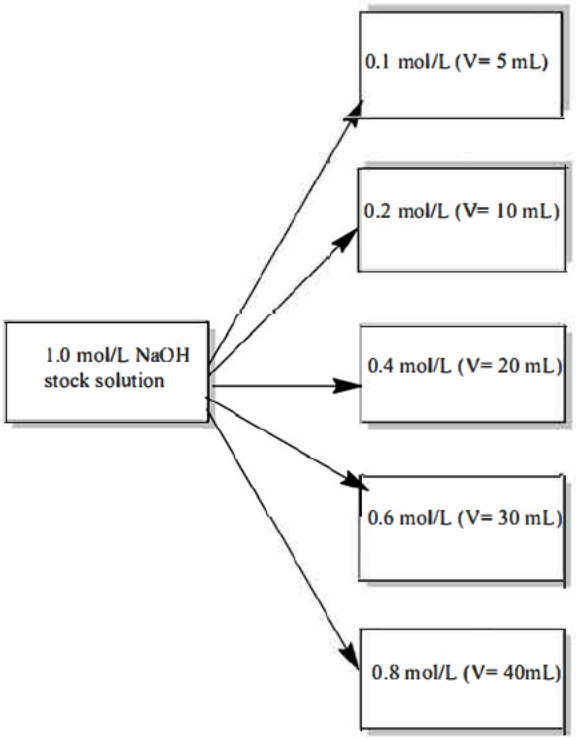

Figure 3.5 Preparation of NaOH working standards from stock solution

Table 3.7 Mass of adsorbents used for the desorption studies

Concentration of NaOH (mol L^{-1})	**Mass (g)**
0.1	0.5020
0.2	0.5005
0.4	0.5010
0.6	0.5013
0.8	0.5002
1.0	0.5023

Desorption and recovery studies were performed by saturating 0.5 g (accurate masses in Table 3.7) of H_3PO_4-AC with 40 mg L^{-1} of mixed dye standard for 2 hours, centrifuged for 30 minutes at 4000 rpm and then the supernatant was filtered. The activated carbon obtained after adsorption was dried overnight at room temperature and not in an oven to prevent burning of the dye particles onto the adsorbent. Sodium hydroxide was used as a desorbing agent for the removal of the dye particles

entrapped within the surface of the activated carbon. A 1 M NaOH stock solution was prepared using NaOH pellets, and by successive dilutions 0.1 M, 0.2 M, 0.4 M, 0.6 M, 0.8 M standard solutions was prepared as stipulated in Figure 3.5 (Appendix 17 shows the mass on NaOH used for stock solution preparation). The dried activated carbon was added to the six different salt standards (50 mL) of different concentration at room temperature for 15 minutes so that the dye particles can be removed from the surface of the adsorbent and go back into solution. The solutions were centrifuged, filtered and then analysed using the UV for the determination of the recovery.

The percentage recoveries were calculated using the following equation 3.3:

$\%\ \text{Regeneration} = \frac{\text{Cf}}{\text{Co}} \times 100$	3.3

3.6 References

Aksu, Z. and Tezer, S. 2005. Biosorption of reactive dyes on the green alga *Chlorella vulgaris*. *Process Biochemistry*, 40 (3): 1347-1361.

Annadurai, G., Juang, R.-S. and Lee, D.-J. 2002. Use of cellulose-based wastes for adsorption of dyes from aqueous solutions. *Journal of Hazardous Materials*, 92 (3): 263-274.

Babel, S. and Kurniawan, T. A. 2003. Low-cost adsorbents for heavy metals uptake from contaminated water: a review. *Journal of Hazardous Materials*, 97 (1): 219-243.

BV Consultants and HYDRAULICS, D. 2000. Absorption spectroscopy.Hydrology project module handbook.

Chiou, M.-S. and Li, H.-Y. 2002. Equilibrium and kinetic modeling of adsorption of reactive dye on cross-linked chitosan beads. *Journal of Hazardous Materials*, 93 (2): 233-248.

Chung, H.-K., Kim, W.-H., Park, J., Cho, J., Jeong, T.-Y. and Park, P.-K. 2015. Application of Langmuir and Freundlich isotherms to predict adsorbate removal efficiency or required amount of adsorbent. *Journal of Industrial and Engineering Chemistry*, 28: 241-246.

Crank, J. 1957. Diffusion with rapid irreversible immobilization. *Transactions of the Faraday Society*, 53: 1083-1091.

Crank, J. and Gupta, R. S. 1975. Isotherm migration method in two dimensions. *International Journal of Heat and Mass Transfer*, 18 (9): 1101-1107.

Dada, A., Olalekan, A., Olatunya, A. and Dada, O. 2012. Langmuir, Freundlich, Temkin and Dubinin–Radushkevich isotherms studies of equilibrium sorption of Zn2+ unto phosphoric acid modified rice husk. *IOSR Journal of Applied Chemistry*, 3 (1): 38-45.

Dubinin, M. M. and Stoeckli, H. F. 1980. Homogeneous and heterogeneous micropore structures in carbonaceous adsorbents. *Journal of Colloid and Interface Science*, 75 (1): 34-42.

El-Zawahry, M. M., Abdelghaffar, F., Abdelghaffar, R. A. and Hassabo, A. G. 2016. Equilibrium and kinetic models on the adsorption of Reactive Black 5 from aqueous solution using Eichhornia crassipes/chitosan composite. *Carbohydrate Polymers*, 136: 507-515.

Foo, K. Y. and Hameed, B. H. 2010. Insights into the modeling of adsorption isotherm systems. *Chemical Engineering Journal*, 156 (1): 2-10.

Freundlich, H. 1926. Colloid and capillary-Translated from the third German edition by H. *Stafford Hartfield. Methuen and Co, Ltd, London*,

Garg, V. K., Amita, M., Kumar, R. and Gupta, R. 2004. Basic dye (methylene blue) removal from simulated wastewater by adsorption using Indian Rosewood sawdust: a timber industry waste. *Dyes and Pigments*, 63 (3): 243-250.

Hameed, B. H., Ahmad, A. L. and Latiff, K. N. A. 2007. Adsorption of basic dye (methylene blue) onto activated carbon prepared from rattan sawdust. *Dyes and Pigments*, 75 (1): 143-149.

Ho, Y. S. and McKay, G. 1999. Pseudo-second order model for sorption processes. *Process Biochemistry*, 34 (5): 451-465.

Konduru R. Ramakrishna, T. V. 1997. Dye removal using low cost adsorbents. *Water Science & Technology*, 36 (2-3): 189-196.

Lagergren, S. 1898. About the theory of so-called adsorption of soluble substances. *Sven. Vetenskapsakad. Handingarl*, 24: 1-39.

Langmuir, I. 1916. The constitution and fundamental properties of solids and liquids. Part I. Solids. *Journal of the American Chemical Society*, 38 (11): 2221-2295.

Langmuir, I. 1918. The adsorption of gases on plane surfaces of glass, mica and platinum. *Journal of the American Chemical Society*, 40 (9): 1361-1403.

Oliveira, L. C. A., Rios, R. V. R. A., Fabris, J. D., Lago, R. M. and Sapag, K. 2004. Magnetic Particle Technology. A Simple Preparation of Magnetic Composites for the Adsorption of Water Contaminants. *Journal of Chemical Education*, 81 (2): 248.

Peter Adkins, J. D. P. 2006. *Physical Chemistry*. 8 ed. United States and Canada: W.H. Freeman and Company.

Ramesh, A., Lee, D. J. and Wong, J. W. C. 2005. Thermodynamic parameters for adsorption equilibrium of heavy metals and dyes from wastewater with low-cost adsorbents. *Journal of Colloid and Interface Science*, 291 (2): 588-592.

Rouquerol, J., Rouquerol, F., Llewellyn, P., Maurin, G. and Sing, K. S. 2013. *Adsorption by powders and porous solids: principles, methodology and applications*. Academic press.

Sabela, M. I., Kunene, K., Kanchi, S., Xhakaza, N. M., Bathinapatla, A., Mdluli, P., Sharma, D. and Bisetty, K. 2019. Removal of copper (II) from wastewater using green vegetable waste derived activated carbon: An approach to equilibrium and kinetic study. *Arabian Journal of Chemistry*,12 (8), 4331-4339.

Sen, T. K. 2011. Equilibrium, kinetics and mechanism of removal of methylene blue from aqueous solution by adsorption onto Pine cone biomass of *Pinus radiata*. *Water, Air, and Soil Pollution*, 218 (1-4): 499-515.

Simonin, J.-P. and Bouté, J. 2016. Intraparticle diffusion-adsorption model to describe liquid/solid adsorption kinetics. *Revista Mexicana de Ingeniería Química*, 15 (1): 161-173.

Singh, R. K., Kumar, S., Kumar, S. and Kumar, A. 2008. Development of parthenium based activated carbon and its utilization for adsorptive removal of p-cresol from aqueous solution. *Journal of Hazardous Materials*, 155 (3): 523-535.

Temkin, M. and Pyzhev, V. 1940. Recent modifications to Langmuir isotherms. *ACTA PHYSICO-CHIMICA SINICA 12,* 217-222.

Weber, W. J. and Morris, J. C. 1963. Kinetics of adsorption on carbon from solution. *Journal of the Sanitary Engineering Division*, 89 (2): 31-60.

CHAPTER FOUR: RESULTS AND DISCUSSION

PART A: Characterization of Activated Carbon and their Adsorption Studies

4.1 Characterization of Activated Carbon

4.1.1 Characterization of Phosphoric Acid Based Activated Carbon

The FTIR spectrum (Figure 4.1) of phosphoric acid based activated carbon (H_3PO_4-AC) shows the OH group as a disordered, strong, wide absorption band at 3500 – 3200 cm^{-1}. These bands are characteristic of cellulose precursor materials present on lignocellulose structures (Myglovets *et al.* 2014; Pereira *et al.* 2014). The irregular profile of this signal is due to the overlap of the -CH stretch of the aliphatic chains with OH groups. The P-OH stretching vibration are observed at frequency 2328 cm^{-1}. Weak bands resembling the overtones of the substituted aromatic structures is observed in the range of 2300 – 1900 cm^{-1}. The band observed at 1576 cm^{-1} represents the P=O stretch from the phosphate esters that shifted to higher frequencies due to the presence of the hydroxyl groups attached to phosphorus (Hampton, Demoin and Glaser 2010). The stretching vibration of the P-O-C group observed at 1118 cm^{-1} is due to the aromatic linkage or phosphate/poly phosphate to the P=OOH, and its bending occur at 472 cm^{-1} (Puziy *et al.* 2002; Myglovets *et al.* 2014; Eisa, Dabbas and Abdulla 2015). The strong, broad signal at 944 cm^{-1} represents the stretching of the P-O-C groups of the aliphatic chain (Corbrjdge 1956; Bellamy 1964; Socrates 1994) or asymmetric stretch from the aromatic structures (Socrates 1994), stretching in -P=OOH (Socrates 1994), P-OH bending (Corbrjdge 1956), asymmetric stretch of the P-O-P in polyphosphates (Bellamy 1964; Socrates 1994), and symmetric stretch of the P=O in phosphate carbon-complexes (Bourbigot *et al.* 1995). This absorption band is the characteristic band of phosphorus-activated carbon materials (Myglovets *et al.* 2014; Eisa, Dabbas and Abdulla 2015).

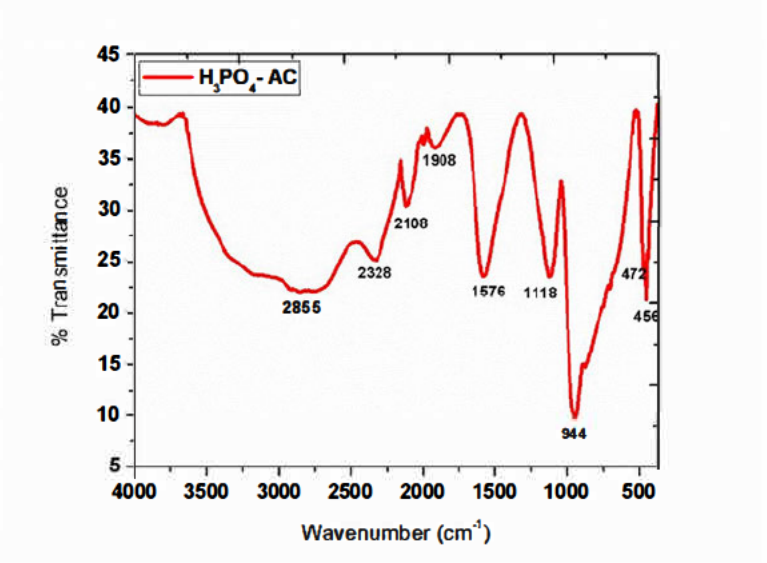

Figure 4.1 The FTIR spectrum of phosphoric acid based activated carbon

The thermal stability of H_3PO_4-AC was determined by TGA at temperatures up to 1000 ºC scanned at a rate of 10ºC/min. The TGA curve (Figure 4.2) depicts a 4-step degradation process. Below 100ºC, a sharp weight loss of about 19% accompanied by a gradual 4.5% mass loss is observed: this is due to the evaporation of water (Xu *et al.* 2014). From 200ºC to 800ºC, there is a mass loss of 28%. From 200ºC to 400ºC there is usually pyrolysis of organic matter and the dehydration of phosphoric acid (Suárez-García, Martínez-Alonso and Tascón 2004; Nahil and Williams 2012). Moreover, phosphoric acid is also known to convert to poly-condensed form such as pyrosphosphoric acid and metasphophoric acid. Above 700ºC, a mass loss of about 25% is attributed to the possible reaction of phosphoric acid on the surface of the precursor material thereby possibly breaking the bonds of structures such as hemicellulose, lignin and cellulose thereby generating pores. The formation of phosphorus complexes such as phosphates (P=O) and polyphosphates (P-O-P) bridges following the dehydration of phosphoric acid during thermal activation (Nahil and Williams 2012; Xu *et al.* 2014) is possible. On the DSC curve between 100ºC to 200ºC, the evaporation of the OH^- ions is noted. The endothermic peak depicts heat flow onto the material. This confirms the phase change or conversion of phosphoric acid and its derivatives.

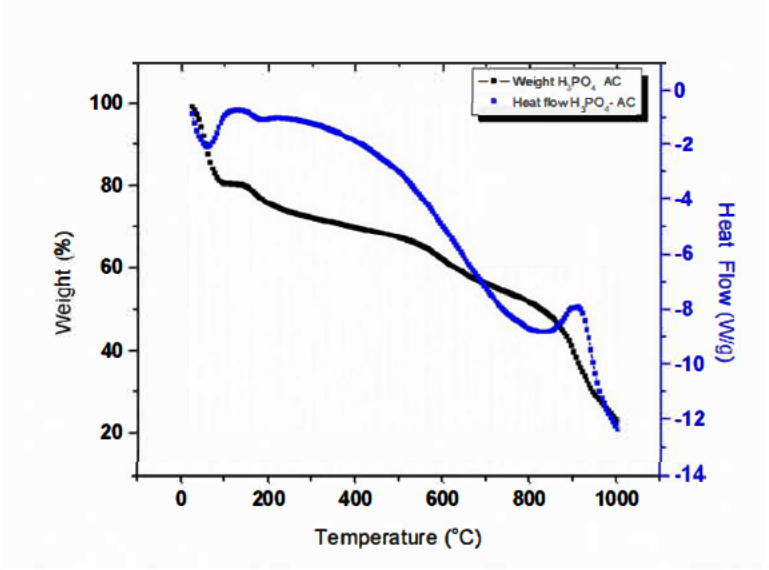

Figure 4.2 TGA/DSC curve of phosphoric acid based activated carbon

The SEM micrographs (Figure 4.3) show the surface morphology of the H_3PO_4-AC adsorbent. Figure 4.3 (a) at 42X magnification shows rough, irregular shapes of particles. They are diverse in structure consisting of various sizes and cavities. In Figure 4.3 (b), agglomeration of the particles that are uniform, well distributed and smooth in texture are noted at 40 000X magnification. This is due to carbonization and activation with phosphoric acid. It is reported that when phosphoric acid, introduced during chemical activation, is evaporated at elevated temperatures as a result of carbonization, it leaves spaces or pores in-between the surface structure of the adsorbent (Deng *et al.* 2010).

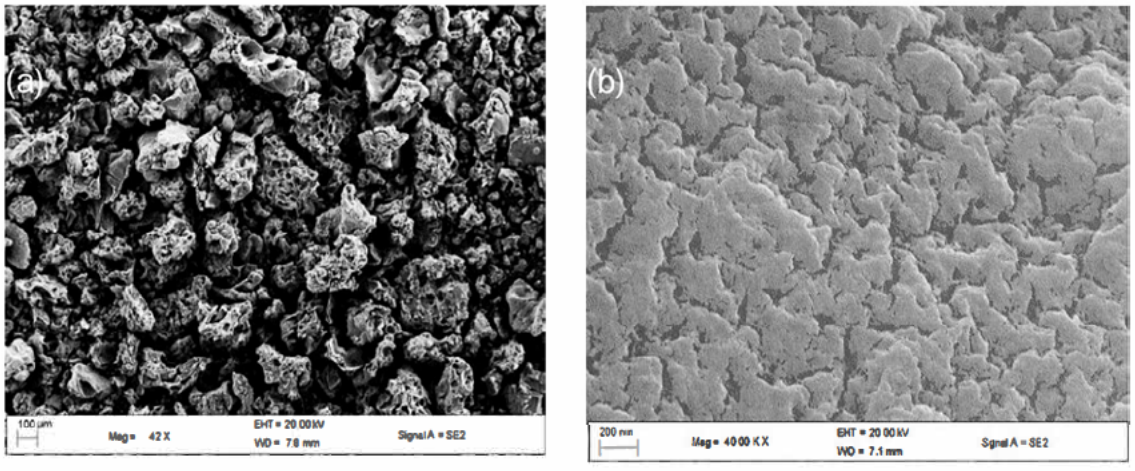

Figure 4.3 SEM images of phosphoric based activated carbon at (a) 42X (b) 40 000X

The EDX spectrum (Figure 4.4 a-b) shows all the major elements present on the activated carbon material. Figure 4.4 (a) shows the quantity of carbon and oxygen as 49.75% and 37.62%, respectively. These important elements stated above, when at high concentrations, facilitates adsorption on carbonaceous materials with these functional groups. 9.28% of phosphorus is due to modification with H_3PO_4 used during sample activation. Traces of Al, Ta and Ir are observed which are possibly the traces of elements present in the plant.

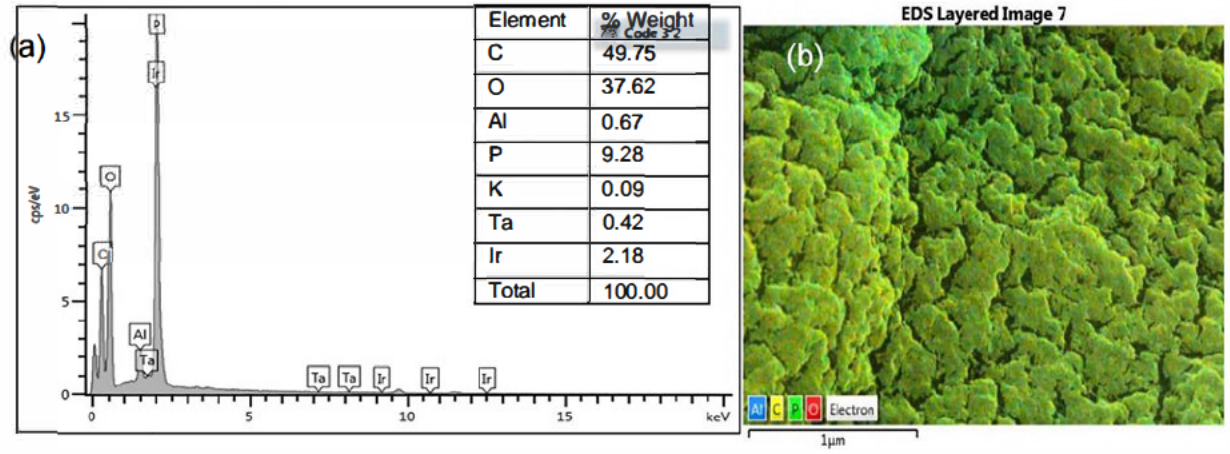

Figure 4.4 Phosphoric acid based activated carbon (a) EDX spectrum (b) EDX mapping for the distribution of elements

TEM micrograms were used to examine the structural crystallinity of H_3PO_4-AC material. Figure 4.5 (a) shows disordered and layered carbon structures whereas the HRTEM (Figure 4.5 b) shows the particles are closely bonded to each other suggestive of crystallinity in the structure of the activated carbon.

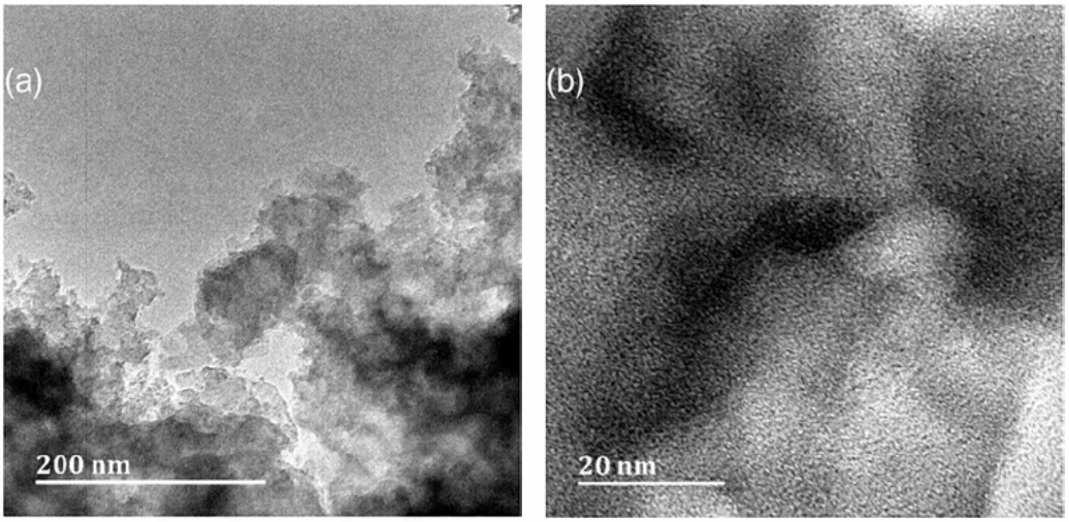

Figure 4.5 Micrograms of phosphoric acid based activated carbon (a) TEM (b)HRTEM

4.1.2 Characterization of Potassium Hydroxide Based Activated Carbon

The FTIR spectrum (Figure 4.6) of potassium hydroxide based activated carbon (KOH-AC) shows a broad absorption at 3208 cm^{-1} which is attributed to the O-H stretch. The band at 2912 cm^{-1} is due to the stretching of -CH, $-CH_2$ and CH_3 (Demiral and Demiral 2008). The C=C stretch, suggesting the presence of aromatics, is observed around 1555 cm^{-1}. The absorption band around 1377 cm^{-1} corresponds to the C-O and K-O-C stretch (Demiral and Demiral 2008; Foo and Hameed 2011). The band at 1056 cm^{-1} is probably due to the Ca-O bond from the precursor material. The vibrations between 866 cm^{-1} to 559 cm^{-1} are associated with K-O, K-C bonds, C-H in plane bends of the aromatic derivatives and -OH bending vibrations (Foo and Hameed 2011).

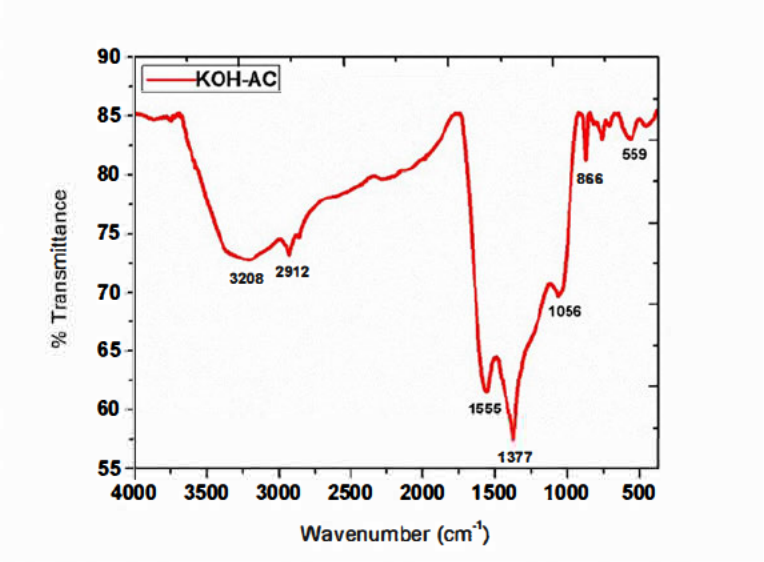

Figure 4.6 FTIR spectrum of potassium hydroxide based activated carbon

The TGA/DSC thermogram (Figure 4.7) shows a 3-step degradation of KOH-AC from 20ºC up to 1000ºC. A sharp mass loss of approximately 8% occurs at 110ºC which is due to the escape of water molecules from the surface of the activated carbon. Below 200ºC, bound water evaporates, and this is in agreement with the OH group in the FT-IR (Figure 4.6). A gradual mass loss of 10.5% is probably due to the pyrolysis of hydrocarbons and any other organic volatiles. A further decomposition of about 15.0%, occurring between 800ºC to 1000ºC, is due to degradation of potassium oxide. The downward peak of the DSC graph suggests that heat flow occurs into the sample

(endothermic reaction) confirming the mass loss was because of breakage of the crystalline structure of the carbon, and vaporization at the initial step.

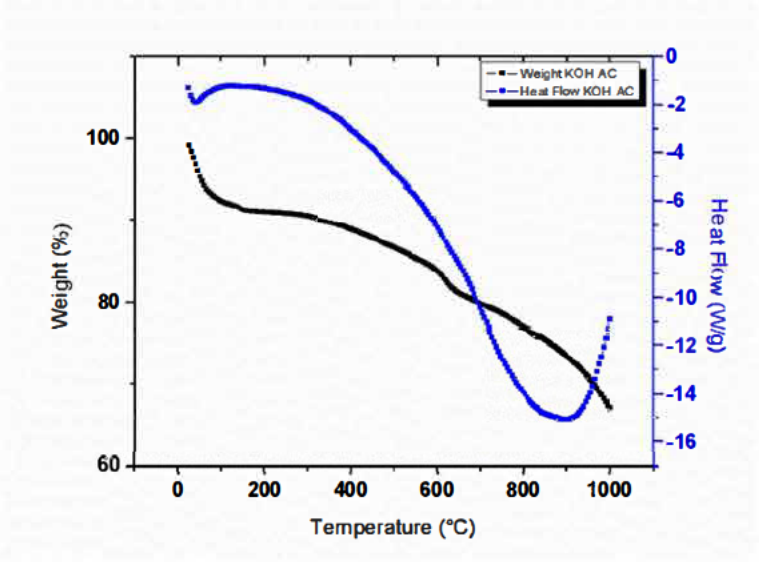

Figure 4.7 TGA/DSC thermogram of potassium hydroxide based activated carbon

The SEM image is presented in Figure 4.8. The profile shows clear distinct pores of various sizes. During the activation process with KOH, the organic volatile matter escapes from the precursor material resulting in pores, thus oxidation between KOH and carbon occurs, as predicted by this reaction:

$$6KOH + 2C \leftrightarrow 2K + 3H_2 + 2K_2CO_3 \qquad 4.1$$

(Gañan et al. 2004; Fiuza *et al.* 2015). Metallic potassium then intercalates in-between the produced carbon layers, creating spaces for adsorption (Chandra *et al.* 2009). This is observed in Figure 4.8 (b) as inhomogeneous white, small, shiny beads/particles The EDX spectrum (Figure 4.8 (c)) indicates 38.09% carbon and 11.28% oxygen, which are sufficient for adsorption. The 25.43% of potassium is attributed to the modifying agent. Calcium (18.64%), zirconium (2.95%), chlorine (1.85) and antimony (1.76%) are also present and occur naturally in most lignocellulose material and soil. The possible reactions that occur (González-García 2018) are:

$$2\,KOH \rightarrow K_2O + H_2O \qquad 4.2$$

$$C + H_2O \rightarrow H_2 + CO \quad 4.3$$

$$CO + H_2O \rightarrow H_2 + CO_2 \quad 4.4$$

$$K_2O + CO_2 \rightarrow K_2CO_3 \quad 4.5$$

$$K_2O + H_2 \rightarrow 2K + H_2O \quad 4.6$$

$$K_2O + C \rightarrow 2K + CO \quad 4.7$$

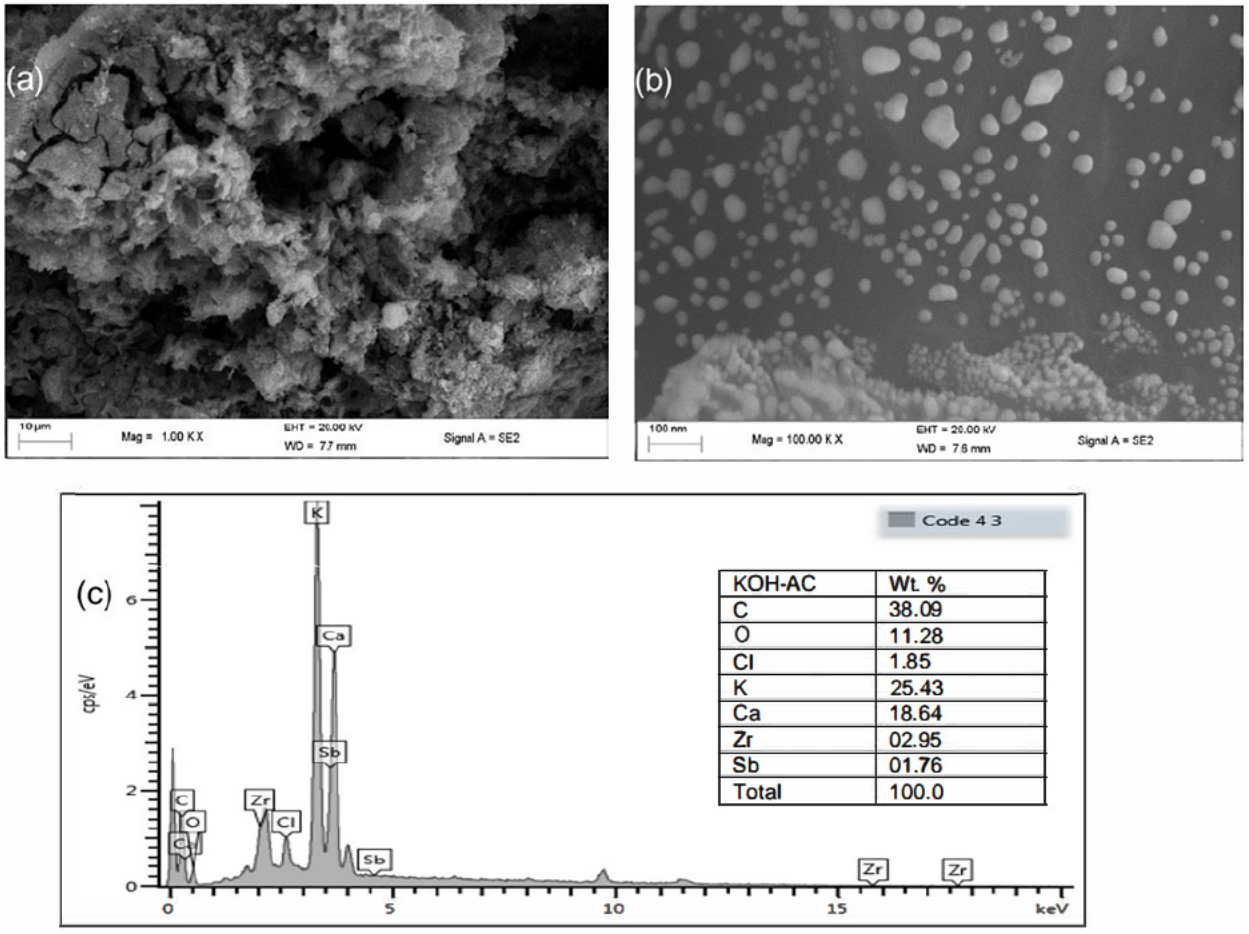

Figure 4.8 Potassium hydroxide based activated carbon (a) SEM image at 1000 magnification (b) SEM image at 10 000 magnification (c) EDS mapping spectrum

The TEM and HRTEM is presented in Figure 4.9. In Figure 4.9 (a) carbon nanofibers (CNFs) are noted. The crystal lattice atomic structural arrangement of the CNFs is also clearly visible at closer magnifications (Figure 4.9 (b)) providing stacked carbon sheets.

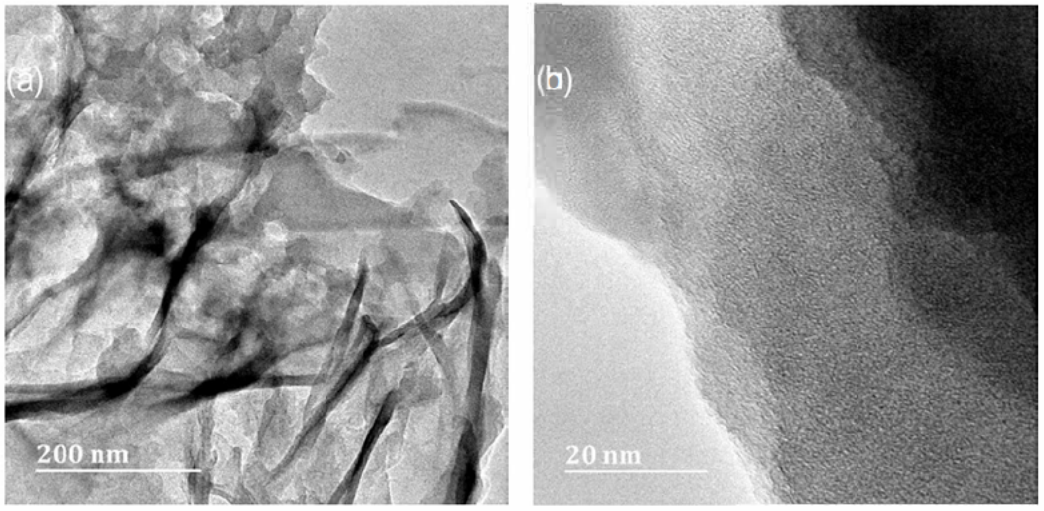

Figure 4.9 Potassium hydroxide based activated carbon micro images (a) TEM, and (b) HRTEM

4.1.3 Characterization of Sulfuric Acid Based Activated Carbon

The FTIR spectrum of sulphuric acid based activated carbon (H_2SO_4-AC) is presented in Figure 4.10. It shows absorption at 3212 cm^{-1} and 2925 cm^{-1} corresponding to the O-H and -S-O-H stretch, respectively. The absorption at 1701 cm^{-1} and 1609 cm^{-1} corresponds to the C=O and C=C stretch, respectively. The C-O stretch is at 1191 cm^{-1} while the C-O bend is at 610 cm^{-1} (Hampton *et. al* 1993).

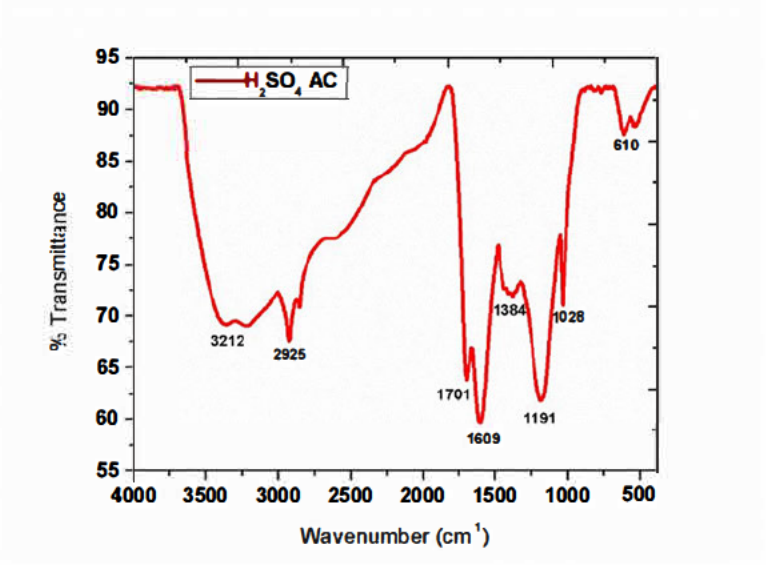

Figure 4.10 FTIR spectrum of sulfuric acid based activated carbon

The TGA/DSC profile for H_2SO_4-AC (Figure 4.11) shows a 3-step mass loss. The initial mass loss of 10.4% is due to loss of moisture and other organic volatiles. The 32.7% mass loss from 100ºC – 750ºC corresponds to the decomposition of hydrocarbons and sulfur. Above the temperature of 800ºC, a steady mass loss of 2.72% is observed which is possibly due to combustion. The DSC thermogram has two downward peaks due to vaporization and decomposition suggesting an endothermic character of the activated carbon.

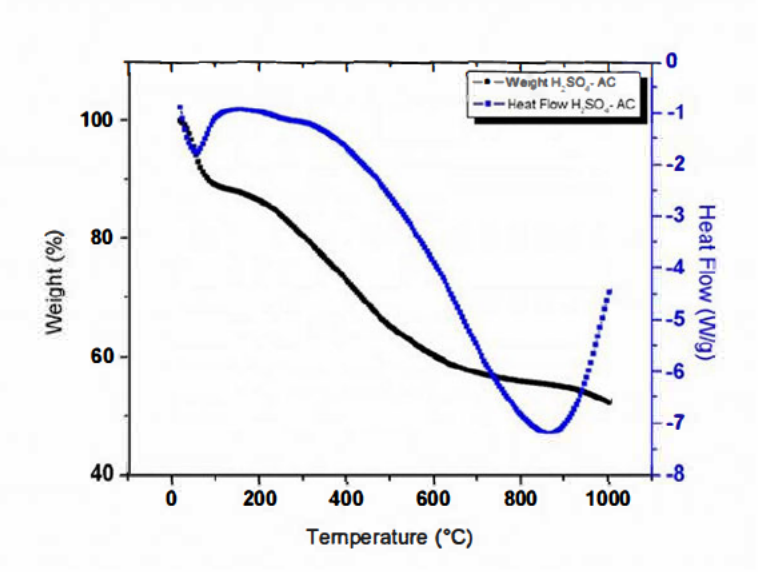

Figure 4.11 TGA/DSC thermogram of sulfuric acid based activated carbon

The SEM image in Figure 4.12 (a) at 100X shows particles of various sizes and shapes, rough in texture and containing cavities on the surface. At 20 000X (Figure 4.12 (b)) the precursor fibres are shown to break to form a mesoporous structure suitable for adsorption. The EDX spectrum (Figure 4.12 (c)) shows 84.02% carbon while oxygen is 13.69%. In addition, sulfur of 1.64% is observed with traces of copper and rubidium at amounts of 0.42% and 0.23%, respectively. The most probable reaction that could occur is:

$$C + 2H_2SO_4 \rightarrow CO_2 + 2SO_2 + 2H_2O \qquad 4.8$$

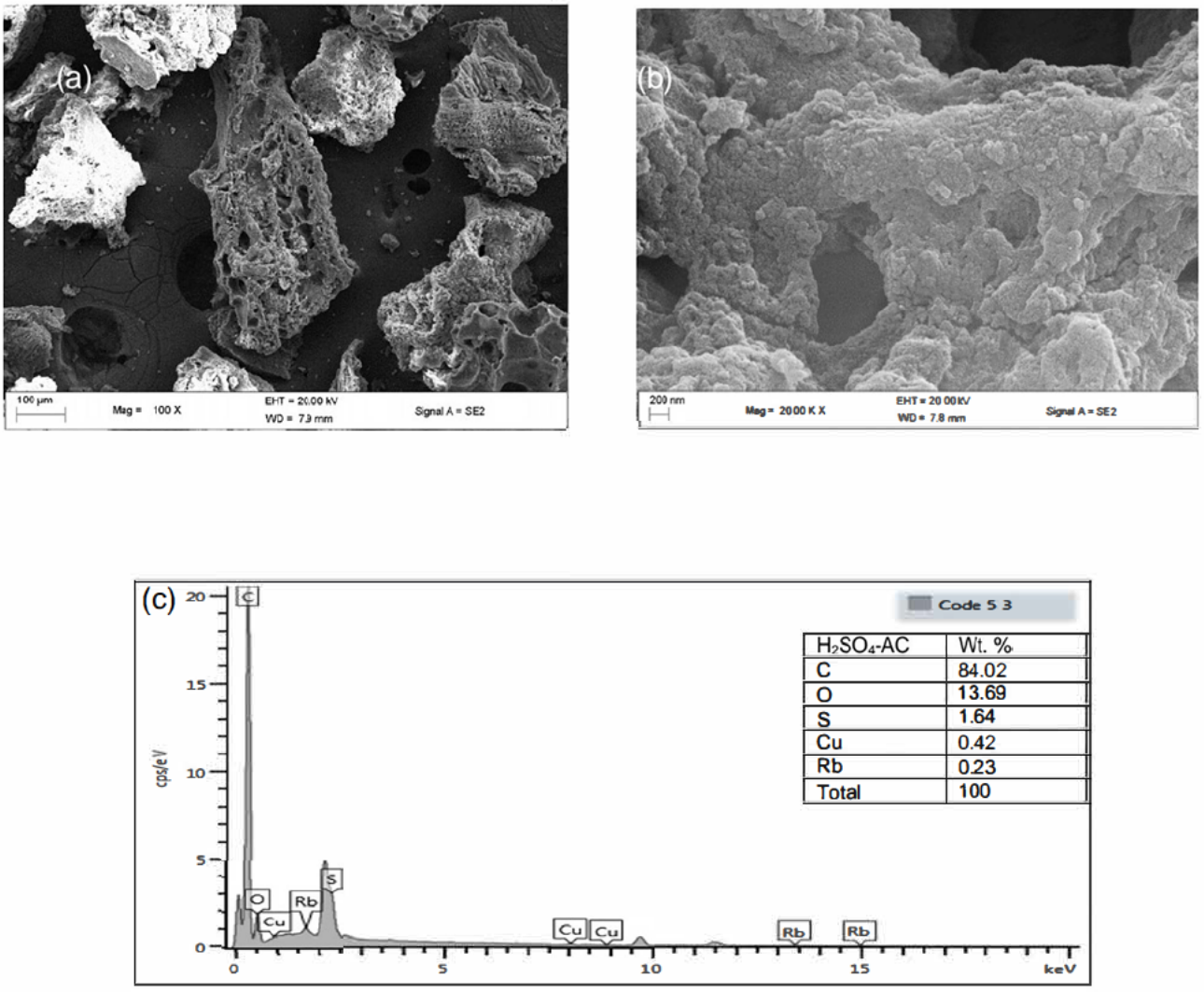

Figure 4.12 SEM images of sulfuric acid based activated carbon at (a) 100X, (b) 2000X, and (c) EDX spectrum

The light microscope was used to determine the inner structure of the H_2SO_4-AC at high and low magnification from high-resolution images shown in Figure 4.13 (a) and (b), respectively. The TEM images show a distinct outer shell of the particle containing the black nanostructured particles on the inside, whilst the HRTEM shows a layered crystalline structure of the activated carbon.

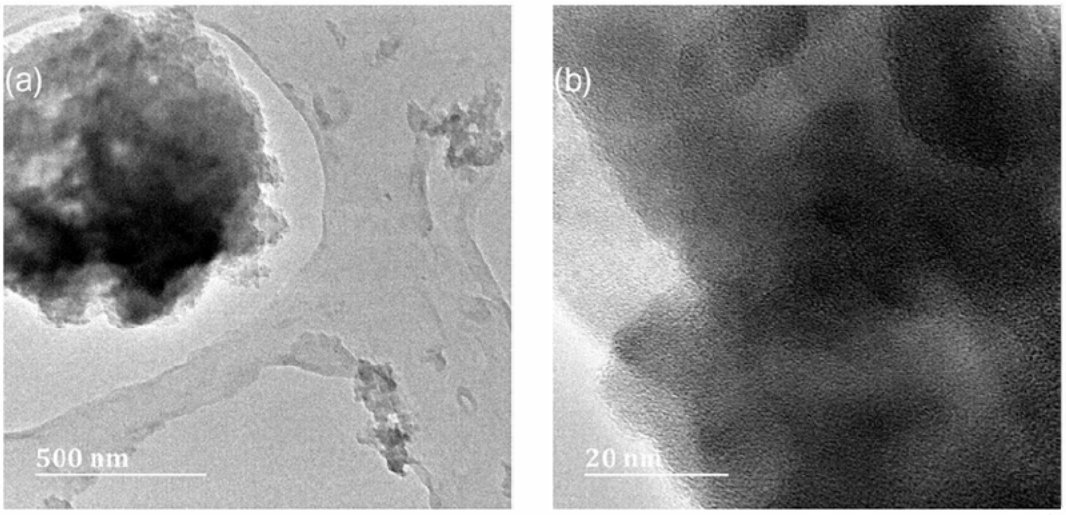

Figure 4.13 TEM micrograph of sulfuric acid activated carbon, and (b) HRTEM micrograph

4.1.4 Characterization of Sodium Hydroxide Based Activated Carbon

The FTIR spectrum sodium hydroxide based activated carbon (NaOH-AC) is presented in Figure 4.14. The O-H stretch is observed at 3337 cm^{-1}, while the C= O stretch and lactone is at 1760 cm^{1} and 1430 cm^{1}, respectively. The absorption at 1414 and 1008 cm^{-1} is the O-H bend. These bands suggest the presence of a carboxylic group from the precursor within the porous material that was an indication that these groups were not completely modified by NaOH. This has also been reported previously by Shim (Shim, Park and Ryu 2001).

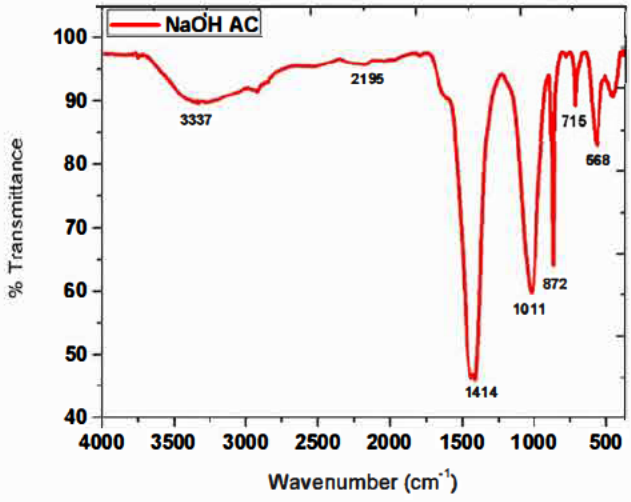

Figure 4.14 FTIR spectrum of sodium hydroxide based activated carbon

Figure 4.15 shows the TGA/DSC thermogram of activated carbon treated with 10% NaOH alkali is a two-step decomposition curve. A loss of 5.4% is seen on the initial step and is attributed to water molecules and organic volatiles. The major decomposition of 40.8% is due to pyrolysis of the carbon which occurs at 100ºC – 1000ºC The endothermic nature of this activated carbon is observed as the phase change occurs in the heat flow thermogram.

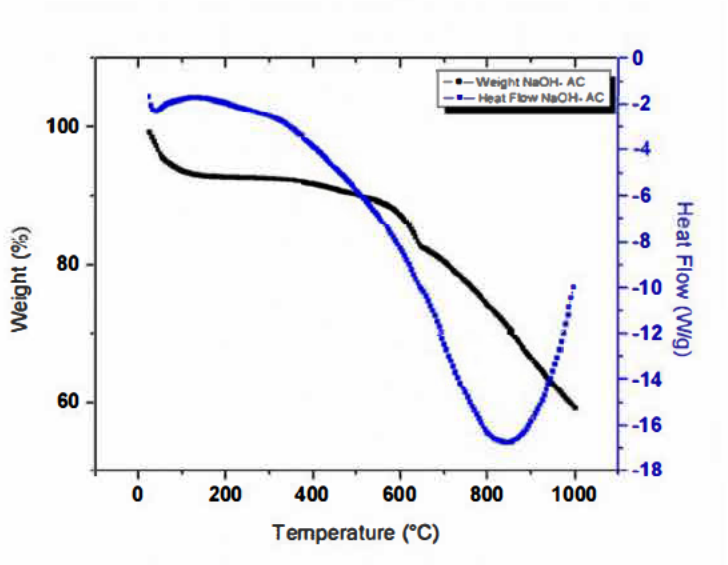

Figure 4.15 TGA/DSC thermogram of sodium hydroxide based activated carbon

In the SEM analysis for NaOH-AC (Figure 4.16 (a)), heterogeneous particles of different irregular shapes and sizes are visible. Cavities, which are vital for surface adsorption, are observed. The agglomeration of particles at 30KX magnification is observed as white shiny particles in Figure 4.15 (b). The EDX mapping of elements (Figure 4.15 (c) and (d)) shows 97.30% carbon, 1.80% sodium, 0.25% silicon, 0.13% sulfur, 0.20% chlorine, 0.24% potassium and 0.07% calcium. These values are in agreement with the FTIR spectrum of NaOH-AC confirming that not all the lignocellulose is broken down and neutralized by the acid. All though the carbon content is very good, however having no functional groups such as oxygen and hydrogen content hinders the adsorption capacity of the material.

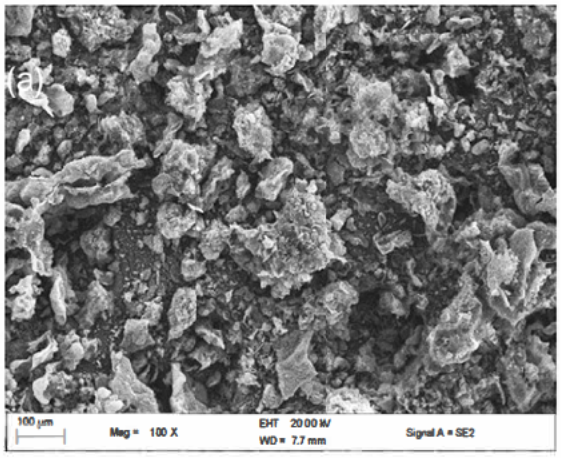

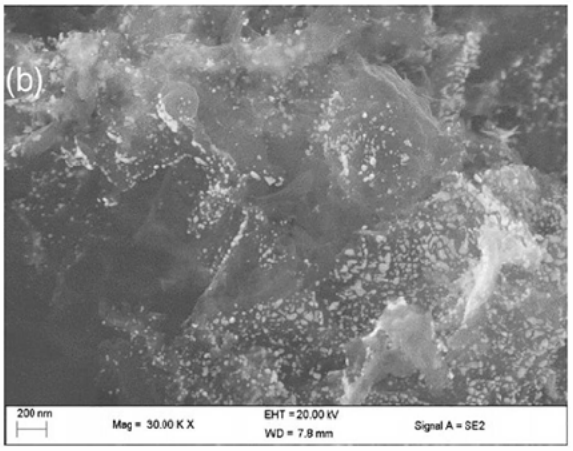

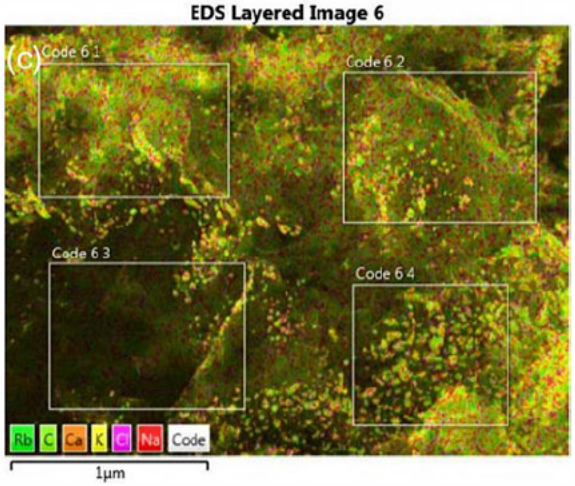

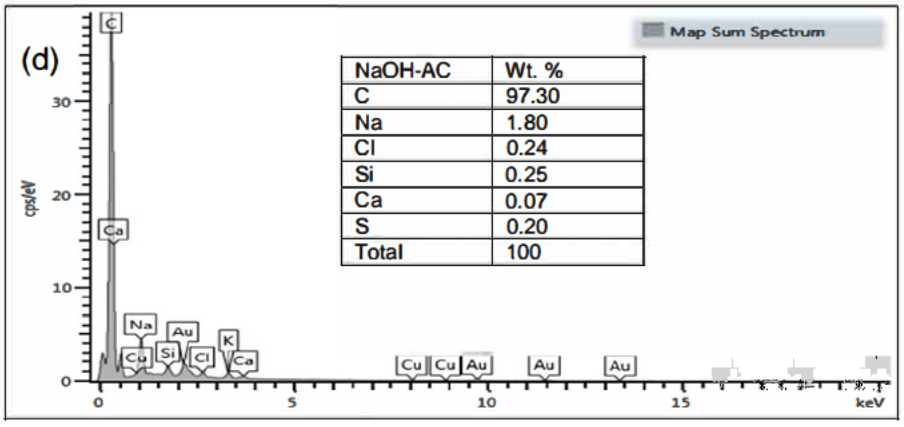

NaOH-AC	Wt. %
C	97.30
Na	1.80
Cl	0.24
Si	0.25
Ca	0.07
S	0.20
Total	100

Figure 4.16 Sodium hydroxide based activated carbon (a) 1000X, (b) 30 000X, (c) EDX layered map of the elements, and (d) EDX spectrum

The TEM image (Figure 4.17 (a)), shows the shape of the capsulated carbon, which resembles the nanotube structure that is seen as black rods. Figure 4.17 (b) shows a closely packed structure of the carbon while Figure 4.17 (c) indicates the presence and scattering of granular nanostructures observed on the electron dark field image.

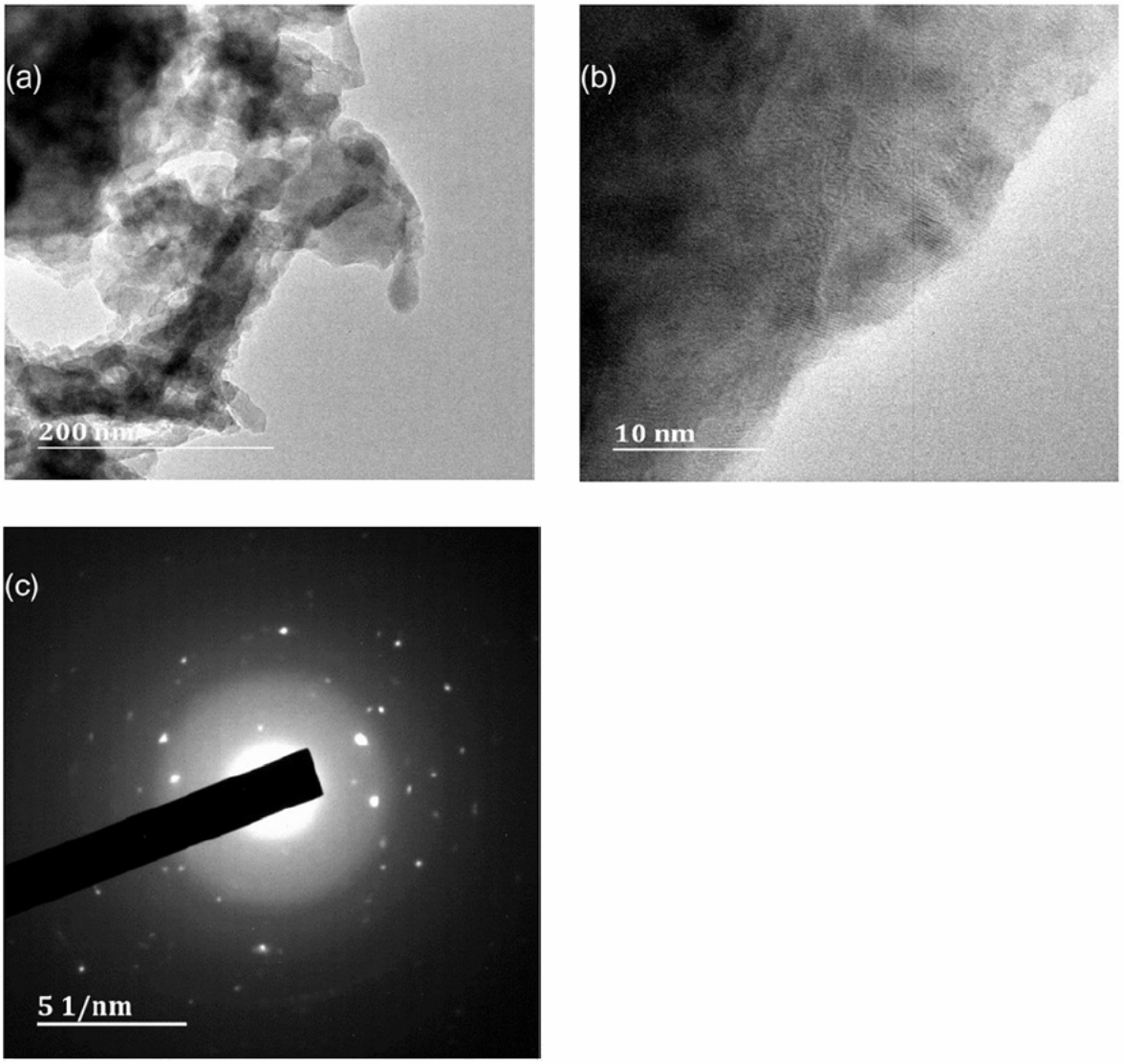

Figure 4.17 Light microscopy of sodium hydroxide based activated carbon (a) TEM, (b) HRTEM, (c) microscopic dark field

4.2 Calibration of the Mixed Dye Standards

The calibration curves were the tool that was used to determine the maximum wavelength, and the exact concentration for each dye. The concentration of the different dye standards was plotted against the absorbance values. This information was also used in the adsorption and desorption studies for the determination of the concentration of the dye that was not adsorbed. The limit of detection and limit of quantification were calculated using equation 4.9 and 4.10, respectively.

$$LOD = 3\ (S_{\frac{y}{x}}) \qquad 4.9$$

$$LOQ = 10\ (S_{\frac{y}{x}}) \qquad 4.10$$

LOD (limit of detection), *S* is the standard error, *x* and *y* represents the values of each axis in the graphs.

Table 4.1 Absorbance values for the textile reactive dyes at different concentrations

Concentration (mg L^{-1})	**Absorbance**		
	Reactive Blue 222	**Reactive Red 195**	**Reactive Yellow 145**
20	0.276	0.324	0.286
40	0.514	0.634	0.584
60	0.743	0.956	0.859
80	0.971	1.304	1.133
100	1.204	1.525	1.410
120	1.438	1.946	1.716
R^2 value	1.0000	0.9997	0.9962
gradient	0.0116	0.0159	0.0116
Sy/x	0.5497	0.58770	0.8379
LOD	1.6491	1.7631	2.5137
LOQ	5.4969	5.8770	8.3792

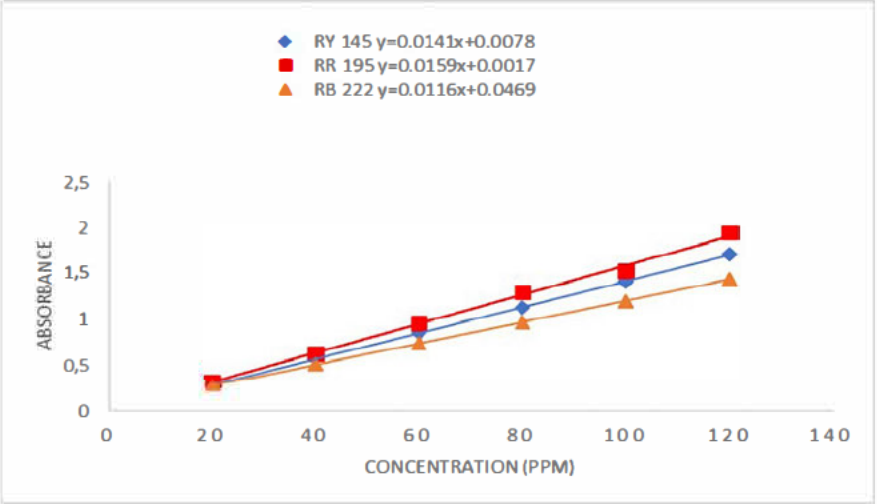

Figure 4.18 Calibration curves for the dyes

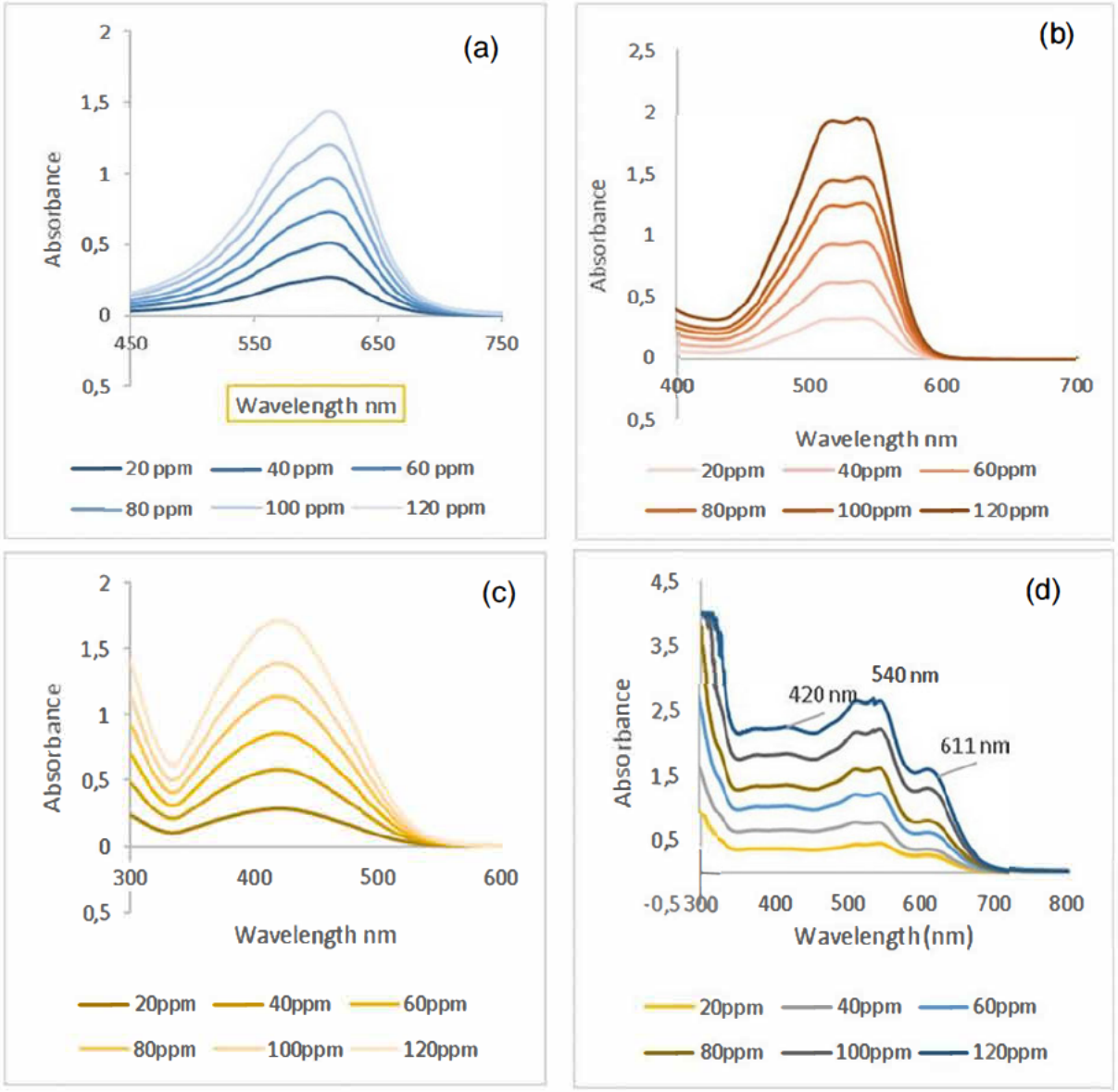

Figure 4.19 UV Spectra of (a) Reactive Blue 222, (b) Reactive Red 195, (c) Reactive Yellow 145, and (d) mixture of dye standards

4.3 Adsorption Studies

Four different adsorbents (H_3PO_4-AC, KOH-AC, H_2SO_4-AC, and NaOH-AC) were prepared from *Plantago Lanceolate* and their potential to remove a mixture of reactive blue 222, reactive red 195 and reactive yellow 145 dyes was investigated against different parameters. The adsorbent with the highest capacity was used to examine the effect of initial concentration, pH, equilibrium, thermodynamics and the kinetics of the reaction.

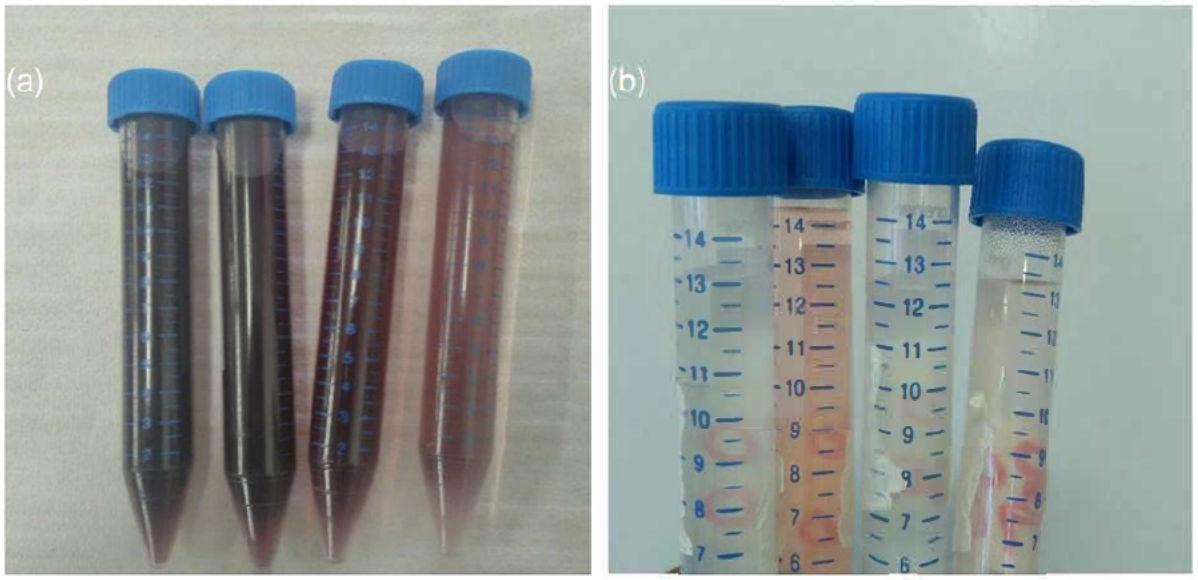

Figure 4.20 Ternary mixture of textile azo dye standards (a) before adsorption, and (b) after adsorption

4.3.1 Comparison of Different Activated Carbons and their Effect on Textile Dye Removal

Modification plays a critical role in the activation of carbonaceous material for the enhancement of adsorption capacity. Carbon can be activated physically by heat. The precursor can be activated in the presence of oxygen, steam, carbon dioxide and nitrogen. Chemical activation includes modifying the substrate with acids, bases or oxidising agents such as H_3PO_4, H_2SO_4, KOH, NaOH, $ZnCl_2$, and Na_2CO_3 (Chen and Wu 2004; Anjum and Murugesan 2016). Modification promotes the necessary

physicochemical properties required for adsorption such as surface area and porosity (Chen and Wu 2004).

The percentage adsorption of the ternary mixture of azo dyes was found to be the highest from 98.98% - 100% (RB), 91.78% -100% (RR), 91.96% - 99.65% for H_3PO_4-AC (Figure 4.21(a)). The KOH-AC resulted in 66.69% – 85.51% (RB), 24.31% - 49.69% (RR), and 26.44% - 48.63% (RY) (Figure 4.21 (b)). For H_2SO_4-AC presented in Figure 4.21 (c), 85.88% - 99.28% (RB), 39.21% - 91.78% (RR), 51.40% - 94.06% (RY), whereas for NaOH-AC (Figure 4.21 (d)) showed 53.55% - 85.14% (RB), 17.16% - 47.22% (RR) and 16.26% - 66.78%. H_3PO_4-AC showed tremendous adsorption capacity when compared to the other prepared activated carbons. This was due to phosphoric acid decomposing the plant material, thus creating an increased surface area-volume-ratio by forming a cross-linked structure, which enhanced porosity as previously reported (Pereira *et al.* 2014) and observed in Figure 4.3 (c). Modification increases the required functional groups whereas oxygen, nitrogen, hydrogen and phosphorus are vital elements that increase adsorption capacity (Lee, Daud and Lee 2010) as illustrated in Figure 4.1 and 4.4 (a). H_2SO_4-AC also showed a clear porous structure (Figure 4.12 (a)). However, it has been reported that activation with H_2SO_4 at temperatures < 100ºC increases the surfaces area but not necessarily the porosity of the carbon as the surface contains fewer oxygen heteroatoms (Jiang *et al.* 2003). This was observed in Figure 4.12 (c) with O_2 13.69% whereas H_3PO_4-AC has 40.52% of oxygen (Figure 4.4 (a)). The removal capacity of KOH-AC and NaOH-AC was slightly different; however, both were low when compared to the acid modified carbon (Figure 4.22). Moreover, this trend has been observed previously as KOH and NaOH treatments resulted in a lower carbon surface area and pore volume when compared to carbon treated with H_3PO_4 and H_2SO_4 (Chen *et al.* 2011). This is possibly due to the presence of the dominant precursor functional groups (Figure 4.14) therefore; structural porosity decreases and hence so does adsorption.

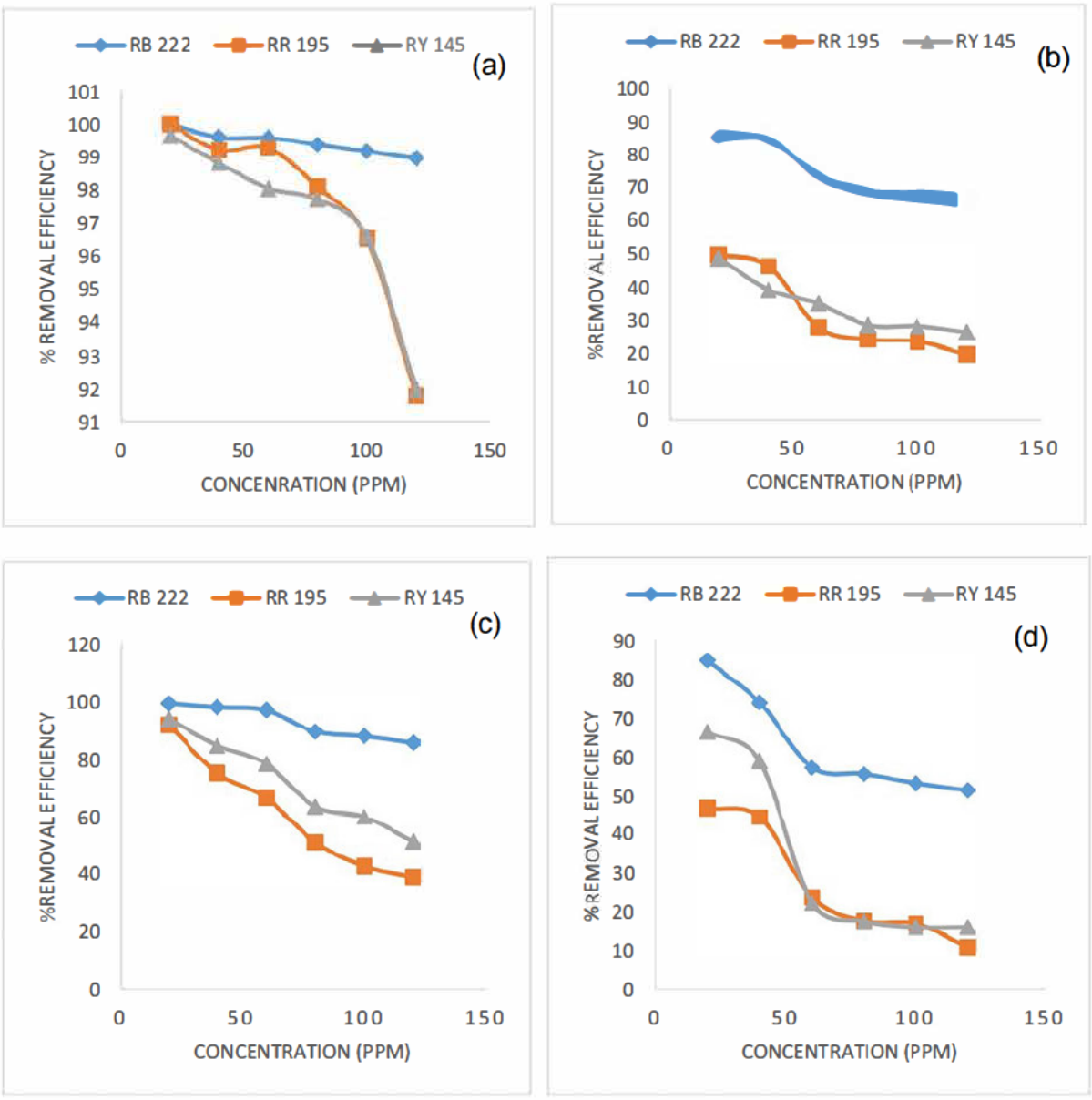

Figure 4.21 The effect of different modifying agents: (a) H_3PO_4, (b) KOH, (c) H_2SO_4, and (d) NaOH (adsorbent = 0.5 g, volume = 30 mL, time =30 min)

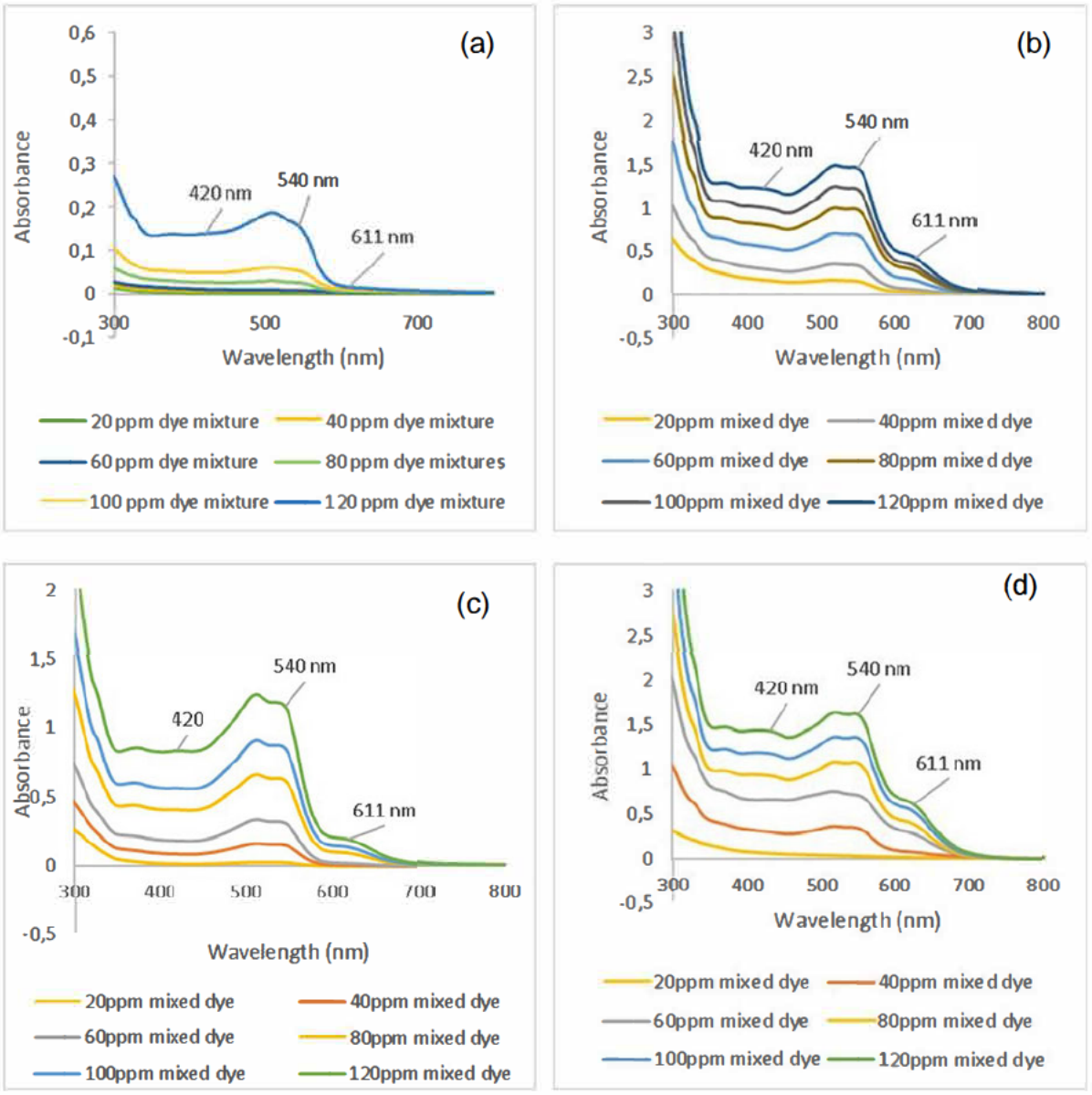

Figure 4.22 UV profiles illustrating absorbance values for the different activated carbons: (a) H_3PO_4-AC, (b) KOH-AC, (c) H_2SO_4-AC, and (d) NaOH-AC

4.3.2 Effect of Initial Dye Concentration and Adsorbent Contact Time on Textile Dye Removal

The rate of dye adsorption was found to be dependent on the initial dye concentration. This relationship is due to the interaction between the vacant sites on the adsorbent and the adsorbate. The effect of initial dye concentration was determined by examining the three reactive dyes at different concentrations (20 mg L^{-1}, 40 mg L^{-1}, 60 mg L^{-1}, 80 mg L^{-1}, 100 mg L^{-1} and 120 mg L^{-1}) at time intervals ranging from 10 minutes up to 90 minutes. The adsorbent dosage was fixed to 0.5 g/50 mL per reaction flask at room temperature. The percentage adsorption for reactive blue 222 was 73.57% - 99.64%,

reactive red 195 was 43.68% - 99.07% and reactive yellow 145 was 40.97% - 98.11% for all the dye concentrations examined. The optimum time for dye removal for all the concentrations was 70 minutes. The removal percentages of the dye solutions decreased with an increase in dye concentration and contact time as shown in Figures 4.23 (a), (c) and (e). This was due to the available number of active sites for adsorption on the surface of the adsorbent decreasing as the dye molecules began saturating these sites, which is suggestive of the monolayer coverage by the dyes. Figures 4.23 (b), (d) and (f) illustrate the adsorption capacity of the activated carbon per unit mass of adsorbate, which increases with time, and with the increase in initial dye concentration. This is the result of a high driving force for mass transfer at higher concentrations (Yagub *et al*. 2014).

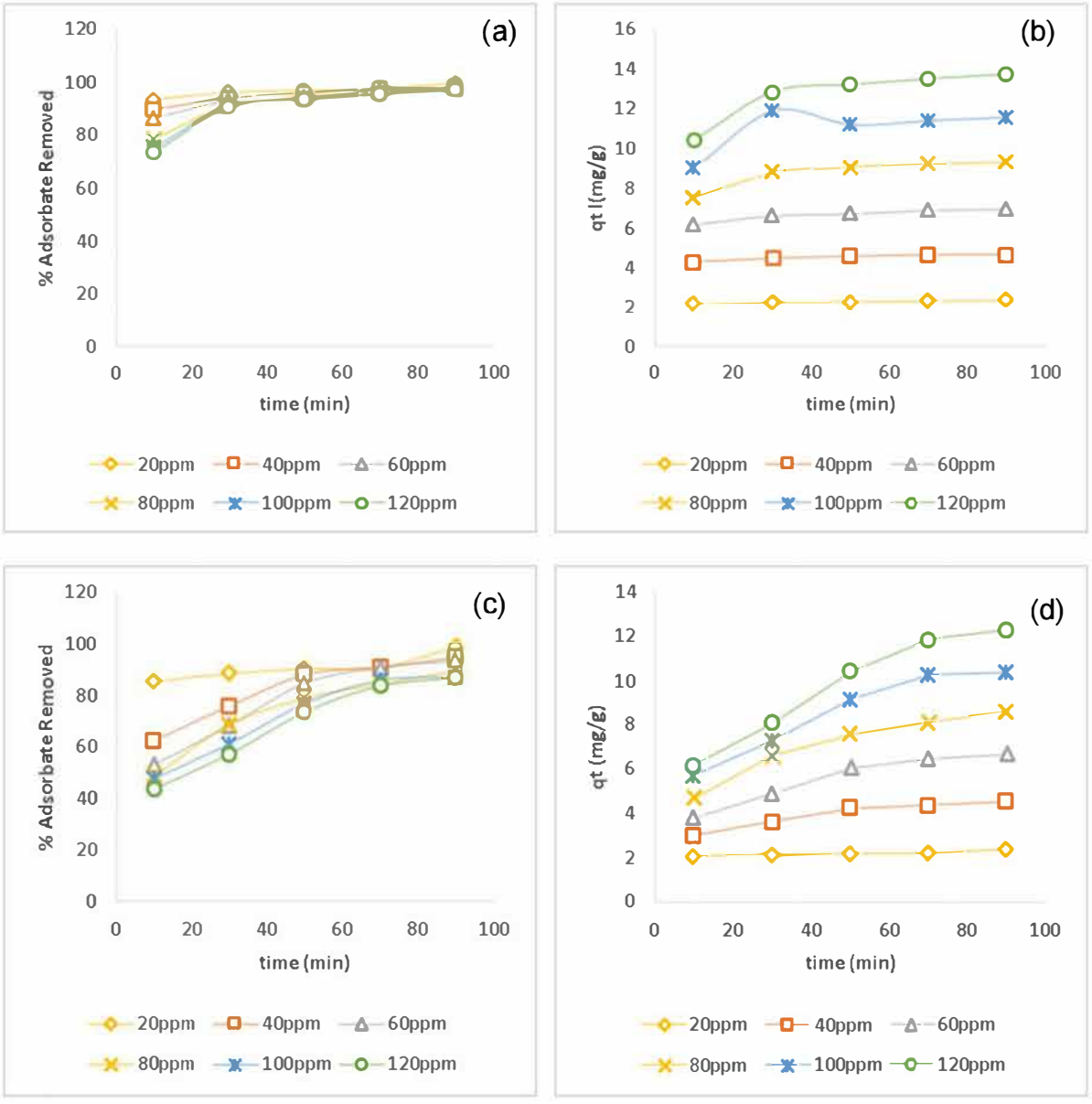

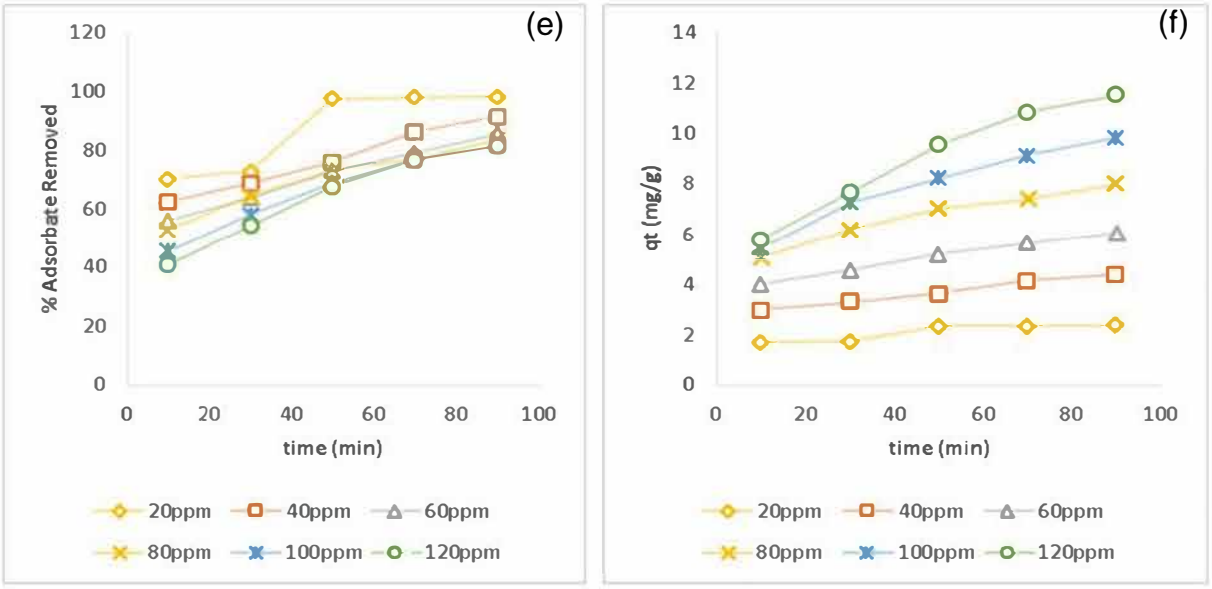

Figure 4.23 Effect of initial dye concentration (a) % dye removed (RB), quantity of dye removed (RB), (c) % dye removed (RR), (d) quantity of dye removed (RR), (e) % dye removed (RY), and (f) quantity of dye removed (RY) at pH=6.1, adsorbent dosage=0.5 g, volume=50 mL

4.3.3 Effect of pH on Textile Dye Removal

The effect of acidity and basicity on the dye medium and its electrostatic interactions with regards to activated carbon was determined. The effect of changes in pH has also been among the role key factors that affect adsorption. The pH values of the mixture of dyes examined were 2.29, 4.02, 6.00, 7.15, 8.76, 10.25, and 12.01 at room temperature and at a fixed sample concentration.

The reason for changing the initial pH of the dyes was because the initial pH was more influential in the adsorption process when compared to the final concentration (Waranusantigul *et al.* 2003). In Figure 4.24 (a), it illustrates that the highest adsorption occurred in the range of pH 6 – 8. However, in Figure 4.24 (b) and (c), it clearly shows that the highest capacity of adsorption occurred at a pH of 6, which makes this the optimum initial pH. This pH was applied in all the studies. Since the mixture of the reactive azo dyes is rich in sulfonate groups ($-SO_3$) that are anionic, it was feasible for the activated carbon to possess positive charges on the surface, for electrostatic interaction. Hence, this was the reason for maximum adsorption at an acidic pH. Activated carbons were reported to be basic and amphoteric in nature (Órfão *et al.* 2006; Al-Degs *et al.* 2008). However, the pH at zero charge is what aided us in

determining the interactions that favour adsorption, since activated carbon possesses repelling charges below zero.

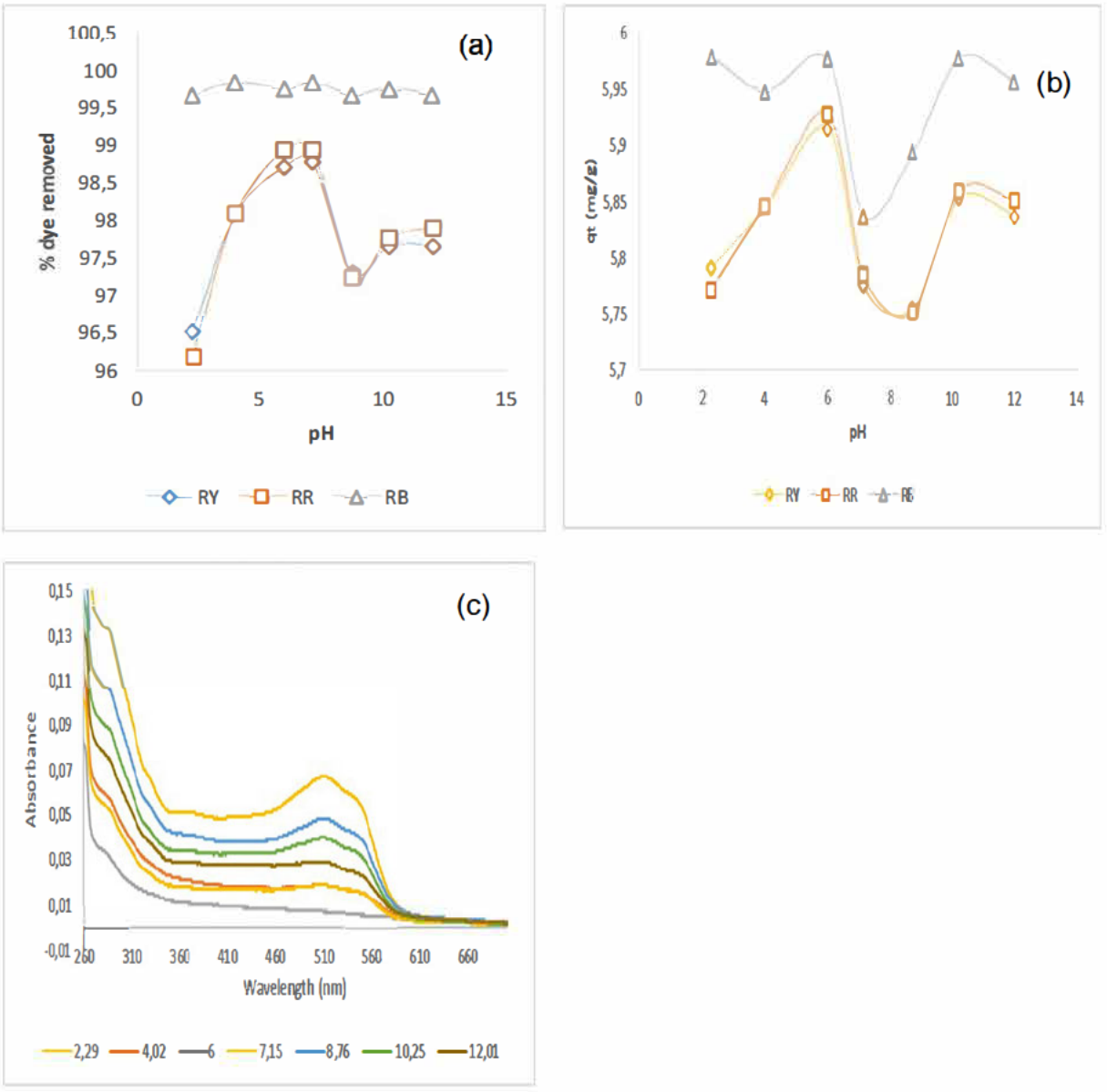

Figure 4.24 Effect of pH on the removal of textile azo dyes (a) % efficiency, (b) amount of dye adsorbed per unit mass (c) UV profiles (concentration=100 mg L^{-1} ,dosage=0.5 g, volume=50 mL, time=30 min)

4.3.4 Effect of Adsorbent Dosage on Textile Dye Removal

The adsorbent dosage plays a critical role in adsorption studies. Hence, its capacity in the removal of the textile azo dyes viz. reactive blue 222, reactive red 195 and reactive yellow 145 in a ternary system was investigated as the function of adsorbent weight.

The study was conducted at room temperature ±25ºC and all the other parameters were kept constant.

The percentage adsorption increased with the quantity of adsorbent as illustrated in Figure 4.25. This is due to an increase in the number of active pore sites available for the dye molecules to bind. The optimum adsorbent dosage for this system was 0.8 g (reactive blue 222) and 1.0 g (reactive red 195 and reactive yellow 145), as is observed since the graph reaches a plateau suggesting monolayer coverage completion. It is also observed that the amount adsorbed per unit mass of activated carbon is inversely proportional to the mass of the adsorbent. Equation 4.11 was used to calculate the amount of dye adsorbed.

$$q_t = \frac{C_0 - C_t}{W} V \qquad 4.11$$

Where q_t represents the amount of reactive dye adsorbed per unit mass of activated carbon, C_0 is the initial dye concentration, C_t is the final concentration at time, W is the mass of the activated carbon and V is the volume of the dye solution.

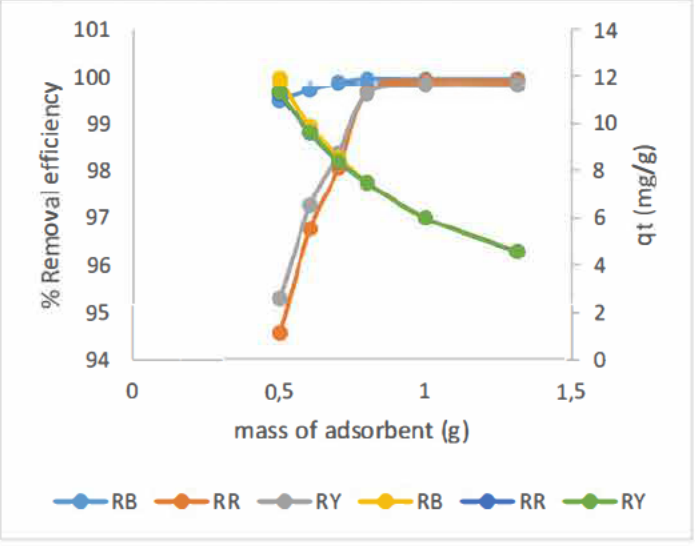

Figure 4.25 Effect of adsorbent dosage illustrating the percentage adsorbate removed and amount removed per gram (volume=50 mL, pH=6.1,C_o=120 mg L^{-1})

4.4 Study of Adsorption Isotherms

Adsorption isotherms were employed to characterize the adsorption process, and to assess the adsorption capacity of H_3PO_4-AC. This study was carried out by varying the mass of the adsorbent at a fixed temperature (25°C) for 50 mL at initial dye concentration of 120 mg L^{-1}, and pH 6.

4.4.1 Langmuir Isotherm Application

The experimental data obtained was analysed using the four types of Langmuir isotherms related to the adsorption process. The linearized Langmuir equations are listed in Table 4.2. Langmuir plots were drawn, and the coefficients were determined as stipulated. All the symbols for the parameters are listed in chapter 2 (equation 2.8).

Table 4.2 Linearized Langmuir isotherm equations

Equation	Linear method	Plot	Parameters
4.2	$\frac{C_e}{q_e} = \frac{1}{K_L q_m} + \frac{C_e}{q_m}$	$\frac{C_e}{q_e}\ vs\ C_e$	$slope = \frac{1}{q_m}$ $y\ intercept = \frac{1}{K_L q_m}$
4.3	$\frac{1}{q_e} = \frac{1}{q_m} + \frac{1}{K_m q_m C_e}$	$\frac{1}{q_e}\ vs\ \frac{1}{C_e}$	$slope = \frac{1}{K_L q_m}$ $y\ intercept = 1/q_m$
4.4	$q_e = q_m - \frac{q_e}{K_L C_e}$	$q_e\ vs\ \frac{q_e}{C_e}$	$slope = -\frac{1}{K_L}$ $y\ intercept = q_m$
4.5	$\frac{q_e}{C_e} = K_L q_m - K_L q_e$	$\frac{q_e}{C_e}\ vs\ q_e$	$slope = -K_L$ $y\ intercept = K_L q_m$

The adsorption process for the removal of the mixture of reactive azo dyes viz. reactive blue 222, reactive red 195 and reactive yellow 145 onto H_3PO_4-AC fitted the Langmuir isotherm Type I as noted in the results presented in Table 4.3 and Figure 4.26 (a). The monolayer adsorption of the dyes per unit mass of the activated carbon was 38.06 g. The highest correlation efficiency (R^2) value (Subramanyam and Das 2009) was closer to 1, which is in agreement with good linearity of the experimental data with the

expected results. The results presented therefore imply that at a higher concentration of the dye solution a monolayer adsorption was achieved, and that there was no interaction of the ternary reactive dye system. Therefore, no further adsorption of the reactive dyes occurred in an occupied site of the H_3PO_4-AC (Subramanyam and Das 2009).

Table 4.3 Langmuir isotherm adsorption parameters

Type of Dye	Langmuir Model Type	q_m (mg g^{-1})	K_L (L mg^{-1})	R^2	Linear Equation
RB	I	15.58	0.829	0.9927	y=0.0642x+0.0774
	II	12.97	1.384	0.9609	Y=0.0557x+0.0771
	III	13.78	1.202	0.8922	Y=-0.8322x+13.783
	IV	14.38	1.072	0.8922	Y=-1.072x+15.415
RR	I	11.24	0.794	0.9957	Y=0.089x+0.1122
	II	10.34	1.332	0.9798	Y=0.0726x+0.0967
	III	10.50	1.266	0.9413	Y=-0.79x+10.501
	IV	10.65	1.192	0.9413	Y=-1.1915x+12.69
RY	I	11.24	0.385	0.9978	Y=0.089x+0.2309
	II	10.34	0.556	0.9780	Y=0.174x+0.0967
	III	10.51	0.518	0.9518	Y=-1.9314x+10.57
	IV	10.71	0.493	0.9518	Y=-0.4928x+5.278

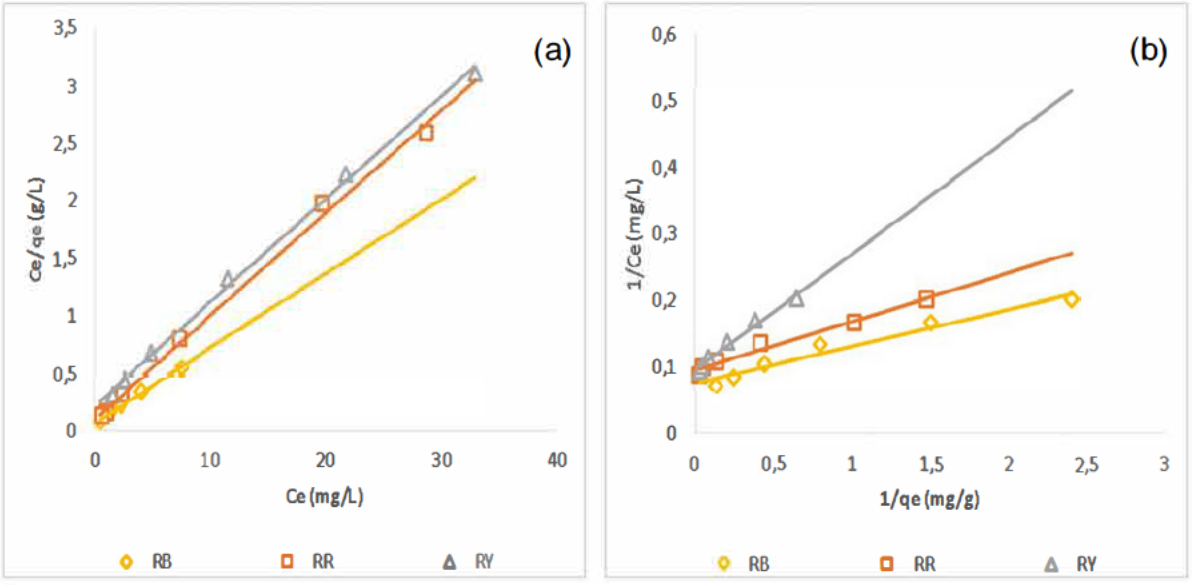

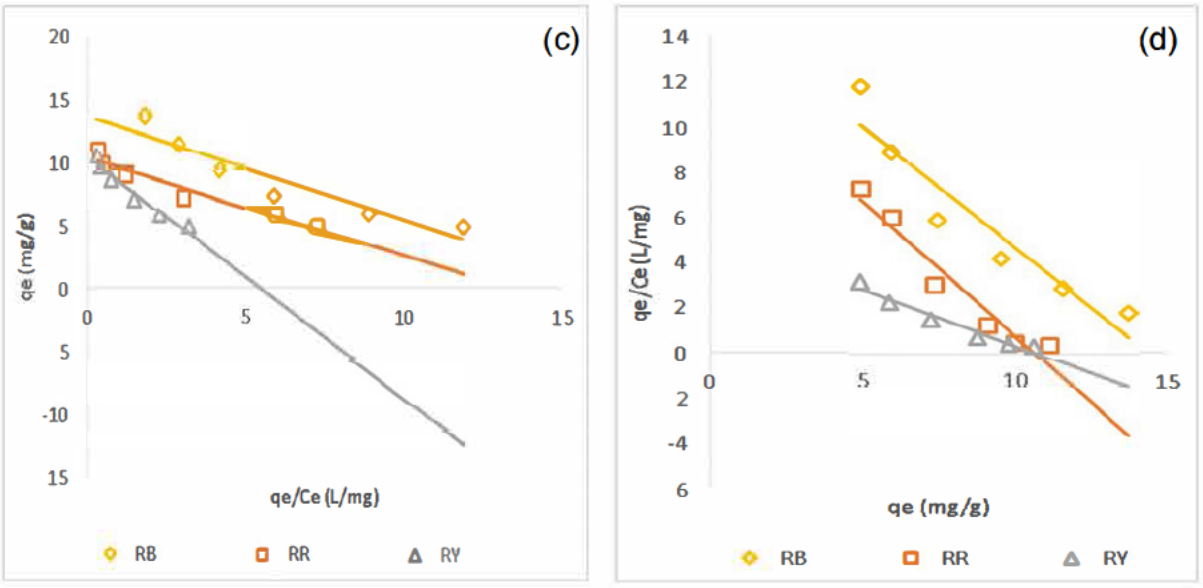

Figure 4.26 Langmuir adsorption isotherm graphs (a)Type I, (b) Type II, (c) Type III, and (d) Type IV (C_o=120 mg L^{-1}, volume=50 mL, pH=6, T=25^{0}C) for the RB, RR, RY

4.4.2 Freundlich Isotherm Application

The Freundlich isotherm (Freundlich 1926) given by equation 4.12 describes the adsorption process that occurs on a multilayer heterogeneous surface (Hamzaoui, Bestani and Benderdouche 2018).

$$\log q_e = \frac{1}{n} \log C_e + \log K_f \qquad 4.12$$

The graph (Figure 4.27) of log q_e as a function of log C_e resulted in a linear plot with the gradient $\frac{1}{n}$ representing the relative distribution of the energy and heterogeneity of the adsorbent sites (Ayawei, Ebelegi and Wankasi 2017), and the y- intercept as log K_f. All the symbols and units for this isotherm are clearly stipulated in chapter 2 (equation 2.9).

Table 4.4 Freundlich isotherm adsorption parameters

Type of Dye	1/n	n (g L^{-1})	K_f (mg g^{-1})	R^2	Linear Equation
RB	0.3584	2.79	6.874	0.9964	Y=0.3584x+0.8372
RR	0.1989	5.03	5.790	0.9663	Y=0.1989x+0.7627
RY	0.2475	4.04	4.615	0.9844	Y=0.2475x+0.6642

The Freundlich isotherm coefficients K_f and n were determined from the graph as presented in Table 4.4. The adsorption process can be described as favourable because n lies between 1 and 10, and normal adsorption occurred due to the intensity of adsorption $\frac{1}{n} < 1$ (Dada *et al.* 2012).

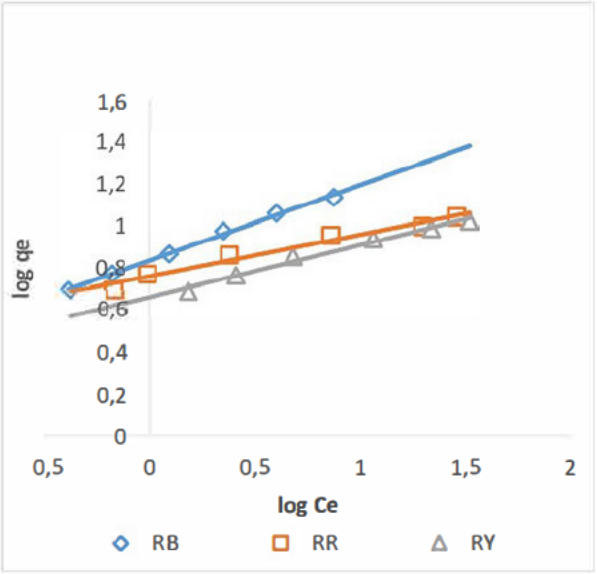

Figure 4.27 Freundlich isotherm plot for RB,RR,RY adsorption onto H_3PO_4-AC (C_o=120 mg L^{-1}, volume=50 mL, pH=6)

4.4.3 Dubinin-Radushkevich Isotherm Application

The Dubinin-Radushkevich isotherm (Dubinin and Stoeckli 1980) for heterogeneous surfaces is based on the Gaussian distribution energy curve (Dada *et al.* 2012) described by equation 4.13. This isotherm is based on a systematic occupation of the porous structure by the solute particles. It is used to differentiate the adsorption taking place as either physisorption or chemisorption. It is based on weak Van der Waals interactions hence favours physical adsorption processes, and is temperature dependent (Ayawei, Ebelegi and Wankasi 2017).

$$\ln q_e = \ln q_s - K_{ad}\,\epsilon^2 \qquad 4.13$$

The D-R coefficients are determined through a linear plot (Figure 4.28) of ln q_e as a function of ϵ^2, producing a gradient of $-K_{ad}$ and the y-intercept of ln q_s. Chapter 2 (equation 2.10) denotes all the coefficients and their meanings.

The Polanyi effect, ϵ was determined by the following expression:

$$\epsilon = RT \ln (1+1/C_f) \qquad 4.5$$

ϵ is the Polanyi potential, R being the gas constant, T is the temperature and C_f is the final concentration. This important parameter determines that the reaction performed in this study is a physical adsorption.

Table 4.5 Dubinin-Radushkevich adsorption parameters

Type of Dye	**K_{ad} ($mol^2\ KJ^{-2}$)**	**q_s ($mg\ g^{-1}$)**	**R^2**	**E ($J\ mol^{-1}$)**	**Linear Equation**
RB	$7X10^{-6}$	11.169	0.8431	267.3	$Y=-7x10^{-6}x+2.4131$
RR	$1X10^{-5}$	9.571	0.8836	223.6	$Y=-1x10^{-5}x+2.2587$
RY	$3X10^{-5}$	9.441	0.7939	129.1	$Y=-3x10^{-5}x+2.2451$

In Table 4.5, it can be seen that the maximum adsorption capacity for the ternary dye adsorption system resulted in a total of 11.169 mg per unit mass of adsorbent, which was lower that the monolayer capacity obtained on the Langmuir application. However, the energy of the total system is 0.62 KJ mol^{-1} that assumes that adsorption was a physical process.

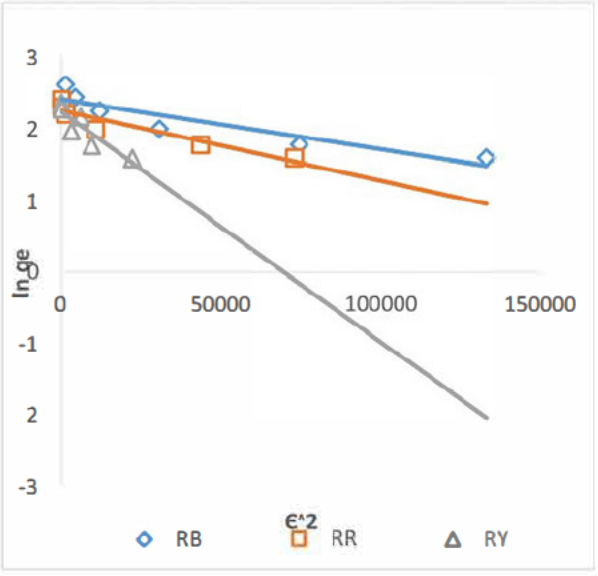

Figure 4.28 D-R isotherm for the RB, RR,RY ternary system onto H_3PO_4-AC (C_o=120 mg L^{-1}, volume=50 mL, pH=6,T=25°C)

4.4.4 Temkin Isotherm Application

This isotherm is based on the interaction between the adsorbent (activated carbon) and the adsorbate (dye solution) in an adsorption process. This model also predicts that the heat of adsorption decreases linearly as the solute coverage increases (Dada *et al.* 2012; Ayawei, Ebelegi and Wankasi 2017). The Temkin isotherm is represented by equation 4.14, with the symbols explained in chapter 2 (equation 2.11).

$$q_e = \frac{RT}{b_T} \ln A_T + \frac{RT}{b_T} \ln C_e \qquad 4.14$$

$$B = \frac{RT}{b_T} \qquad 4.15$$

A plot of q_e as a function of ln C_e yields a straight line presented in Figure 4.29 with the gradient of $\frac{RT}{b_T}$ and the y-intercept of $\frac{RT}{b_T} ln\ ln\ A_T$. The heat of adsorption, B for RB, RR and RY dyes: 3.1, 1.5 and 1.9 J mol^{-1} respectively are presented in Table 4.6 are very low, suggesting the physical adsorption process (Dada *et al.* 2012).

Table 4.6 Temkin adsorption isotherm parameters

Type of Dye	**B (J mol^{-1})**	**b_T**	**A_T (L g^{-1})**	**R^2**	**Linear Equation**
RB	3.0749	805.74	10.468	0.9900	Y=3.0749x+7.221
RR	1.5445	1604.13	43.079	0.9867	Y=1.5445x+5.812
RY	1.8522	1337.64	9.392	0.9988	Y=1.8522x+4.1487

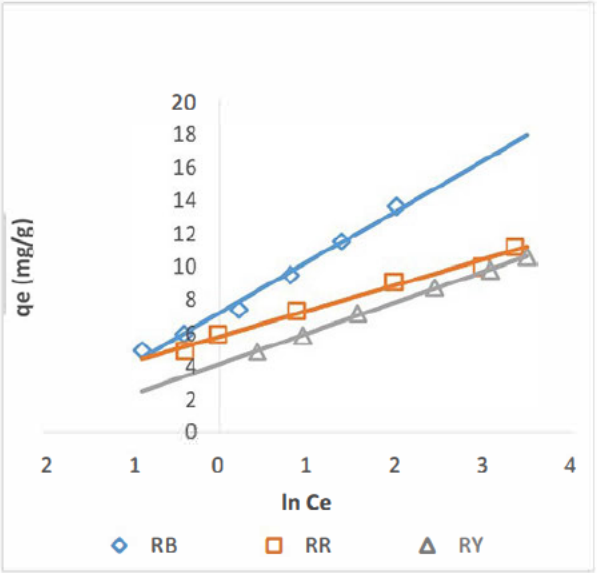

Figure 4.29 Temkin isotherm plot for RB,RR,RY ternary system onto H_3PO_4-AC (C_o=120 mg L^{-1}, volume=50 mL, pH=6,T=25°C)

4.5 Adsorption Kinetics Study of the Adsorption Process

It is important to determine the rate limiting steps and the rate laws involved in the adsorption process. This was determined at varying time intervals, at room temperature for the mixture of RB, RR, and RY ternary system of initial concentration 20, 40, 60, 80,100 and 120 mg L^{1}. The experimental data was applied to Lagergren's pseudo first order (Lagergren 1898), Ho and McKay's pseudo second order (Ho and McKay 1999), and Intraparticle diffusion (Weber and Morris 1963) kinetic models.

4.5.1 Lagergren's Pseudo 1st Order Kinetic Model

The experimental data was fitted into Largergren pseudo first order (Lagergren 1898) kinetic model represented by equation 4.16.

$$\log (q_m - q_t) = \log q_e - \frac{K_{L1}}{2.303} t \qquad 4.16$$

The graph (Figure 4.30 (a-c)) of log (q_m – q_t) as a function of time was plotted to yield a descending straight line with gradient of $-\frac{K_{L1}}{2.303}$ and the y-intercept of log q_e, which

was used to determine the Lagergren pseudo kinetic constant and the amount of reactive azo dyes adsorbed at equilibrium, presented in Table 4.7.

Table 4.7 Parameters for the Lagergren pseudo 1st order kinetic model for the reactive dyes

Dye Concentration	**Linear Equation**	**R^2**	**K_{L1} (min^{-1})**	**q_e ($mg\ g^{-1}$)**
RB 20 ppm	$y = -5.0x10^{-5}x + 1.1268$	0.9454	$1.152\ x10^{-4}$	13.391
40 ppm	$y = -2.0x10^{-4}x + 1.0555$	0.8556	$4.606\ x10^{-4}$	11.363
60 ppm	$y = -2.0x10^{-4}x + 0.9591$	0.9168	$4.606\ x10^{-4}$	9.1012
80 ppm	$y = -1.2x10^{-3}x + 0.8948$	0.7779	$2.764\ x10^{-3}$	7.8487
100 ppm	$y = -2.4x10^{3}x + 0.7933$	0.7779	$5.527\ x10^{-3}$	6.2130
120ppm	$y = -5.0x10^{-3}x + 0.6781$	0.8343	$1.152\ x10^{-2}$	4.7654
RR 20 ppm	$y = -2.0x10^{4}x + 0.9655$	0.8605	$4.606\ x10^{-4}$	9.2363
40 ppm	$y = -1.1x10^{-3}x + 0.9173$	0.9235	$2.533\ x10^{-3}$	8.2661
60 ppm	$y = -2.8x10^{3}x + 0.8827$	0.9394	$6.448\ x10^{-3}$	7.6331
80 ppm	$y = -4.8x10^{-3}x + 0.8332$	0.9695	$1.105\ x10^{-2}$	6.8108
100 ppm	$y = -1.1x10^{2}x + 0.8744$	0.9688	$2.579\ x10^{-2}$	7.4886
120 ppm	$y = -2.0x10^{2}x + 0.9679$	0.9282	$4.583\ x10^{-2}$	9.2875
RY 20 ppm	$y = -5.0\ x10^{-4}x + 0.9836$	0.7805	$1.152\ x10^{-3}$	9.2694
40 ppm	$y = -1.0\ x10^{3}x + 0.9290$	0.9887	$2.303\ x10^{-3}$	8.4918
60 ppm	$y = -1.8\ x10^{-3}x + 0.8765$	0.9962	$4.145\ x10^{-3}$	7.5249
80 ppm	$y = -3.4\ x10^{3}x + 0.8129$	0.9860	$7.830\ x10^{-3}$	6.4998
100 ppm	$y = -7.6\ x10^{-3}x + 0.8398$	0.9966	$1.750\ x10^{2}$	6.9151
120 ppm	$y = -1.3\ x10^{2}x + 0.8884$	0.9666	$2.971\ x10^{-2}$	7.7339

This model does not fit this adsorption process, as the amount of reactive dyes adsorbed at equilibrium ($q_{e,\ cal}$) does not correlate with the experimental values ($q_{e,\ exp}$). The values obtained are disproportionate as with the model a decrease with increasing temperature is observed. Hence, these values cannot be used to describe this adsorption process.

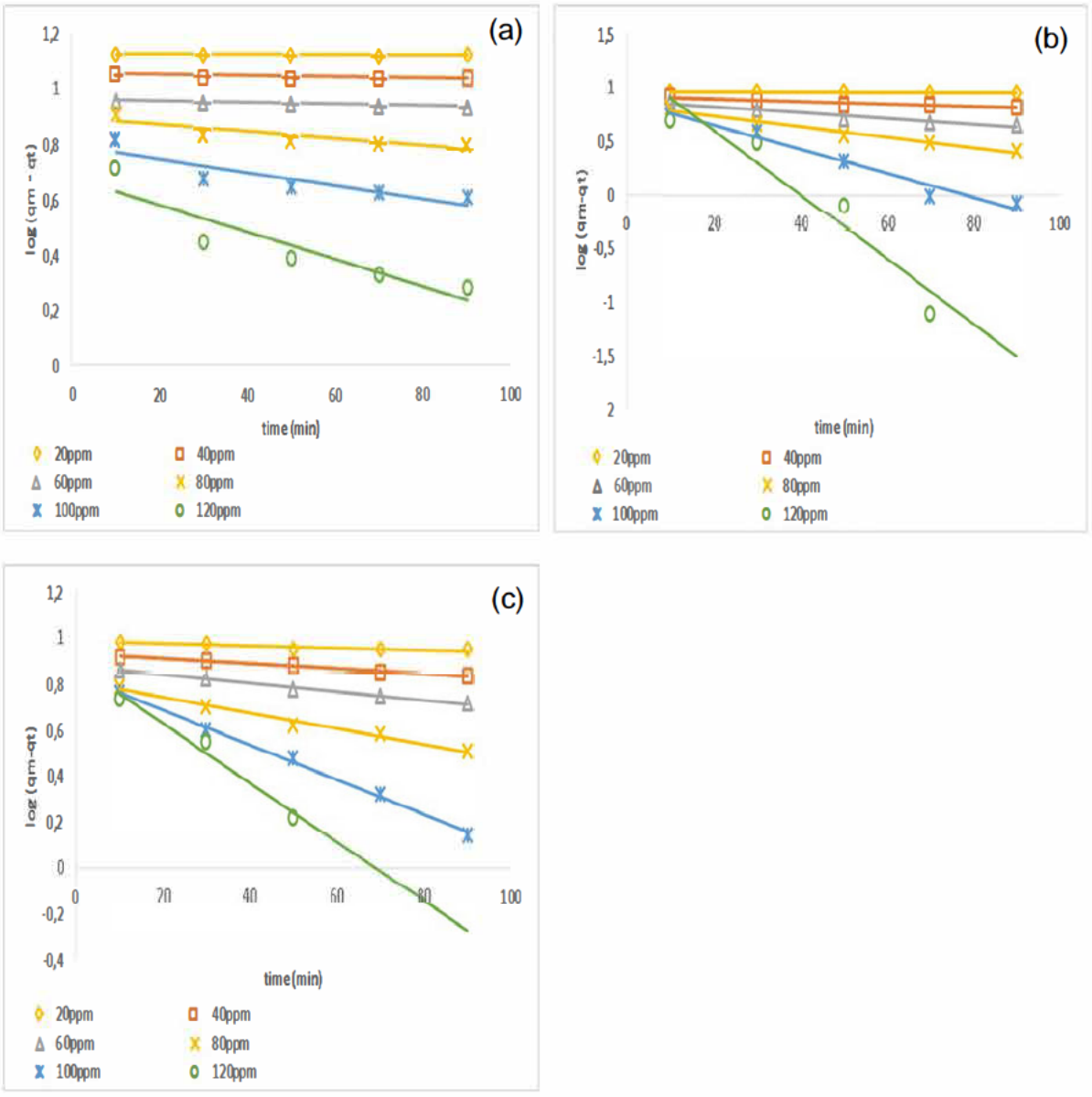

Figure 4.30 Lagergren pseudo 1st order plot for (a) reactive blue 222, (b) reactive red 195, and (c) reactive yellow 145 (volume=50 mL, adsorbent dosage=0.5 g, pH=6)

4.5.2 Ho and McKay's Pseudo 2nd Order Kinetic Model

The Ho and McKay's pseudo second order (Ho and McKay 1999) kinetic model was used to fit the experimental data obtained in the removal of the reactive azo dyes from textile industries using activated carbon (H_3PO_4-AC) using the expression 4.17:

$$\frac{t}{q_t} = \frac{1}{K_{H2} q_e} + \frac{t}{q_e} \qquad 4.17$$

Linear graphs were obtained for this system (Figures 4.31 a-c) by plotting $\frac{t}{q_t}$ as a function of t, to obtain the gradient $\frac{1}{q_e}$ and the y-intercept$\frac{1}{K_{H2}q_e}$. The pseudo second order coefficients (Table 4.8) were calculated from the intercept and slope, respectively.

Table 4.8 Parameters for the Ho and McKay's pseudo 2nd order kinetic model for the reactive dyes

Dye Concentration	**Linear Equation**	**R^2**	**K_{H2} (g mg^{-1})**	**q_e (mg g^{-1})**
RB 20 ppm	y = 0.3384x + 2.3918	0.9749	0.1415	2.9551
40 ppm	y = 0.1706x + 1.2929	0.9714	0.1320	5.8617
60 ppm	y = 0.1154x + 0.8569	0.9695	0.1347	8.6655
80 ppm	y = 0.0845x + 0.7708	0.9719	0.1096	11.834
100 ppm	y = 0.0678x + 0.6506	0.9738	0.1042	14.749
120 ppm	y = 0.0570x + 0.5747	0.9738	0.0992	17.544
RR 20 ppm	y = 0.3425x + 3.2274	0.9789	0.1061	2.9197
40 ppm	y = 0.1653x + 2.6091	0.9706	0.0634	6.0496
60 ppm	y = 0.1064x + 2.3057	0.9595	0.0462	9.3985
80 ppm	y = 0.0841x + 1.7676	0.9706	0.0476	11.891
100 ppm	y = 0.0664x + 1.6466	0.9443	0.0403	15.060
120 ppm	y = 0.0567x + 1.5681	0.9605	0.0362	17.637
RY 20 ppm	y = 0.3126x + 5.0199	0.9536	0.0623	3.1990
40 ppm	y = 0.1702x + 3.2121	0.9454	0.0530	5.8754
60 ppm	y = 0.1239x + 2.2570	0.9604	0.0549	8.0710
80 ppm	y = 0.094x + 1.6642	0.9712	0.565	10.638
100 ppm	y = 0.0734x + 1.6613	0.9595	0.0442	13.624
120 ppm	y = 0.0617x + 1.6310	0.9434	0.0378	16.207

The correlation coefficients for the pseudo second order kinetic model, R^2 for the ternary system removal viz. reactive blue 222, reactive red 195 and reactive yellow 145 onto H_3PO_4-AC was found to be higher than the one fitted into a pseudo first order kinetic model. $R^2 > 0.9434$ for all systems; however it has been mentioned that the correlation efficient is not an important determining factor for the best-fit model. But

the $q_{e,\,cal}$ value is in agreement with the $q_{e,\,exp}$ (Simonin 2016). Moreover, for the pseudo second order model the $q_{e,\,cal}$ is the same is the experimental quantity adsorbed at equilibrium for the reactive dyes. Hence, the best fit is the Ho and McKay's pseudo second order kinetic model for the removal of reactive azo dyes.

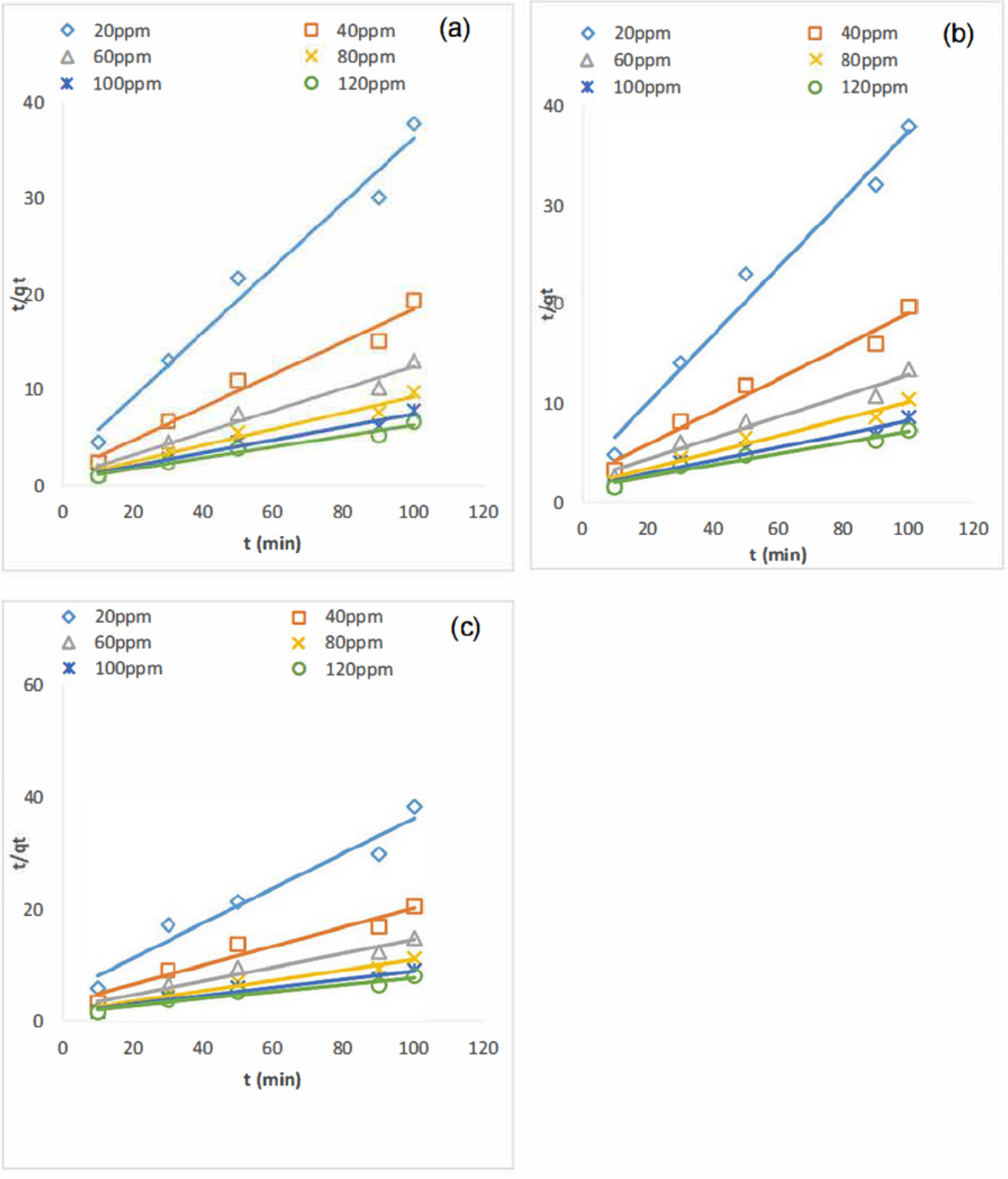

Figure 4.31 Ho and McKay's pseudo 2nd order plot for (a) reactive blue 222, (b) reactive red 195, and (c) reactive yellow 145 (volume=50mL, adsorbent dosage=0.5g, pH=6)

4.5.3 Intraparticle Diffusion Model

The adsorption process is governed by three steps viz. diffusion of the adsorbate through the film layer, adsorbate within the particles of the adsorbent that varies with pore size referred to as the internal diffusion/intraparticle diffusion and lastly the adsorption/desorption of the adsorbate molecules to the active sites on the surface of the adsorbent (Cheung, Szeto and McKay 2007). Equation 4.18 represents the Weber/Morris model of diffusion that relates adsorbate diffusion to be independent of the contact time, but varies with the half-life, $t^{0.5}$ (Weber and Morris 1963; Qiu *et al.* 2009).

$$q_t = K_{IPD} t^{0.5} + I \qquad 4.18$$

The intraparticle diffusion model was employed to determine the rate controlling mechanism for this adsorption process. In Figure 4.32 multi-linearity plots are depicted, which is observed as a 2-step process. However, intraparticle diffusion of the solute to the surface was not the only kinetic limiting step, since the graph does not pass through the origin. Table 4.9 shows the gradient, K_{IPD1} with values greater than zero (Qiu *et al.* 2009).

Table 4.9 Intraparticle diffusion model parameters for the reactive dyes

Dye Concentration	**K_{IPD1}**	**K_{IPD2}**
RB 20 mg L^{-1}	0.4572	0.0203
40 mg L^{-1}	0.5423	0.0482
60 mg L^{-1}	0.4328	0.0872
80 mg L^{-1}	0.5300	0.1362
100 mg L^{-1}	0.8114	0.1679
120 mg L^{-1}	1.0481	0.2194
RR 20mg L^{-1}	0.4629	0.0555
40 mg L^{-1}	0.7044	0.2200
60 mg L^{-1}	0.4636	0.4476
80 mg L^{-1}	0.8322	0.4922

100 mg L^{-1}	0.6844	0.7976
120 mg L^{-1}	0.8184	1.0138
RY 20 mg L^{-1}	0.4561	0.1444
40 mg L^{-1}	0.5618	0.2802
60 mg L^{-1}	0.6675	0.3685
80 mg L^{-1}	0.4776	0.4407
100 mg L^{-1}	0.7804	0.6493
120 mg L^{-1}	0.8143	0.8701

All the reactive dyes showed the first step progressing sequentially when compared to the last which is gradual since the adsorbent is reaching monolayer coverage, especially at lower concentration. It has been reported that especially in physisorption, the diffusion through a boundary film layer phase (mass transfer) is very rapid at the onset of the reaction (Qiu *et al.* 2009; Malash and El-Khaiary 2010). The results presented in Table 4.15 and Figures 4.32 confirm that intraparticle diffusion is not the rate limiting step, and may however, be one or two diffusional processes taking place simultaneously or perhaps the diffusivity of the dyes onto different pores of the adsorbent surfaces (Qiu *et al.* 2009).

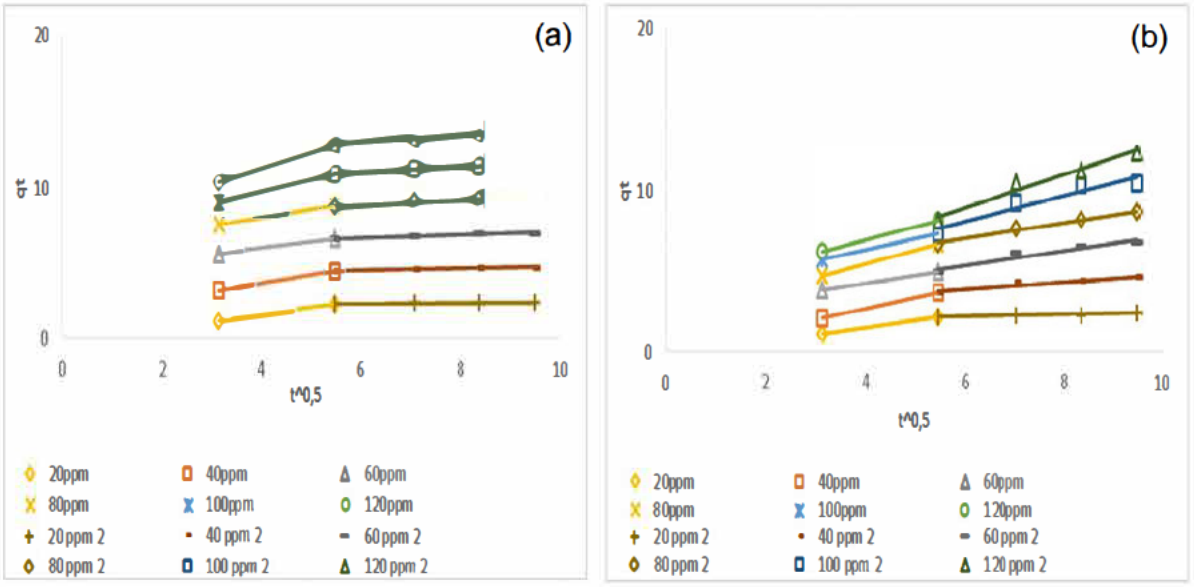

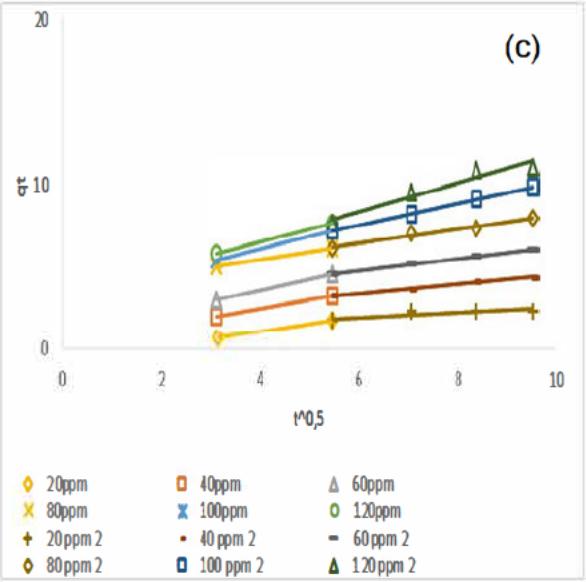

Figure 4.32 Intraparticle diffusion plot (a) reactive blue 222, (b) reactive red 195, and (c) reactive yellow 145 (volume=50 mL, adsorbent dosage=0.5 g, pH=6)

4.6 Thermodynamic Studies for the Adsorption of Reactive Dyes

To determine the nature and the viability of the adsorption process, thermodynamics for the adsorption studies were employed using equations 4.19-4.21.

$$\Delta G^0 = \Delta H^0 - T\Delta S^0 \qquad 4.19$$

$$\ln K_a = \frac{\Delta S^0}{R} \quad \frac{\Delta H^0}{RT} \qquad 4.20$$

$$Ea = \Delta H^0 + RT \qquad 4.21$$

The graph of ln K_a as the function of reciprocal of temperature (1/T) yielded a straight line with gradient of $-\frac{\Delta H^0}{R}$ with the y-intercept of $\frac{\Delta S^0}{R}$. All the symbols are listed with details in chapter 2. The activation parameters: Gibbs free energy (ΔG^o), change in enthalpy (ΔH^o), change in entropy (ΔS^o) and E_a were calculated from the Van't Hoff plot (Figure 4.33).

Table 4.10 Thermodynamic parameters for the removal of reactive dyes using H_3PO_4-AC

Dyes	T (K)	R^2	ΔH^o (kJ mol^{-1})	ΔS^o (J mol^{-1} K^{-1})	ΔG^o (kJ mol^{-1})	Ea (kJ mol^{-1})	Equation
RB	293.15				-9.399	2.402	Y=4216.2x
	303.15	0.9932	-35.05	-87.50	-8.524	2.485	-10.525
	313.15				-7.649	2.568	
RR	293.15				-3.612	2.412	Y=2765.6x
	303.15	0.9844	-25.20	-73.64	-2.876	2.495	-7.7764
	313.15				-2.140	2.578	
RY	293.15				-4.038	2.414	Y=3031.4x
	303.15	0.9125	-22.99	-64.65	-3.391	2.497	-8.8579
	313.15				-2.745	2.580	

The thermodynamic studies of the removal of the textile reactive azo dyes were performed at temperatures: 20ºC, 30ºC and 40ºC using H_3PO_4-AC as an adsorbent. The Gibbs free energy of activation, ΔG^o is classified in 3 categories with physisorption between -20 to 0 kJ mol^{-1}, physisorption/chemisorption between -20 to -80 kJ mol^{-1} and chemisorption at -80 to -400 kJ mol^{-1} (Gerçel *et al.* 2007). The negative ΔG^o values listed in Table 4.10 represent the spontaneity of the physical adsorption process. The enthalpy change of the system was also negative for all the dyes with RB < RR < RY (-35.05, -25.20 and -22.99 kJ mol^{-1}) representing the exothermic nature of the adsorption process. The change in enthalpy and change in entropy values are also negative (Table 4.10) suggesting that the concentration of the reactive dye molecules was decreasing with the increased temperature of the reaction, and begins to saturate the H_3PO_4-AC. This was also observed in the removal of direct blue 106 with activated carbon prepared from pomegranate peel (Amin 2009). The adsorption capacity decreased with an increase in reaction temperature confirming weak physical attractions (Özcan and Özcan 2004) responsible for binding the dye molecules to the adsorbent surface. The activation energies of solutions were calculated from equation 4.19 as stipulated by Atkins (Adkins 2006). The activation energies between 5-50 kJ mol^{-1} and 60-800 kJ mol^{-1} correlates to the physisorption and chemisorption processes, respectively (Doğan, Abak and Alkan 2009). The negative activation

energies signify that physical adsorption (Adkins 2006; Amin 2009) for the removal of reactive dyes onto H_3PO_4-AC requires no activation energy as physisorption is a rapid process. Furthermore, these results are also in agreement with the Gibbs free energy confirming that the reaction is indeed spontaneous.

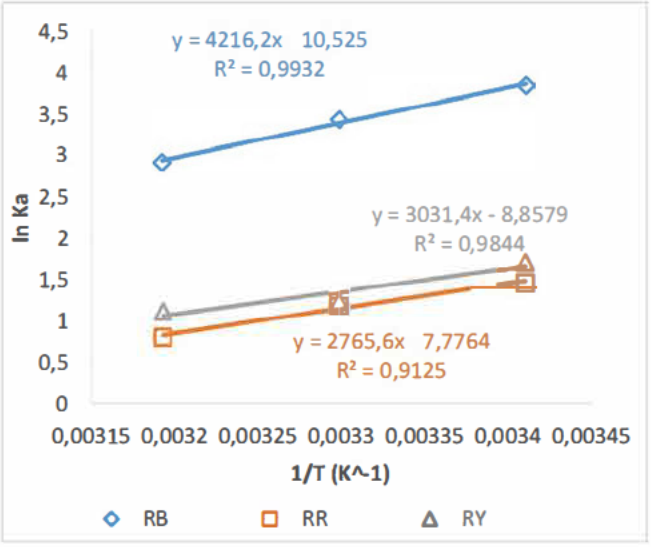

Figure 4.33 Van't Hoff plot for adsorption of reactive dyes (C_o=60 mg L^{-1}, volume=50 mL, adsorbent dosage=0.5 g, pH=6)

4.7 Desorption Studies

Desorption studies of the three reactive dyes (RB, RR and RY) onto H_3PO_4-AC at room temperature were conducted to determine the feasibility and recyclability of the activated carbon to adhere to the green chemistry regulations. This was done to conclude if the adsorbent prepared can be used as a replacement for the costly and non-regenerative commercial activated carbon. Determining the percentage recovery of the dyes is essential. Sodium hydroxide was used as a desorbing agent in this investigation, and its excellent capability to recover the dyes and/ metals in water has been reported by many researchers (Li *et al.* 2009; Raghunath *et al.* 2016; Pathania, Sharma and Singh 2017). Various NaOH standards (0.1 mol L^{-1}, 0.2 mol L^{1}, 0.4 mol L^{1}, 0.6 mol L^{-1}, 0.8 mol L^{1} and 1.0 mol L^{-1}) were used to desorb 40 mg/ 100 mL of a mixture of reactive dyes. The reactive dyes are rich in sulfonate groups ($-SO_3$) that attach on the cationic surface of the activated carbon. The anionic hydroxyl (OH^-) from the desorbing agent attaches itself, thus removing the dye molecules to the desorbing medium.

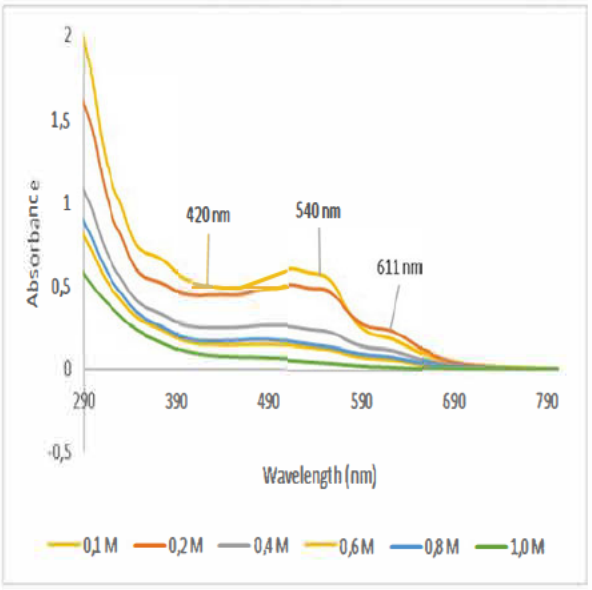

Figure 4.34 UV profile for the recoveries of RB, RR, and RY using NaOH

The formula used to calculate the regeneration of the ternary reactive dye system:

$$\% \, Recoveries = \frac{Cf}{Co} \times 100 \qquad 4.22$$

Figures 4.34 and 4.35 clearly show that the higher the concentration of the salt, there is a decrease in percentage recovery. The percentage recoveries for all the dyes using 0.1, 0.2, 0.4, 0.6, 0.8 and 1.0 mol/L were 86-96%, 75-77%, 42-63%, 29-55%, 25-32% and 14-23%, respectively. It was observed that after adsorption of the dyes, washing with deionized water and drying the adsorbent at a temperature >80ºC as previously carried out in some desorption studies of dyes (Peláez-Cid *et al.* 2016; Raghunath *et al.* 2016), dyes could not be desorbed due to the decomposition of the organic dye molecules at high temperature. However, when the adsorbent was dried at room temperature, regeneration of the dyes was possible. A 0.1 mol L^{1} NaOH solution was the optimum medium for the removal of dye molecules from the adsorbent surface. This confirmed the weak attractions that can be attributed to π-interactions. Since regeneration was possible, this implies that the adsorption process was a reversible physical adsorption.

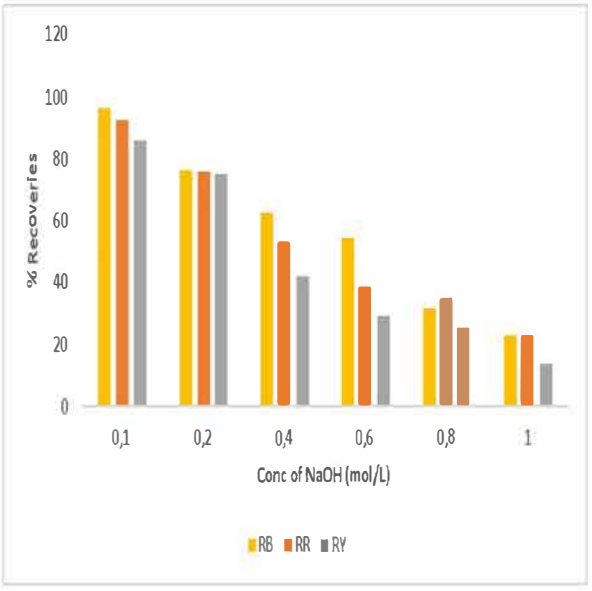

Figure 4.35 Recoveries of mixture of dyes (C_o=40 mg L^{-1}, volume=60 mL, pH=6, T=+-25^oC)

PART B: Characterization of the Ferromagnetic/H_3PO_4-AC Nanocomposite and its Adsorption Capacity on the Removal of Textile Dyes

4.8 Characterization Studies of Iron Oxide/H_3PO_4-AC Nanocomposite

The FTIR spectrum of the iron oxide/H_3PO_4-AC nanocomposites (Figure 4.36) with the characteristic absorption band at 3224 cm^{-1} indicates the O-H stretch of the hydroxyl group. The peak at 1496 cm^{-1} is assigned to the bend of either the O-H groups or the C=C of the aromatic rings. C-O stretch of the ether groups was observed at 1338 cm^{1}. Fe-O stretch was observed at 1077 cm^{1} in agreement with the presence of iron oxide such as maghemite (Cazetta *et al.* 2016).

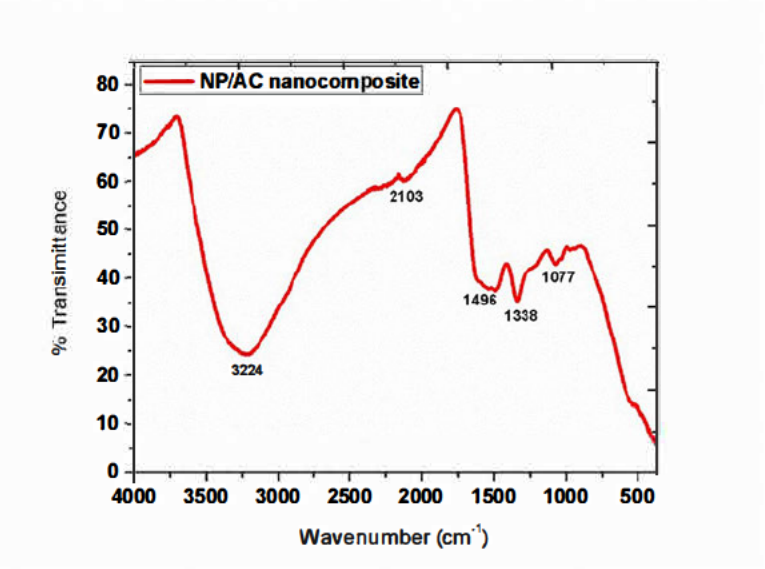

Figure 4.36 FTIR spectrum of iron oxide/phosphoric acid based activated carbon nanocomposite

The thermal behavior and stability of the nanoparticle-activated composite was examined using thermogravimetric analysis and differential scanning calorimetry under nitrogen flow, at a scanning rate of 10ºC/min; a temperature range of 20ºC to 1000ºC. In Figure 4.37, a 3-step degradation process is illustrated. The initial mass loss of approximately 33% at temperatures < 100ºC is due to moisture content and the hydroxyl ions on the material. A gradual weight loss of 18% from 100ºC to 700ºC is followed by a rapid loss of 21% from 700ºC to 850ºC which is attributed to the oxidation

of activated carbon and the iron oxide (e.g. maghemite) (Oliveira *et al.* 2002). The observed endothermic peaks indicate the removal of bound water, and the conversion of the iron oxide.

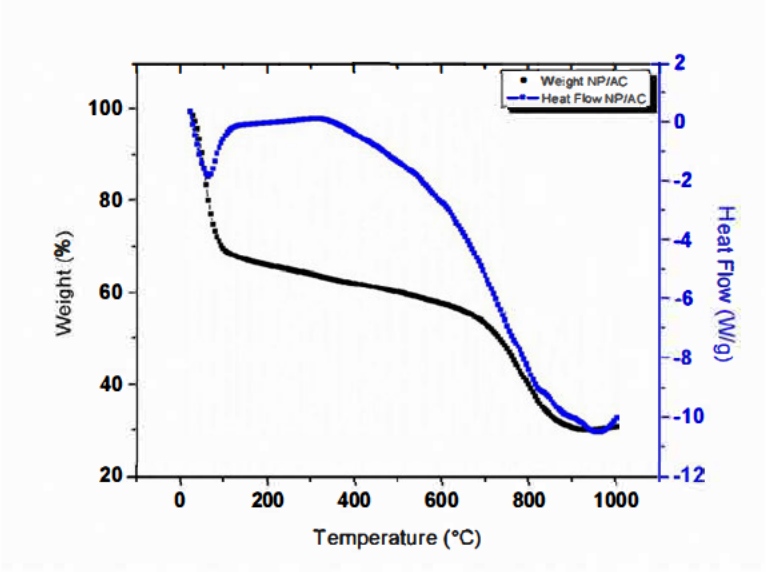

Figure 4.37 TGA/DSC thermogram of the iron oxide/phosphoric acid based activated carbon nanocomposite

The SEM micrographs (Figure 4.38) show heterogeneity of the particles. These particles are smooth and irregular, with different sizes and shapes. The diameter of the smallest particles has a radius of 2.97 µm and the largest being 50.8 µm as depicted in Figure 4.38 (b). Agglomeration of particles forming a cluster was noted.

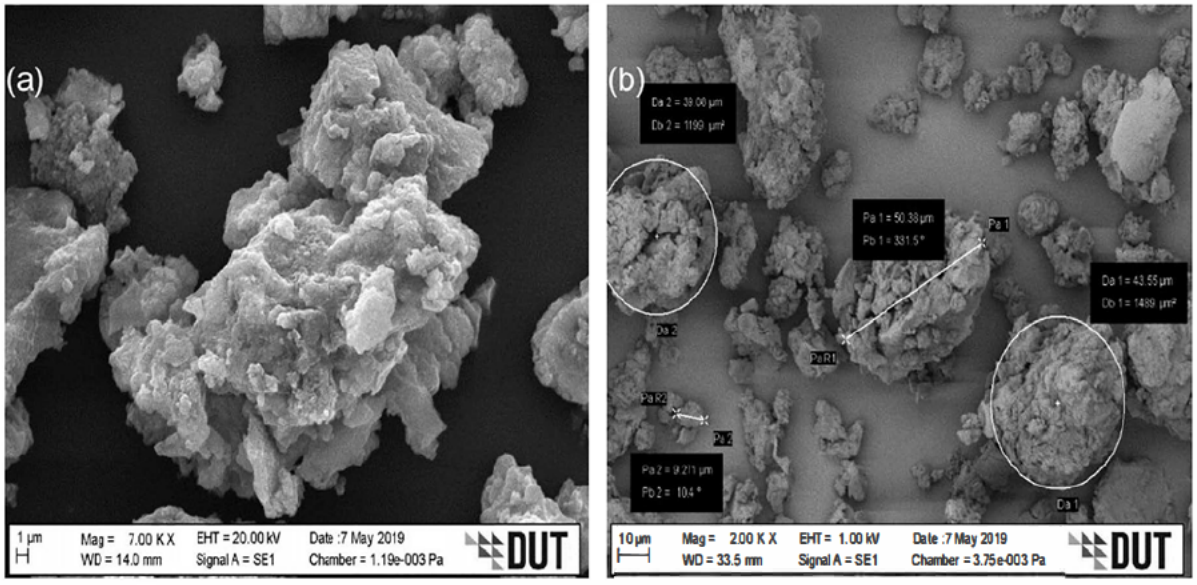

Figure 4.38 SEM images for iron oxide/phosphoric acid based activated carbon nanocomposite (a) 7000X, and (b) 2000X

The energy dispersive X-ray analysis show 3 major elements on the surface of the iron oxide/H_3PO_4-AC composite, namely C (20.55 Wt.%), O (60.59 Wt.%) and Fe (16.43 Wt.%) as illustrated in Figure 4.39 (a-c). This confirmed that the activated carbon produced was successfully incorporated with iron to produce an iron oxide-activated carbon composite. The EDX spectrum (Figure 4.39 (c)) shows iron forming different oxides thus confirming a production of hematite (β- Fe_2O_3)/ maghemite (ϒ-Fe_2O_3) or magnetite (Fe_3O_4) as observed by the Fe peak at 0.6 keV, generally known as zerovalent iron (Fe^0) (Yazdanbakhsh, Hashempour and Ghaderpouri 2018). The micro-zerovalent iron produced forms part of a core shell that is surrounded by layers of iron hydroxides and oxides observed at 6.4 keV and 7.2 keV, respectively (Shi *et al.* 2015; Yazdanbakhsh, Hashempour and Ghaderpouri 2018).

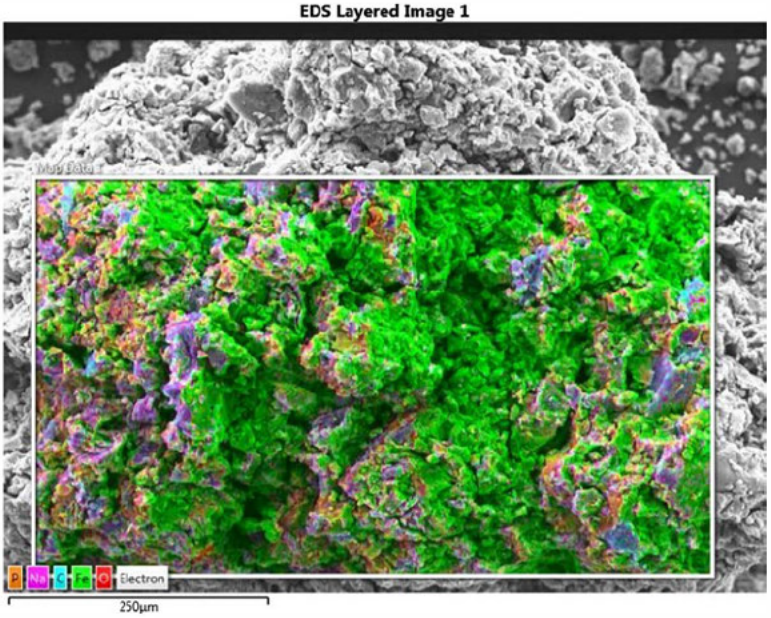

(a)

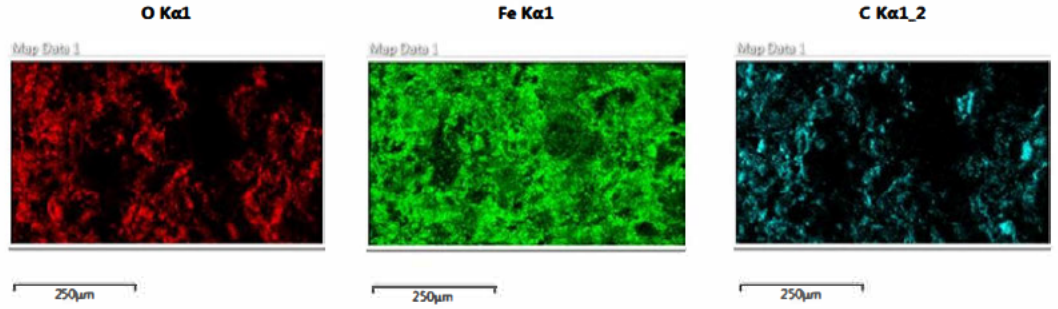

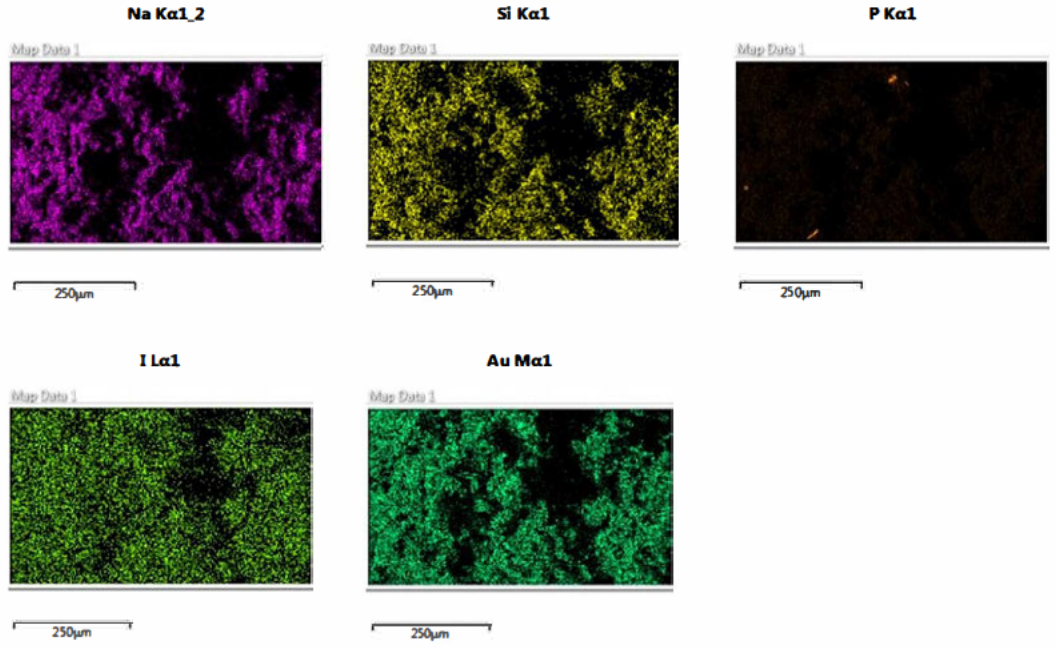

(b)

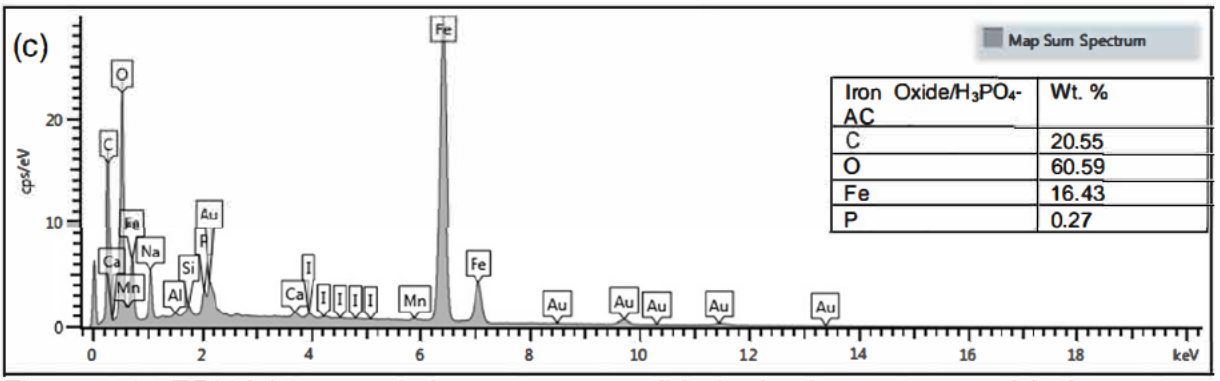

Figure 4.39 EDX (a) Layered elementary map, (b) single element maps, (c) elementary spectrum for the iron oxide/ phosphoric acid based activated carbon composite

The TEM images (Figure 4.40 (a)) shows the spherical particles of fairly proportional sizes of the iron oxide-activated carbon composite while HRTEM shows stacked structures with iron core, in agreement with the EDX map spectrum.

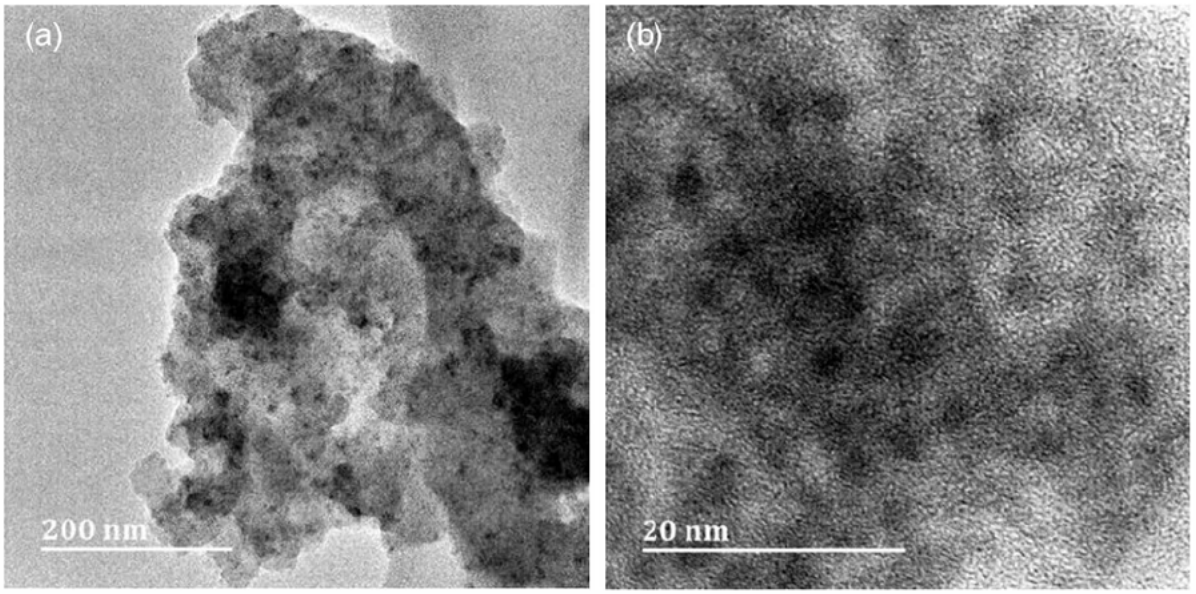

Figure 4.40 Iron oxide/phosphoric acid based activated carbon composite (a) TEM, and (b) HRTEM

4.9 Optimization of Adsorption Factors Using Iron Oxide/H_3PO_4-AC Composite

4.9.1 Effects of Initial Dye Concentration in Remediation of Synthetic Effluents

The percentage dye removed was calculated and it was found to be dependent on the initial dye concentration. As the initial dye concentration on the system increased, the dye removed decreased. The reaction mixture that contained reactive blue 222, reactive red 195 and reactive yellow 145 dyes were studied at different concentration ranges from 20 mg L^{1} up to 120 mg L^{-1}, between 10 minutes up to 90 minutes using 0.5g/50 mL dye working standards. In the mixture containing the three dyes, reactive blue 222 had a much stronger and faster interaction with the adsorbate, as it has the highest adsorption capacity when compared to the other dyes. The optimum dye removal for the ternary dye system was around 70 minutes, however 50 minutes was sufficient to remove reactive blue 222 dye. Dyes removed by the iron oxide/ H_3PO_4-AC composite were: (RB) 99.60 – 100%, (RR) 99,59 – 100%, and (RY) 99,48 – 100% as illustrated in Figure 5.6 (a-c). This inverse relationship between the initial dye concentration and the % dye removal, is due to the interaction of the adsorbate particle and the active sites available for adsorption in an adsorbate. As the adsorbate, particles saturate the adsorbent, the availability of the adsorbent active sites decreases.

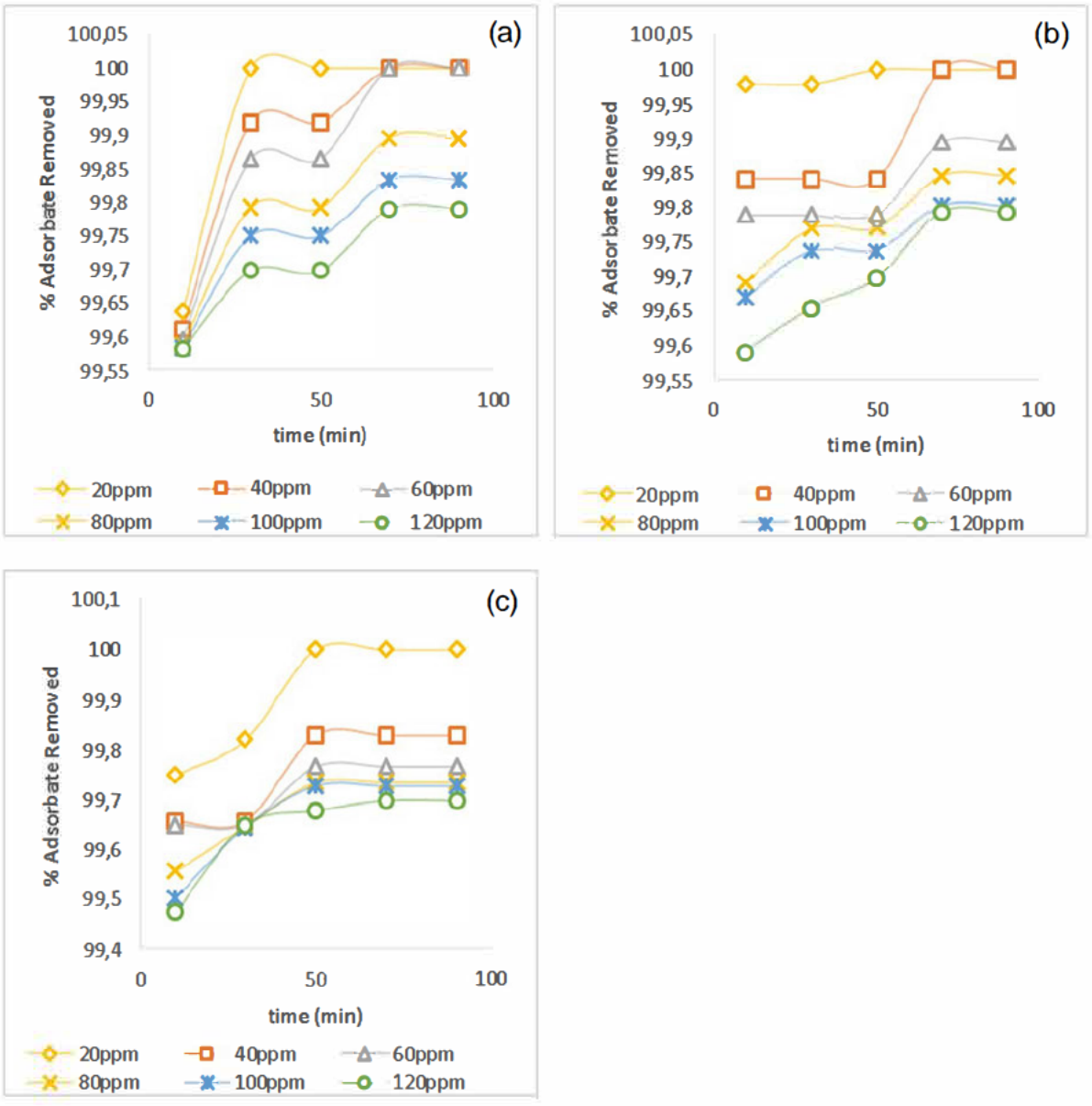

Figure 4.41 % dye removal plots for the effects of initial dye concentration for iron oxide/H_3PO_4-AC composite (a) RB, (b) RR, and (c) RY (volume=50 mL, adsorbent dosage=0.5 g, pH=6)

4.9.2 Effect of Adsorbent Dosage on the Remediation of Textile Synthetic Effluents

The adsorbent dosage had a positive impact on the adsorption capacity, as the adsorbent active sites available for adsorption for the mixture of reactive blue 222, reactive red 195 and reactive yellow 145 dyes increased. The optimum adsorbent mass for iron oxide/ H_3PO_4-AC composite for the ternary mixture was 1 g, as observed in Figure 4.42 for the 120 mg L^{-1} of dye sample. As the adsorbent dosage increased, the amount of dye removed also increased until equilibrium was attained.

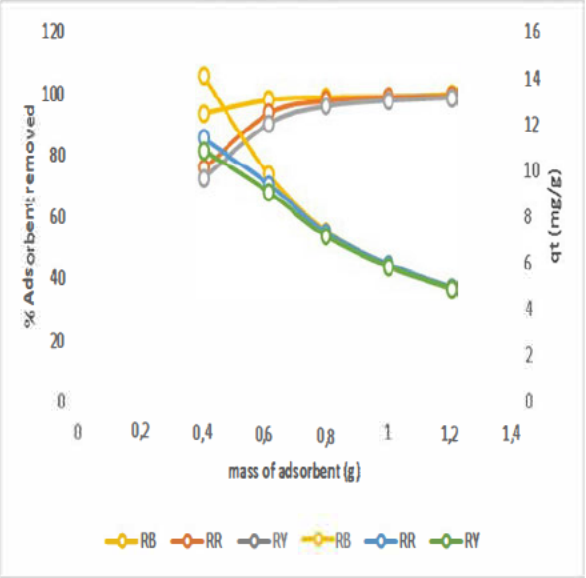

Figure 4.42 Effect of adsorbent dosage plot for the mixture of reactive dyes using iron oxide/H_3PO_4-AC composite as the adsorbent (C_o=120mg L^{-1}, volume=60 mL, adsorbent dosage=0.5 g, pH=6)

4.10 Adsorption Isotherms of Iron Oxide/H_3PO_4-AC Composite

4.10.1 Langmuir Isotherm Application

The experimental data was fitted into the Langmuir isotherm model (Langmuir 1916) as illustrated in Figure 4.43 (a-d). The model symbols and equations are stipulated in chapter 2 of this dissertation in equation 2.8. The reaction system of the ternary mixture of reactive blue 222, reactive red 195 and reactive yellow 145 when using iron oxide/H_3PO_4-AC composite was the best fit to Langmuir type I adsorption model with the highest correlation (R^2) values for the linear plots. The maximum amount adsorbed pertaining to Langmuir isotherm type I for the dyes are as follows: RB, RR and RY are 14.16 mg g^{-1}, 11.20 mg g^{-1} and 11.59 mg g^{-1} respectively, with the Langmuir isotherm constants as stipulated in Table 4.11. These results suggest that a monolayer coverage of the dye molecules was formed on the surface of the iron oxide/H_3PO_4-AC composite.

Table 4.11 Langmuir isotherm parameters of the iron oxide/H_3PO_4-AC composite for the reactive dye mixture

Type of Dye	Langmuir Model Type	q_m (mg g^{-1})	K_L (L mg^{-1})	R^2	R_L	Linear Equation
RB	I	14.16	8.2093	0.9717	0.00101	Y=0.0706x+0.0086
	II	14.06	0.9999	0.6885	0.00826	Y=0.0114x+0.1012
	III	13.41	9.8814	0.9750	0.00084	Y=-0.1012x+13.409
	IV	13.55	9.6313	0.9750	0.00086	Y=-9.6313x+130.47
RR	I	11.20	3.2122	0.9837	0.00259	Y=0.0893x+0.0278
	II	9.881	8.8772	0.8452	0.00092	Y=0.0085x+0.0711
	III	10.02	0.1038	0.8703	0.07432	Y=-0.1131x+10.019
	IV	10.34	7.6972	0.8703	0.00108	Y=-7.6972x+79.571
RY	I	11.59	2.6554	0.9856	0.00313	Y=0.0863x+0.0325
	II	10.54	4.6749	0.8460	0.00178	Y=0.0203x+0.0949
	III	10.54	4.8876	0.8808	0.00170	Y=-0.2046x+10.541
	IV	10.90	4.3048	0.8808	0.00193	Y=-4.3048x+46.912

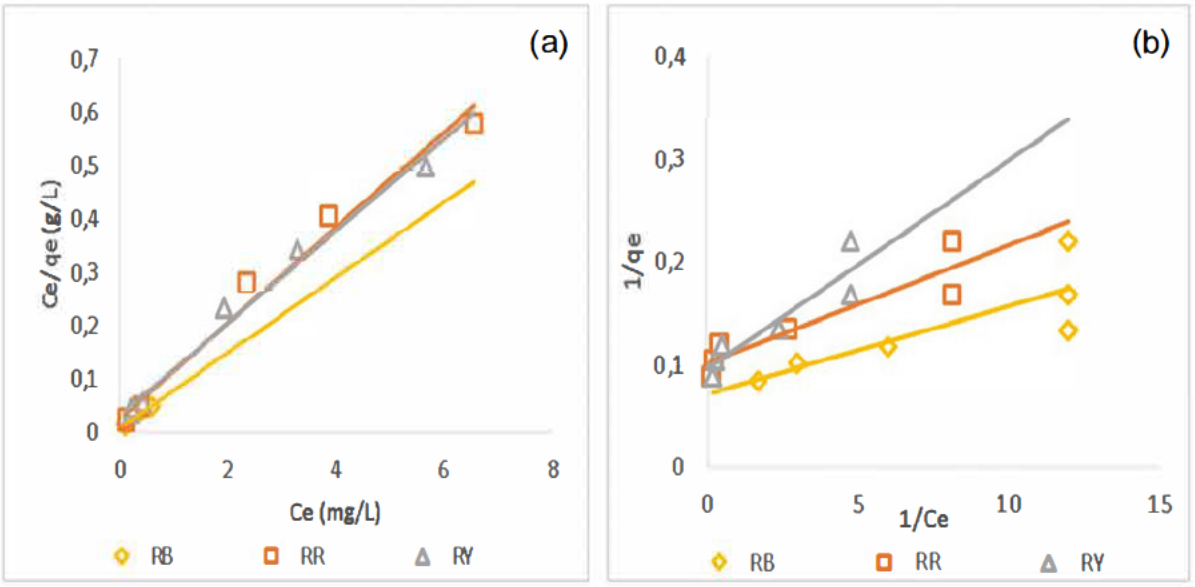

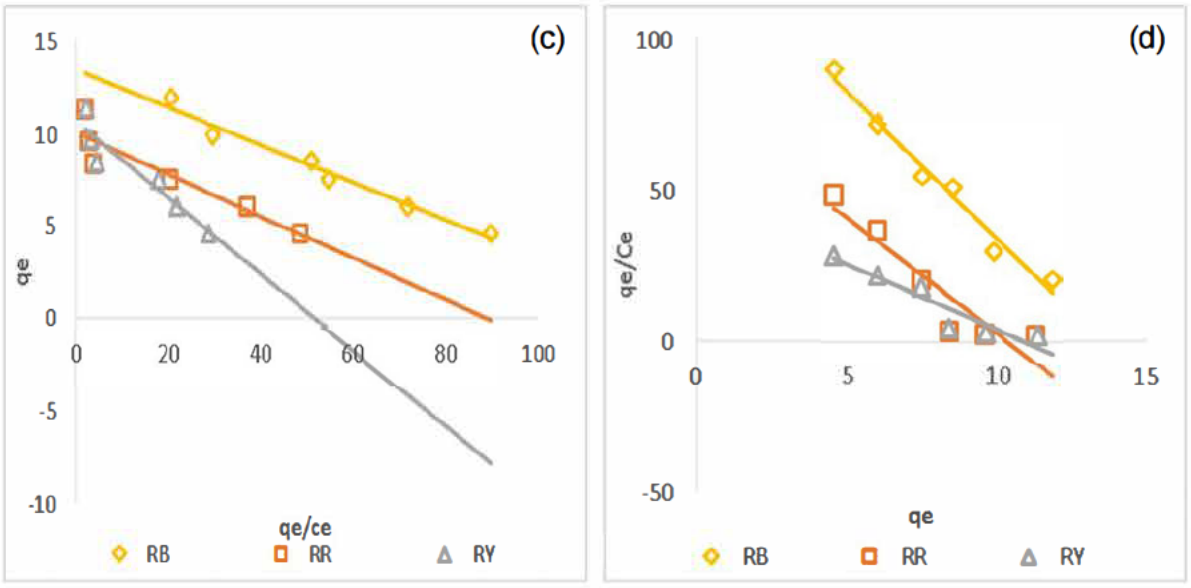

Figure 4.43 Iron oxide/H_3PO_4-AC Langmuir isotherm plots type (a)I, (b)II, (c) III, and (d) IV (C_o=120 mg L^{-1}, volume=50 mL, pH=6, T=25°C)

4.10.2 Freundlich Isotherm Application

The experimental data was also fitted on the Freundlich isotherm model (Freundlich and Hatfield 1926), with the equation, symbols and meanings represented in chapter 2 of this dissertation in equation 2.9. This system was tested to determine the heterogeneity of the reaction that took place between the RB, RR, RY dye molecules onto the surface of the iron oxide/H_3PO_4-AC composite adsorbent. The intensity of the reaction n lies between 1-10 for all three dyes, meaning that the reaction was favourable (Dada *et al.* 2012).

Table 4.12 Freundlich isotherm adsorption parameters for the iron oxide/H_3PO_4-AC composite

Type of Dye	**1/n**	**n (g L^{-1})**	**K_f (mg g^{-1})**	**R^2**	**Linear Equation**
RB	0.3645	2.74	14.87	0.7751	Y=0.3645x+1.1722
RR	0.1736	5.76	7.791	0.8780	Y=0.1736x+0.8916
RY	0.2131	4.69	7.674	0.8692	Y=0.2131x+0.855

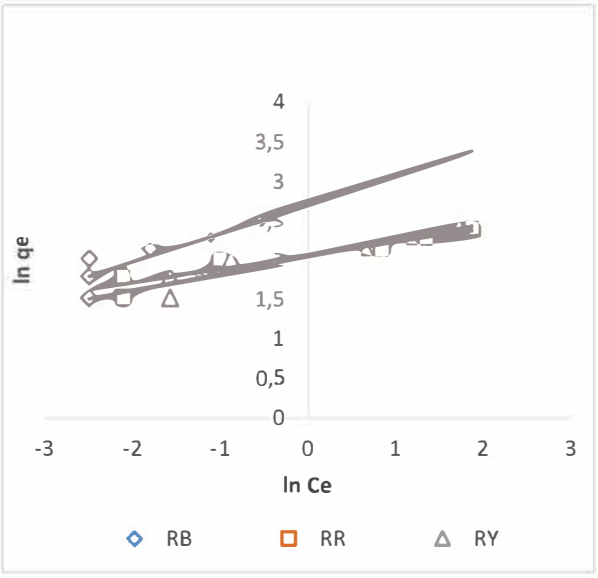

Figure 4.44 Iron oxide/H_3PO_4-AC composite Freundlich isotherm plot (C_o=120 mg L^{-1}, pH=6, T=25°C)

4.10.3 Dubinin-Radushkevich Isotherm Application

Figure 4.45 and Table 4.13 show the experimental data for the RB, RR and RY dye mixture of 120 mg/L fitted on the Dubinin Radushkevich isotherm model (Dubinin and Stoeckli 1980) onto the surface of the iron oxide/H_3PO_4-AC composite to determine the homogeneity or heterogeneity of the adsorbent surface to distinguish if the reaction is physical or chemical adsorption (Ayawei, Ebelegi and Wankasi 2017). The equations and meaning of this isotherm are illustrated in chapter 2 of this dissertation in equation 2.10. The total amount of dye molecules adsorbed was 32.7232 per unit mass, which was lower than that of Langmuir isotherm type I, which resulted in 36.9500 total molecules of dye per unit mass. The total energy required was 1.9142 kJ mol^{-1} confirming the physisorption process occurred.

Table 4.13 Dubinin-Radushkevich adsorption isotherm parameters for iron oxide/H_3PO_4-AC

Type of Dye	K_{ad} ($mol^2\ KJ^{-2}$)	q_s ($mg\ g^{-1}$)	R^2	E ($J\ mol^{-1}$)	Linear Equation
RB	$1X10^{-6}$	13.067	0.7876	707.1	$Y=-1x10^{-6}x+2.5701$
RR	$1X10^{6}$	9.683	0.8619	707.1	$Y=-1x10^{-6}x+2.2704$
RY	$2X10^{-6}$	9.9732	0.8619	500.0	$Y=-2x10^{-6}x+2.2999$

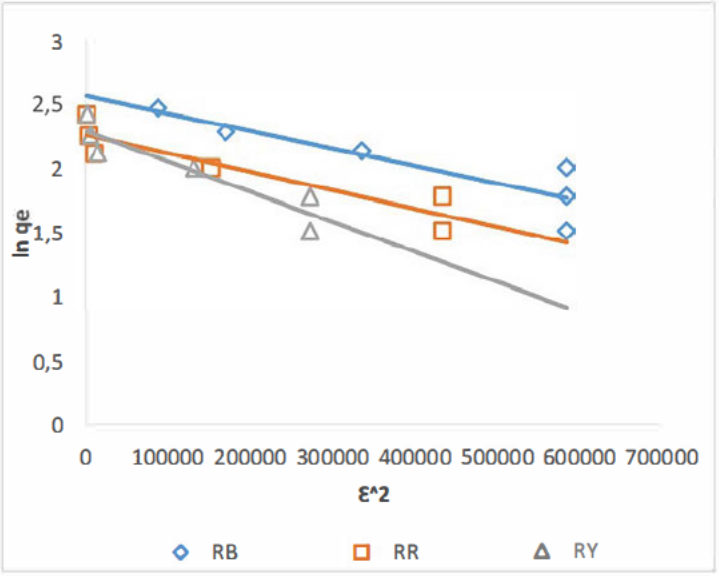

Figure 4.45 Iron oxide/H_3PO_4-AC composite D-R isotherm plot (C_o=120mg L^{-1}, pH=6, volume=50 mL, T=25ºC)

4.10.4 Temkin Isotherm Application

The Temkin isotherm (Temkin and Pyzhev 1940) was employed on the experimental data to obtain the heat of adsorption required for either a physical or chemical process. The equations used with definitions are illustrated in chapter 2 of this dissertation in equation 2.11. The Temkin isotherm heat of adsorption constant calculated from the plots in Figure 4.46, and stipulated in Table 4.14 for the RB, RR and RY dye mixture are: 2.9533 J mol^{-1}; 1.3066 J mol^{-1}; 1.6231 J mol^{-1} respectively. This indicates the physical adsorption nature of the reaction that took place between the adsorbent (iron oxide/H_3PO_4-AC) and the adsorbate (mixture of reactive azo dyes).

Table 4.14 Temkin adsorption isotherm parameters for iron oxide/H_3PO_4-AC composite

Type of Dye	**B (J mol^{-1})**	**b_T**	**A_T (L g^{-1})**	**R^2**	**Linear Equation**
RB	2.9533	557.82	93.723	0.8523	Y=2.7238x+12.842
RR	1.3066	1260.8	499.00	0.9042	Y=1.3066x+8.1174
RY	1.6231	1014.9	139.67	0.9126	Y=1.7449x+8.1712

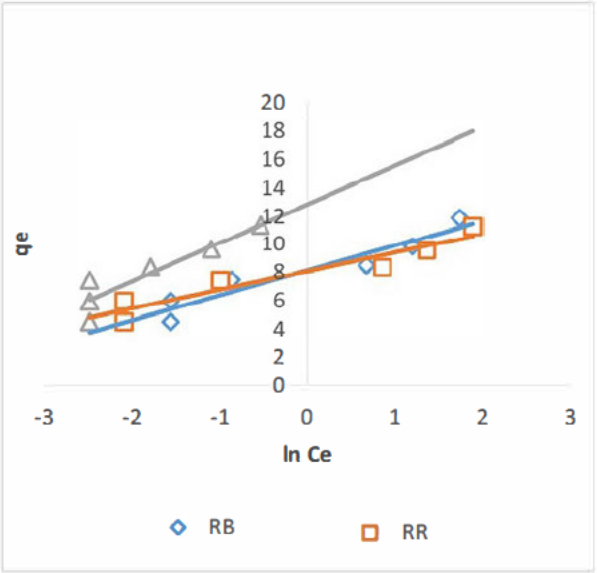

Figure 4.46 Iron oxide/H_3PO_4-AC composite for Temkin isotherm plot (C_o=120 mg L^{-1}, volume=50 mL, pH=6) for RB, RR, RY ternary system

4.11 Adsorption Kinetics Studies of Iron Oxide/H_3PO_4-AC Composite

The adsorption process was further tested using the famous Lagergren's pseudo 1st order (Lagergren 1898) and Ho & McKay's pseudo 2nd order (Ho and McKay 1999) kinetic models. The experimental data was also employed using the intraparticle diffusion equation (Weber and Morris 1963) to determine the mechanism of the solute/ the rate limiting steps of the adsorption process. The equations, symbols and definitions are stipulated in chapter 2 of this dissertation, in section 2.4.1.2 adsorption kinetics: equations 2.12, 2.13 and 2.14. This adsorption process did not fit the Lagergren's pseudo 1st order as the q_e values (Table 4.15) did not correlate with the experimental data, hence discrediting the suitability of the model for the removal of the mixture of reactive azo dyes on the surface of iron oxide/H_3PO_4-AC composite. The correlation coefficient (R^2) values for the Ho and McKay's pseudo 2nd order kinetic model was the best fit within the linear plot for all 3 dyes as they are above 0.9726, with q_e values are in good agreement with experimental values (Table 4.16 and figure 4.48). In Table 4.17, the parameters of the intraparticle diffusion model are displayed. Figure 4.50 (a-c) show that adsorption is not the only rate limiting step as the graph does not pass through the origin (Qiu *et al.* 2009). However, only a major gradual step is observed which confirms the monolayer coverage (Gong *et al.* 2009) that correlates well with the Langmuir isotherm type I model.

4.11.1 Lagergren Pseudo 1st Order Kinetic Model

Table 4.15 Lagergren pseudo 1st order kinetic parameters for the iron oxide/H_3PO_4-AC composite as an adsorbent

Dye Concentration	Linear Equation	R^2	K_{L1} (min^{-1})	q_e (mg g^{-1})
RB 20 ppm	$y = -4.0x10^{-6}x + 1.1795$	0.7500	$9.212 x10^{-6}$	15.118
40 ppm	$y = -8.0x10^{6}x + 1.1068$	0.8929	$1.842 x10^{-5}$	12.788
60 ppm	$y = -1.0x10^{5}x + 1.0120$	0.7503	$2.303 x10^{-5}$	10.280
80 ppm	$y = -2.0x10^{-5}x + 0.9022$	0.7209	$4.606 x10^{-5}$	7.9836
100 ppm	$y = -5.0x10^{-4}x + 0.7555$	0.8574	$1.152 x10^{-4}$	5.6951
120ppm	$y = -6.0x10^{-4}x + 0.5232$	0.6758	$1.382 x10^{-4}$	3.3358
RR 20 ppm	$y = -4.0x10^{6}x + 1.0871$	0.7500	$9.212 x10^{-6}$	12.221
40 ppm	$y = -5.0x10^{-6}x + 0.9949$	0.7500	$1.152x10^{-5}$	9.8833
60 ppm	$y = -7.0x10^{6}x + 0.8679$	0.7500	$1.612 x10^{-5}$	7.3773
80 ppm	$y = -2.0x10^{-5}x + 0.7062$	0.9412	$4.606 x10^{-5}$	5.0839
100 ppm	$y = -4.0x10^{5}x + 0.4444$	0.9426	$9.212 x10^{-5}$	2.7823
120 ppm	$y = -3.0x10^{-4}x - 0.3678$	0.7235	$6.909 x10^{-4}$	0.4287
RY 20 ppm	$y = -3.0 x10^{6}x + 1.0870$	0.5000	$6.909 x10^{-6}$	12.218
40 ppm	$y = -5.0 x10^{-6}x + 0.9950$	0.7500	$1.152 x10^{-5}$	9.8855
60 ppm	$y = -1.0 x10^{-5}x + 0.8679$	0.8000	$2.303 x10^{-5}$	7.3773
80 ppm	$y = -3.0 x10^{-5}x + 0.7067$	0.9425	$6.909 x10^{-5}$	5.0898
100 ppm	$y = -7.0 x10^{-5}x + 0.4460$	0.7816	$1.612 x10^{-4}$	2.7925
120 ppm	$y = -4.0 x10^{4}x - 0.3492$	0.7758	$9.212 x10^{-4}$	0.4475

4.11.2 Ho and McKay's Pseudo 2nd Order Kinetic Model

Table 4.16 Ho and McKay's pseudo 2nd order kinetic parameters of iron oxide/H_3PO_4-AC as an adsorbent

Dye Concentration	Linear Equation	R^2	K_{H2} (g mg^{-1})	q_e (mg g^{-1})
RB 20 ppm	y = 0.3356x + 1.9910	0.9729	1.4533	2.8935
40 ppm	y = 0.1730x + 0.9975	0.9727	0.1734	5.7803
60 ppm	y = 0.1127x + 0.6453	0.9732	0.1746	8.8731
80 ppm	y = 0.0854x + 0.4875	0.9730	0.1752	11.710
100 ppm	y = 0.0686x + 0.3938	0.9729	0.1742	14.577
120 ppm	y = 0.0573x + 0.3267	0.9730	0.1754	17.452
RR 20 ppm	y = 0.3456x + 2.0019	0.9726	0.1726	2.8935
40 ppm	y = 0.1731x + 0.9923	0.9728	0.1744	5.7770
60 ppm	y = 0.1127x + 0.6438	0.9728	0.1751	8.8731
80 ppm	y = 0.0853x + 0.4886	0.9729	0.1746	11.723
100 ppm	y = 0.0687x + 0.3922	0.9731	0.1752	14.556
120 ppm	y = 0.0570x + 0.3345	0.9738	0.1704	17.544
RY 20 ppm	y = 0.3462x + 1.9964	0.9735	0.1734	2.8885
40 ppm	y = 0.1734x + 0.9903	0.9729	0.1751	5.7670
60 ppm	y = 0.1128x + 0.6441	0.9732	1.7513	8.8652
80 ppm	y = 0.0855x + 0.4890	0.9731	0.1748	11.696
100 ppm	y = 0.0687x + 0.3929	0.9730	0.1749	14.556
120 ppm	y = 0.0573x + 0.3273	0.9730	0.1751	17.4520

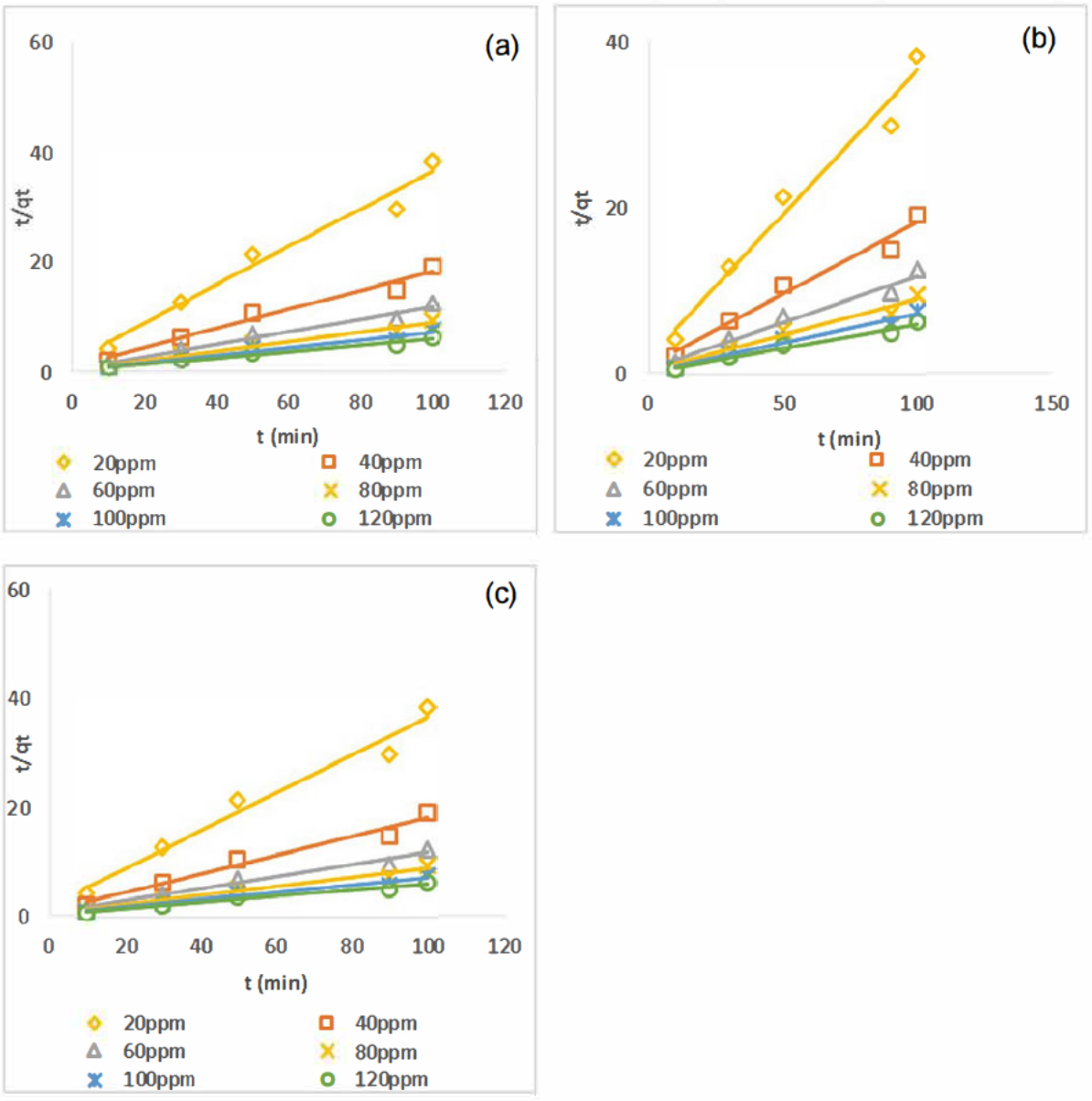

Figure 4.47 Ho and McKay's pseudo 2nd order plot for (a) RB, (b) RR, and (c) RY using iron oxide/H_3PO_4-AC composite (C_o=120mg L^{-1}, volume=50 mL, pH=6, T=25°C)

4.11.3 Intraparticle Diffusion Model of Iron Oxide/H_3PO_4-AC Composite

Table 4.17 Intraparticle diffusion of the dye mixture using iron oxide/H_3PO_4-AC composite as an adsorbent

	DYES ($mg\ L^{-1}$)					
RB	**20**	**40**	**60**	**80**	**100**	**120**
K_{IPD}	0.0016	0.0029	0.0039	0.0047	0.0065	0.0062
R^2	0.7725	0.9211	0.8230	0.8416	0.9626	0.8045
RR						
K_{IPD}	0.0013	0.0013	0.0013	0.038	0.0035	0.0035
R^2	0.6619	0.6619	0.6619	0.0038	0.0035	0.0035
RY						
K_{IPD}	0.0009	0.0016	0.0021	0.0038	0.0057	0.0059
R^2	0.3895	0.7725	0.8102	0.9613	0.8794	0.8760

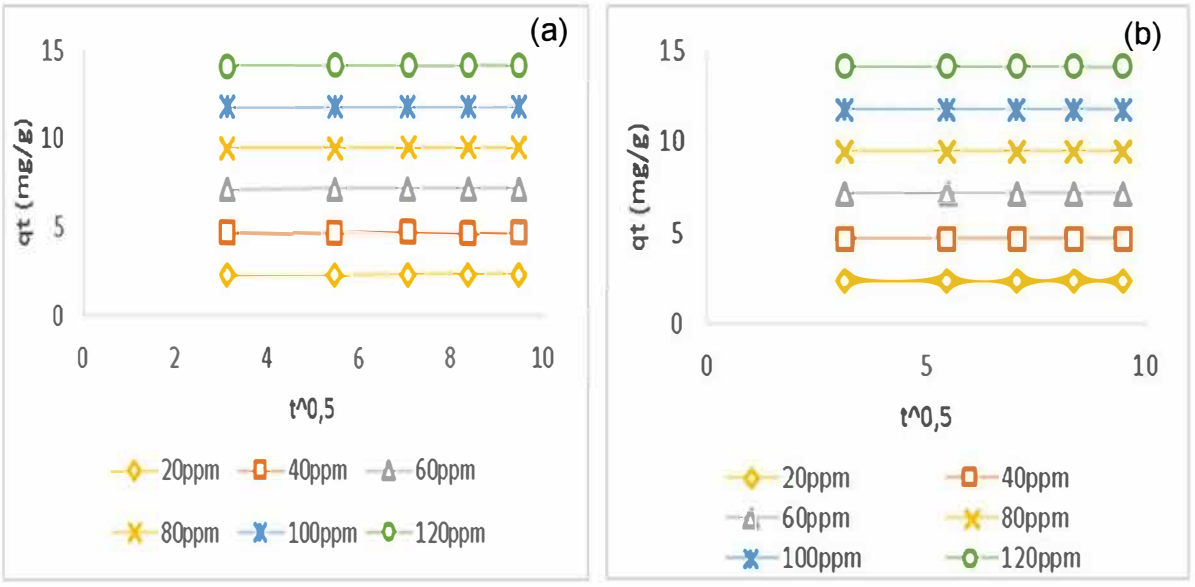

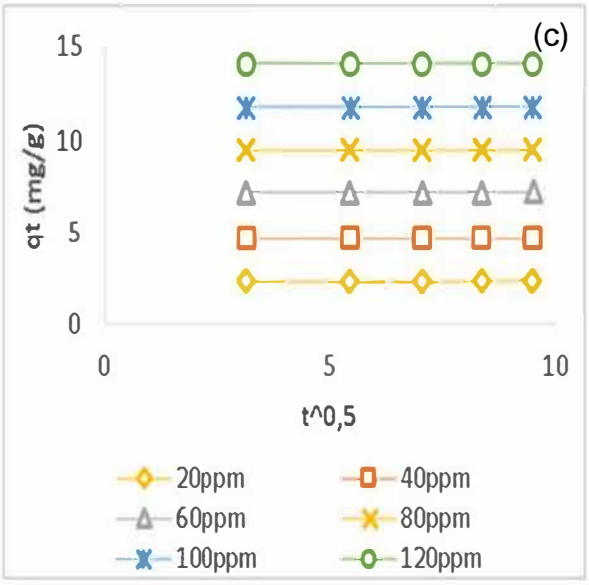

Figure 4.48 Intraparticle diffusion plot of (a) RB, (b) RR, and (c) RY using iron oxide/H_3PO_4-AC composite (C_o=120 mg L^{-1}, volume=50 mL, pH=6, T=25^{o}C)

4.12 References

Al-Degs, Y. S., El-Barghouthi, M. I., El-Sheikh, A. H. and Walker, G. M. 2008. Effect of solution pH, ionic strength, and temperature on adsorption behaviour of reactive dyes on activated carbon. *Dyes and Pigments*, 77 (1): 16-23.

Amin, N. K. 2009. Removal of direct blue-106 dye from aqueous solution using new activated carbons developed from pomegranate peel: Adsorption equilibrium and kinetics. *Journal of Hazardous Materials*, 165 (1): 52-62.

Anjum, H. and Murugesan, T. 2016. Effect of Functionalization Condition on Characterization of Carbonaceous Adsorbent. *Procedia Engineering*, 148: 1346-1350.

Ayawei, N., Ebelegi, A. N. and Wankasi, D. 2017. Modelling and interpretation of adsorption isotherms. *Journal of Chemistry*, 2017:1-11.

Bellamy, L. J. 1975. The infra-red spectra of complex molecules. *Chapman and Hall London* (3rd edition).

Bourbigot, S., Le Bras, M., Delobel, R., Bréant, P. and Trémillon, J.-m. 1995. Carbonization mechanisms resulting from intumescence-part II. Association with an ethylene terpolymer and the ammonium polyphosphate-pentaerythritol fire retardant system. *Carbon*, 33 (3): 283-294.

Cazetta, A. L., Pezoti, O., Bedin, K. C., Silva, T. L., Paesano Junior, A., Asefa, T. and Almeida, V. C. 2016. Magnetic activated carbon derived from biomass waste by concurrent synthesis: efficient adsorbent for toxic dyes. *ACS Sustainable Chemistry & Engineering*, 4 (3): 1058-1068.

Chandra, T. C., Mirna, M. M., Sunarso, J., Sudaryanto, Y. and Ismadji, S. 2009. Activated carbon from durian shell: Preparation and characterization. *Journal of the Taiwan Institute of Chemical Engineers*, 40 (4): 457-462.

Chen, J. P. and Wu, S. 2004. Acid/base-treated activated carbons: characterization of functional groups and metal adsorptive properties. *Langmuir*, 20 (6): 2233-2242.

Chen, Y., Zhu, Y., Wang, Z., Li, Y., Wang, L., Ding, L., Gao, X., Ma, Y. and Guo, Y. 2011. Application studies of activated carbon derived from rice husks produced by chemical-thermal process—A review. *Advances in Colloid and Interface Science*, 163 (1): 39-52.

heung, W. H., Szeto, Y. S. and McKay, G. 2007. Intraparticle diffusion processes during acid dye adsorption onto chitosan. *Bioresource Technology*, 98 (15): 2897-2904.

Corbrjdge, D. 1956. Infra-red analysis of phosphorus compounds. *Journal of Applied Chemistry*, 6 (10): 456-465.

Dada, A., Olalekan, A., Olatunya, A. and Dada, O. 2012. Langmuir, Freundlich, Temkin and Dubinin–Radushkevich isotherms studies of equilibrium sorption of Zn2+ unto phosphoric acid modified rice husk. *IOSR Journal of Applied Chemistry*, 3 (1): 38-45.

Demiral, H. and Demiral, İ. 2008. Surface properties of activated carbon prepared from wastes. Surface and Interface Analysis: An International Journal devoted to the development and application of techniques for the analysis of surfaces, interfaces and thin films, 40 (3-4): 612-615.

Deng, H., Zhang, G., Xu, X., Tao, G. and Dai, J. 2010. Optimization of preparation of activated carbon from cotton stalk by microwave assisted phosphoric acid-chemical activation. Journal of Hazardous Materials, 182 (1): 217-224.

Doğan, M., Abak, H. and Alkan, M. 2009. Adsorption of methylene blue onto hazelnut shell: Kinetics, mechanism and activation parameters. Journal of Hazardous Materials, 164 (1): 172-181.

Dubinin, M. M. and Stoeckli, H. F. 1980. Homogeneous and heterogeneous micropore structures in carbonaceous adsorbents. *Journal of Colloid and Interface Science*, 75 (1): 34-42.

Eisa, M. Y., Dabbas, M. and Abdulla, F. H. 2015. Quantitative identification of phosphate using X-Ray diffraction and Fourier transfor infra red (FT-IR) spectroscopy. *International Journal of Current Microbiology and Applied Science*, 4 (1) 270-283.

Fiuza, R. A., Medeiros de Jesus Neto, R., Correia, L. B. and Carvalho Andrade, H. M. 2015. Preparation of granular activated carbons from yellow mombin fruit stones for CO2 adsorption. *Journal of Environmental Management*, 161: 198-205.

Foo, K. Y. and Hameed, B. H. 2011. Utilization of rice husks as a feedstock for preparation of activated carbon by microwave induced KOH and K2CO3 activation. *Bioresource Technology*, 102 (20): 9814-9817.

Freundlich, H. 1926. Colloid and capillary-Translated from the third German edition by H. *Stafford Hartfield. Methuen and Co, Ltd, London.*

Freundlich, H. and Hatfield, H. S. 1926. *Colloid and capillary chemistry*. Methuen And Co. Ltd; London.

Gañan, J., González-García, C. M., González, J. F., Sabio, E., Macías-García, A. and Díaz-Díez, M. A. 2004. Preparation of activated carbons from bituminous coal pitches. *Applied Surface Science*, 238 (1): 347-354.

Gerçel, Ö., Özcan, A., Özcan, A. S. and Gerçel, H. F. 2007. Preparation of activated carbon from a renewable bio-plant of Euphorbia rigida by H2SO4 activation and its adsorption behavior in aqueous solutions. *Applied Surface Science*, 253 (11): 4843-4852.

Gong, J.-L., Wang, B., Zeng, G.-M., Yang, C.-P., Niu, C.-G., Niu, Q.-Y., Zhou, W.-J. and Liang, Y. 2009. Removal of cationic dyes from aqueous solution using magnetic multi-wall carbon nanotube nanocomposite as adsorbent. *Journal of Hazardous Materials*, 164 (2): 1517-1522.

González-García, P. 2018. Activated carbon from lignocellulosics precursors: A review of the synthesis methods, characterization techniques and applications. *Renewable and Sustainable Energy Reviews*, 82: 1393-1414.

Hampton, C., Demoin, D. and Glaser, R. E. 2010. Vibrational spectroscopy tutorial: sulfur and phosphorus. Organic Spectroscopy, *University of missouri.* Chemistry webbook.

Hamzaoui, M., Bestani, B. and Benderdouche, N. 2018. The use of linear and nonlinear methods for adsorption isotherm optimization of basic green 4-dye onto sawdust-based activated carbon. *Journal of Material and Environmental Science*, 9 (4): 1110-1118.

Ho, Y. S. and McKay, G. 1999. Pseudo-second order model for sorption processes. *Process Biochemistry*, 34 (5): 451-465.

Jiang, Z., Liu, Y., Sun, X., Tian, F., Sun, F., Liang, C., You, W., Han, C. and Li, C. 2003. Activated carbons chemically modified by concentrated H2SO4 for the adsorption of the pollutants from wastewater and the dibenzothiophene from fuel oils. *Langmuir*, 19 (3): 731-736.

Lagergren, S. 1898. About the theory of so-called adsorption of soluble substances. *Sven. Vetenskapsakad. Handingarl*, 24: 1-39.

Langmuir, I. 1916. The constitution and fundamental properties of solids and liquids. Part I. Solids. *Journal of the American Chemical Society*, 38 (11): 2221-2295.

Lee, S.-W., Daud, W. M. A. W. and Lee, M.-G. 2010. Adsorption characteristics of methyl mercaptan, dimethyl disulfide, and trimethylamine on coconut-based activated carbons modified with acid and base. *Journal of Industrial and Engineering Chemistry*, 16 (6): 973-977.

Li, Q., Yue, Q.-Y., Su, Y., Gao, B.-Y. and Li, J. 2009. Two-step kinetic study on the adsorption and desorption of reactive dyes at cationic polymer/bentonite. *Journal of Hazardous Materials*, 165 (1): 1170-1178.

Malash, G. F. and El-Khaiary, M. I. 2010. Piecewise linear regression: A statistical method for the analysis of experimental adsorption data by the intraparticle-diffusion models. *Chemical Engineering Journal*, 163 (3): 256-263.

Myglovets, M., Poddubnaya, O. I., Sevastyanova, O., Lindström, M. E., Gawdzik, B., Sobiesiak, M., Tsyba, M. M., Sapsay, V. I., Klymchuk, D. O. and Puziy, A. M. 2014. Preparation of carbon adsorbents from lignosulfonate by phosphoric acid activation for the adsorption of metal ions. *Carbon*, 80: 771-783.

Nahil, M. A. and Williams, P. T. 2012. Pore characteristics of activated carbons from the phosphoric acid chemical activation of cotton stalks. *Biomass and Bioenergy*, 37: 142-149.

Oliveira, L. C. A., Rios, R. V. R. A., Fabris, J. D., Garg, V., Sapag, K. and Lago, R. M. 2002. Activated carbon/iron oxide magnetic composites for the adsorption of contaminants in water. *Carbon*, 40 (12): 2177-2183.

Órfão, J. J. M., Silva, A. I. M., Pereira, J. C. V., Barata, S. A., Fonseca, I. M., Faria, P. C. C. and Pereira, M. F. R. 2006. Adsorption of a reactive dye on chemically modified activated carbons—Influence of pH. *Journal of Colloid and Interface Science*, 296 (2): 480-489.

Özcan, A. S. and Özcan, A. 2004. Adsorption of acid dyes from aqueous solutions onto acid-activated bentonite. *Journal of Colloid and Interface Science*, 276 (1): 39-46.

Pathania, D., Sharma, S. and Singh, P. 2017. Removal of methylene blue by adsorption onto activated carbon developed from Ficus carica bast. *Arabian Journal of Chemistry*, 10: S1445-S1451.

Peláez-Cid, A.-A., Herrera-González, A.-M., Salazar-Villanueva, M. and Bautista-Hernández, A. 2016. Elimination of textile dyes using activated carbons prepared from vegetable residues and their characterization. *Journal of Environmental Management*, 181: 269-278.

Pereira, R. G., Veloso, C. M., da Silva, N. M., de Sousa, L. F., Bonomo, R. C. F., de Souza, A. O., Souza, M. O. d. G. and Fontan, R. d. C. I. 2014. Preparation of activated carbons from cocoa shells and siriguela seeds using H3PO4 and ZnCL2 as activating agents for BSA and α-lactalbumin adsorption. *Fuel Processing Technology*, 126: 476-486.

Peter Adkins, J. D. P. 2006. *Physical Chemistry*. 8 ed. United States and Canada: W.H. Freeman and Company.

Puziy, A. M., Poddubnaya, O. I., Martínez-Alonso, A., Suárez-García, F. and Tascón, J. M. D. 2002. Synthetic carbons activated with phosphoric acid: I. Surface chemistry and ion binding properties. *Carbon*, 40 (9): 1493-1505.

Qiu, H., Lv, L., Pan, B.-c., Zhang, Q.-j., Zhang, W.-m. and Zhang, Q.-x. 2009. Critical review in adsorption kinetic models. *Journal of Zhejiang University-Science A*, 10 (5): 716-724.

Raghunath, S., Anand, K., Gengan, R. M., Nayunigari, M. K. and Maity, A. 2016. Sorption isotherms, kinetic and optimization process of amino acid proline based polymer nanocomposite for the removal of selected textile dyes from industrial wastewater. *Journal of Photochemistry and Photobiology B: Biology*, 165: 189-201.

Shi, Z., Fan, D., Johnson, R. L., Tratnyek, P. G., Nurmi, J. T., Wu, Y. and Williams, K. H. 2015. Methods for characterizing the fate and effects of nano zerovalent iron during groundwater remediation. *Journal of Contaminant Hydrology*, 181: 17-35.

Shim, J.-W., Park, S.-J. and Ryu, S.-K. 2001. Effect of modification with HNO3 and NaOH on metal adsorption by pitch-based activated carbon fibers. *Carbon*, 39 (11): 1635-1642.

Simonin, J.-P. 2016. On the comparison of pseudo-first order and pseudo-second order rate laws in the modelling of adsorption kinetics. *Chemical Engineering Journal*, 300: 254-263.

Socrates, G. 1994. Infrared characteristic group frequencies 2nd edition. *John Wiely & Sons*.

Suárez-García, F., Martínez-Alonso, A. and Tascón, J. M. D. 2004. Activated carbon fibers from Nomex by chemical activation with phosphoric acid. *Carbon*, 42 (8): 1419-1426.

Subramanyam, B. and Das, A. 2009. Linearized and non-linearized isotherm models comparative study on adsorption of aqueous phenol solution in soil. *International Journal of Environmental Science & Technology*, 6 (4): 633-640.

Temkin, M. and Pyzhev, V. 1940. Recent modifications to Langmuir isotherms.

Waranusantigul, P., Pokethitiyook, P., Kruatrachue, M. and Upatham, E. S. 2003. Kinetics of basic dye (methylene blue) biosorption by giant duckweed (Spirodela polyrrhiza). *Environmental Pollution*, 125 (3): 385-392.

Weber, W. J. and Morris, J. C. 1963. Kinetics of adsorption on carbon from solution. *Journal of the Sanitary Engineering Division*, 89 (2): 31-60.

Xu, J., Chen, L., Qu, H., Jiao, Y., Xie, J. and Xing, G. 2014. Preparation and characterization of activated carbon from reedy grass leaves by chemical activation with H3PO4. *Applied Surface Science*, 320: 674-680.

Yagub, M. T., Sen, T. K., Afroze, S. and Ang, H. M. 2014. Dye and its removal from aqueous solution by adsorption: A review. *Advances in Colloid and Interface Science*, 209: 172-184.

Yazdanbakhsh, A., Hashempour, Y. and Ghaderpouri, M. 2018. Performance of granular activated carbon/nanoscale zero-valent iron for removal of humic substances from aqueous solution based on experimental design and response surface modeling. *Global Nest Journal*, 20 (1): 57-68.

CHAPTER 5: CONCLUSION AND RECOMMENDATIONS

Activated carbon materials were prepared from the leaves of *Plantago lanceolate* and activators H_3PO_4, H_2SO_4, NaOH and KOH. The structural morphology, functional groups, and other physico-chemical properties were determined using FTIR, TGA/DSC, SEM/EDX, and HRTEM. The activated carbon materials were used to determine the adsorption of a ternary mixture of three textile azo dyes after optimizing the initial concentration, dosage, contact time, pH and temperature. The phosphoric acid-based activated carbon (H_3PO_4-AC) material displayed the highest removal efficiency of 98,98%-100% compared to the other three activated materials. The Langmuir, Freundlich, Temkin and Dubinin-Radushkevich isotherms were applied; however, the data best fitted the Langmuir isotherm type 1 model. Furthermore, the rate of reaction followed the pseudo second-order kinetic model. In addition, an iron oxide-phosphoric acid-based activated carbon nanomaterial was prepared, characterized, and displayed a marginal improvement of removal efficiency of the ternary dye mixture.

Although the activated carbon materials displayed excellent adsorption capacity to remove some selected azo dyes, it is recommended that the optimum dosage of the activated materials and other classes of pigments such as acid dyes, mordant dyes, sulfur dyes and dispersive dyes be investigated. In addition, a fixed-bed column method could be compared against the batch method to ascertain the best methodology for dye removal.

APPENDICES

Appendix 1

SANBI
Biodiversity for Life

South African National Biodiversity Institute

Ref: **Plant Identification Dispatch List** **27 October 2016**

Client: Kaunda Thabisile
Address: Durban University Of Technology
Durban
4000

Tel:
Cell: 073 882 1580
Email: kaundathabisile@gmail.com

ID CODES:

0 = No challenges
1 = Specimen too poor to ID
2 = Label information inadequate
3 = Cannot match specimen in herbarium
4 = Specialist not available to do ID
5 = Genus requiring/under revision
6 = Specimen closest to name listed (cf)
7 = Please send more material
8 = Please refer to attached note/letter
9 = New record

FATE:

K = specimen kept for herbarium
R = specimen returned
S = specimen scrapped

	Collector	No.	Plant Name	Det. By	Det. Notes	ID Code	Fate
1	Kaunda Thabisile	s.n.	*Plantago lanceolata L.*	Ngwenya, A.M. 27/10/2016			R

Curator

Please note a handling fee is charged for each specimen received for identification. 1

Appendix 1 Sample identification: *Plantago Lanceolata L.*

Appendix 2

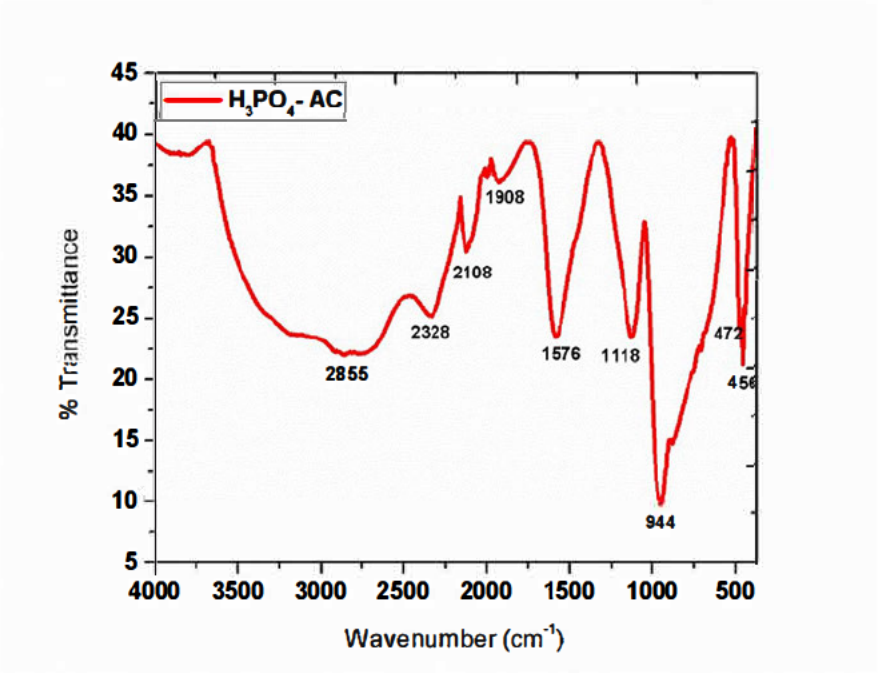

Appendix 2 FTIR spectra of phosphoric acid based activated carbon

Appendix 3

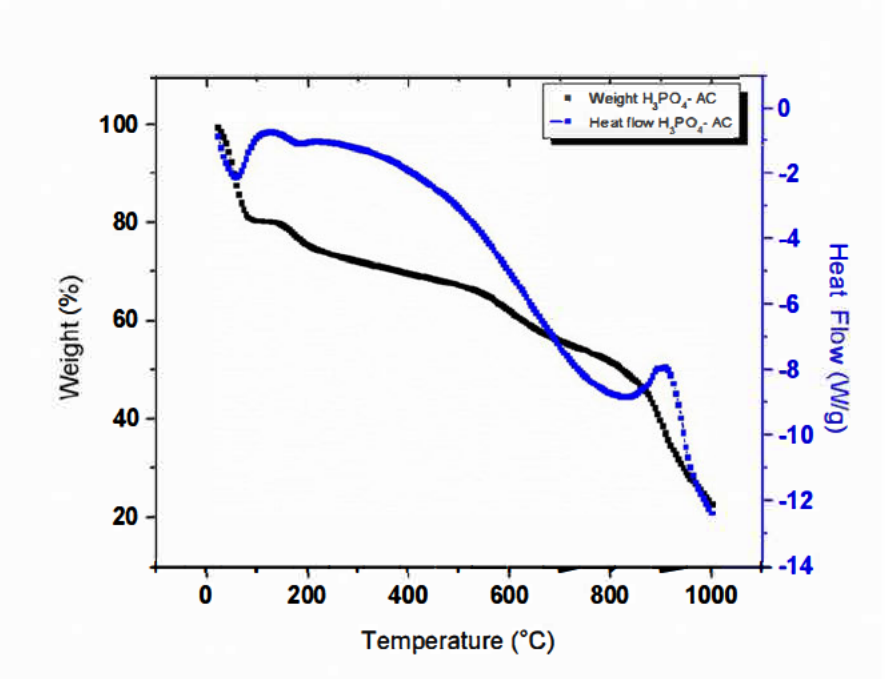

Appendix 3 TGA/DSC curve of phosphoric acid based activated carbon

Appendix 4

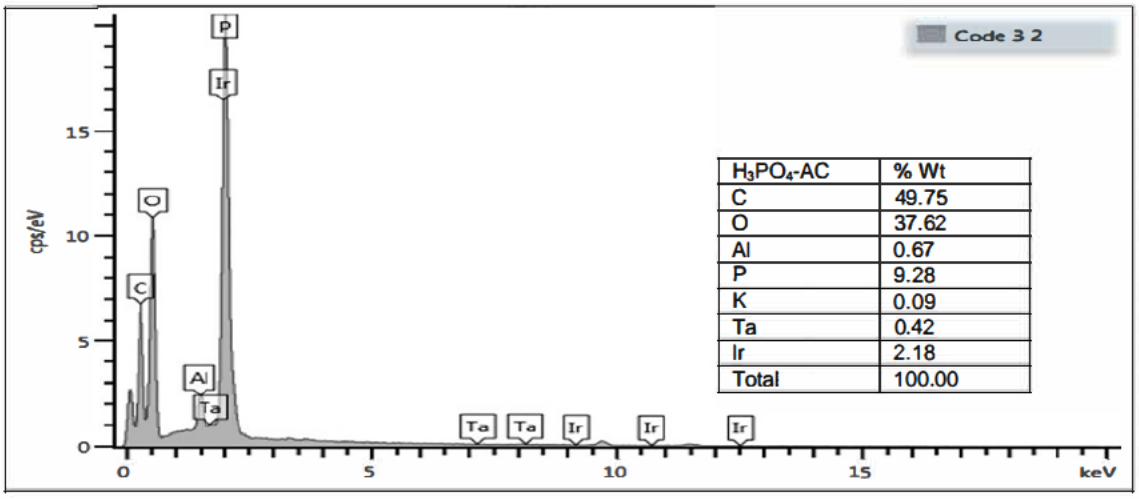

H_3PO_4-AC	% Wt
C	49.75
O	37.62
Al	0.67
P	9.28
K	0.09
Ta	0.42
Ir	2.18
Total	100.00

Appendix 4 EDX spectrum of phosphoric acid based activated carbon

Appendix 5

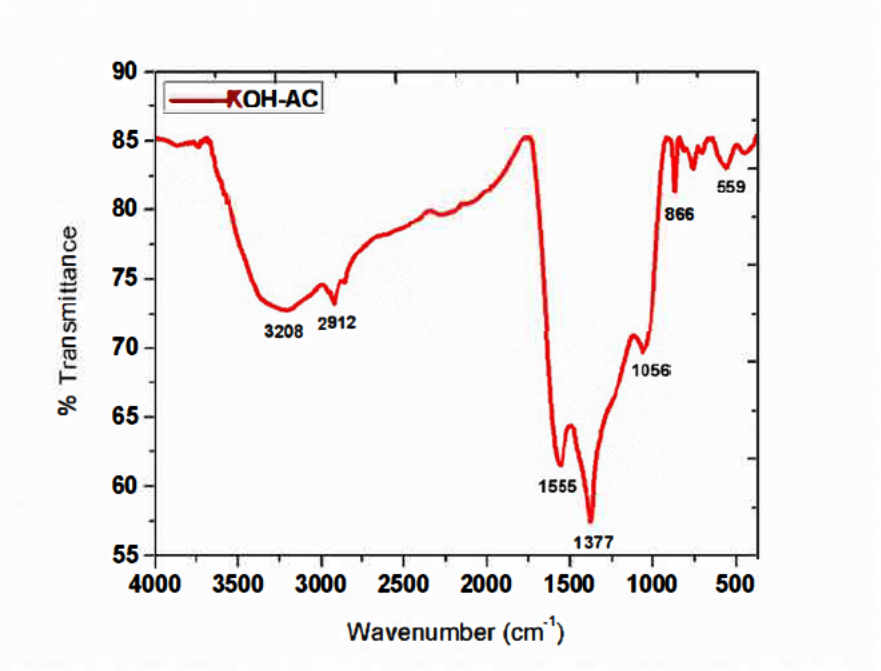

Appendix 5 FTIR spectrum of potassium hydroxide based activated carbon

Appendix 6

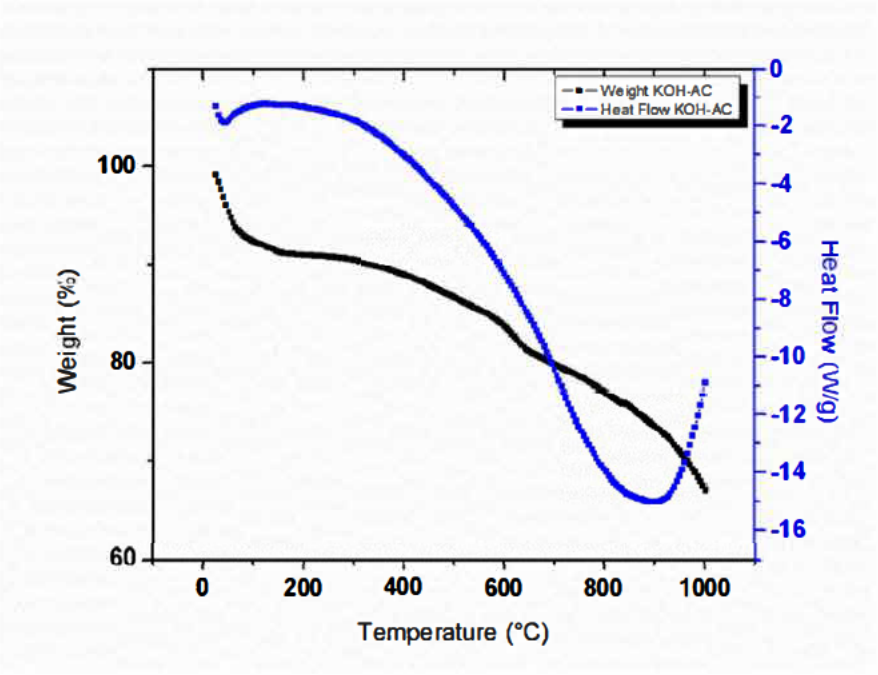

Appendix 6 TGA/DSC curve of potassium hydroxide based activated carbon

Appendix 7

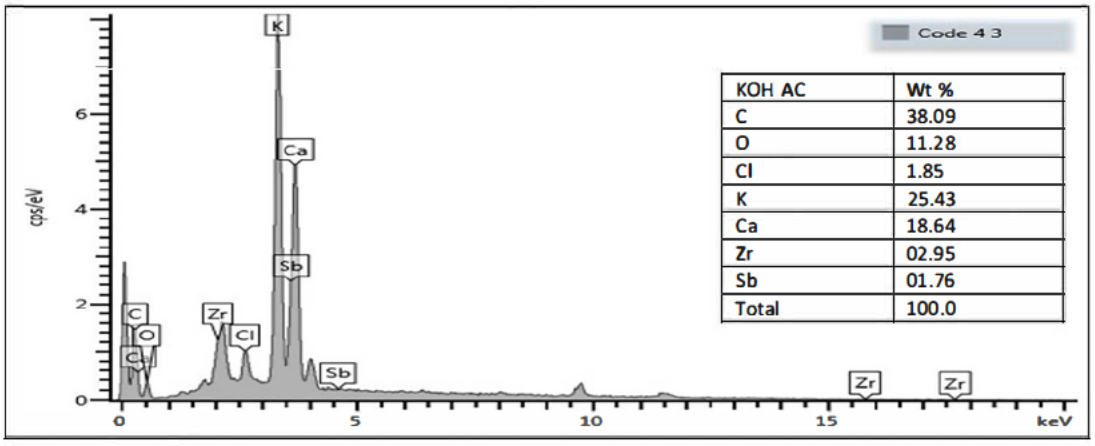

Appendix 7: EDS mapping spectrum of potassium hydroxide based activated carbon

Appendix 8

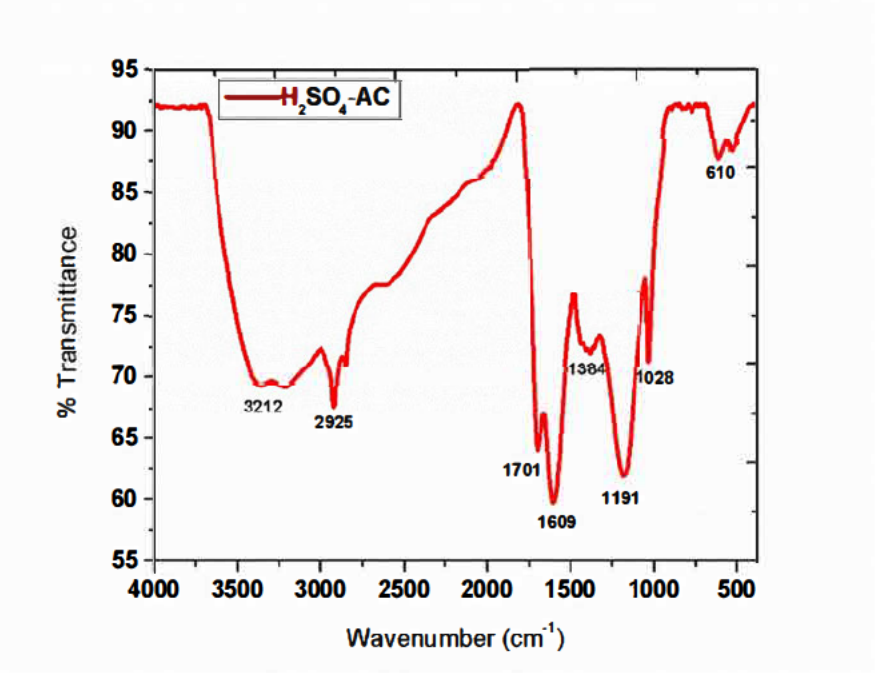

Appendix 8 FTIR spectrum of sulphuric acid based activated carbon

Appendix 9

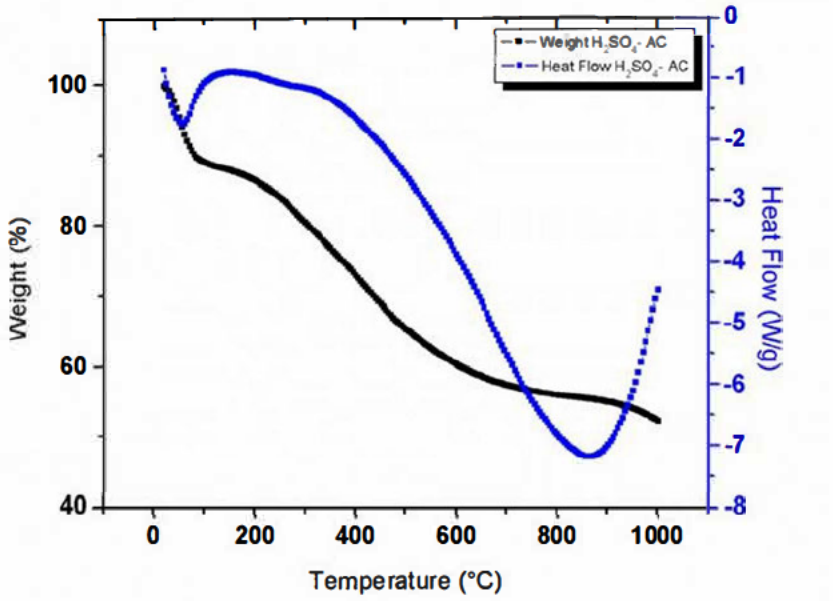

Appendix 9 TGA/DSC curve of sulphuric acid based activated carbon

Appendix 10

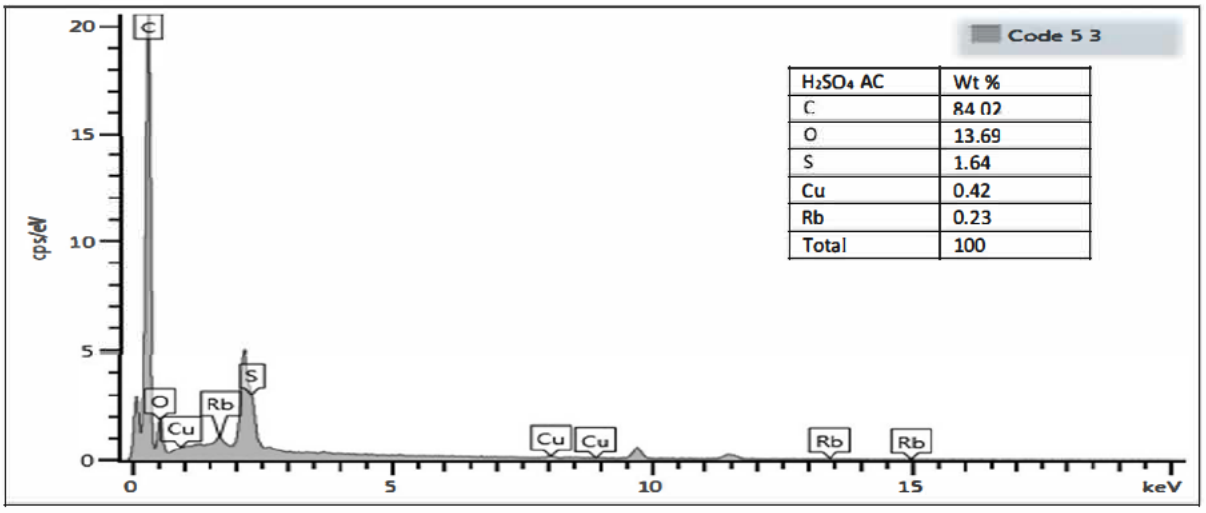

H_2SO_4 AC	Wt %
C	84.02
O	13.69
S	1.64
Cu	0.42
Rb	0.23
Total	100

Appendix 10 EDX spectrum of sulphuric acid based activated carbon

Appendix 11

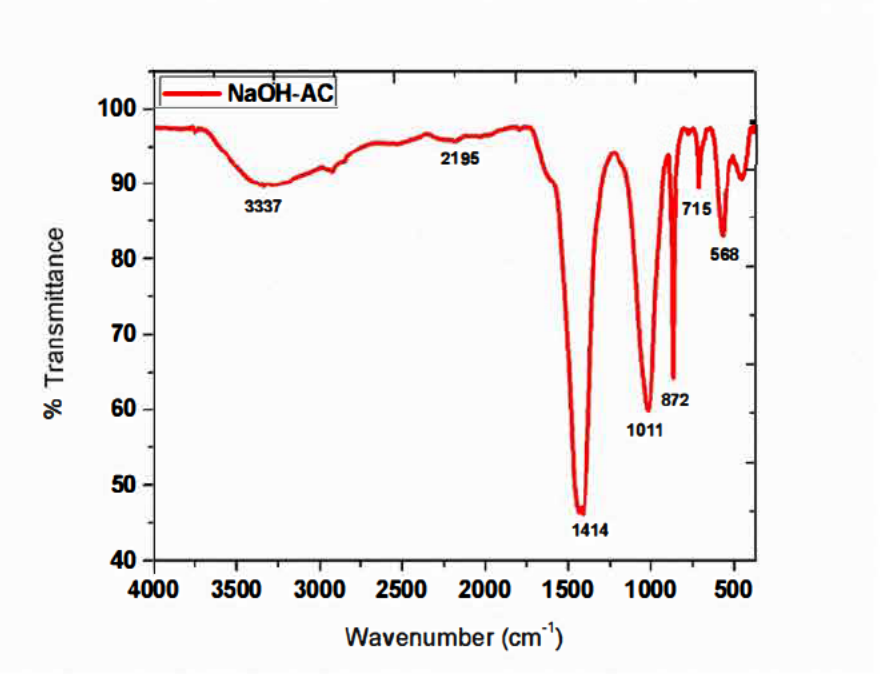

Appendix 11 FTIR spectrum of sodium hydroxide based activated carbon

Appendix 12

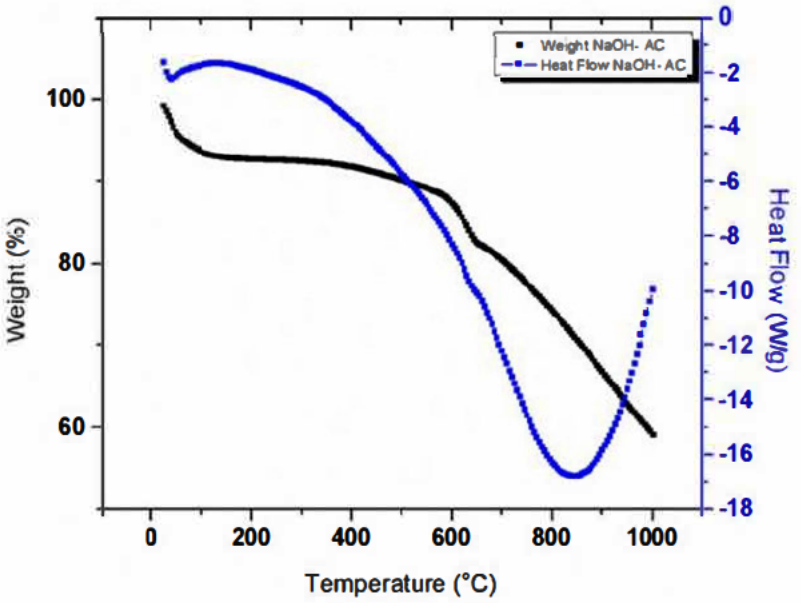

Appendix 12 TGA/DSC curve of sodium hydroxide based activated carbon

Appendix 13

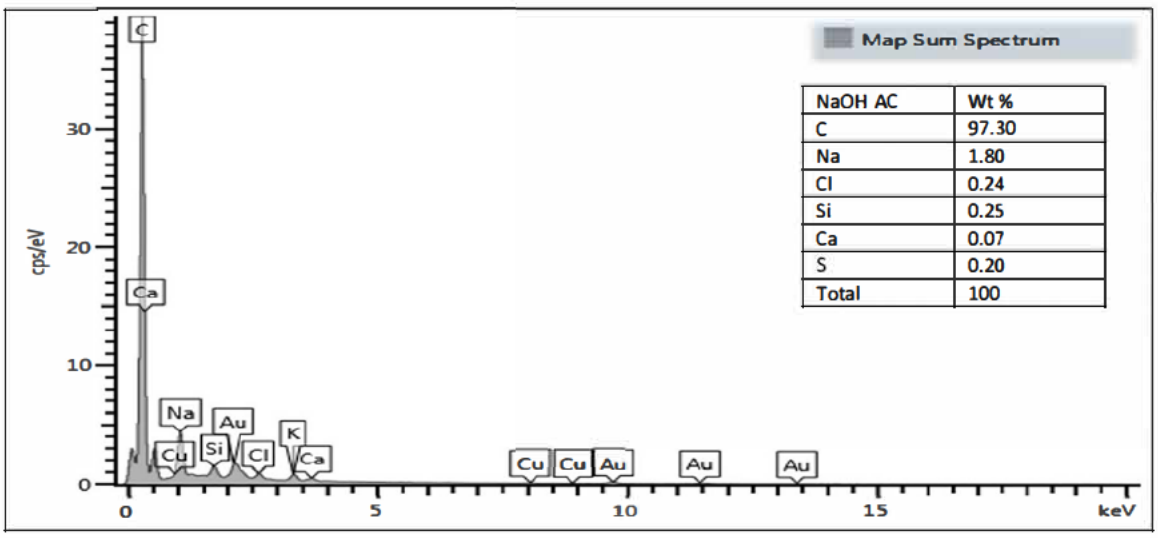

NaOH AC	Wt %
C	97.30
Na	1.80
Cl	0.24
Si	0.25
Ca	0.07
S	0.20
Total	100

Appendix 13 EDX spectrum of sodium hydroxide based activated carbon

Appendix 14

(a)

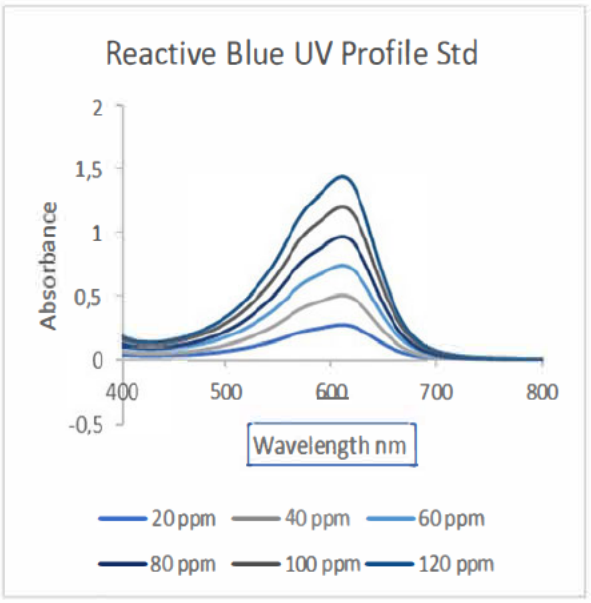

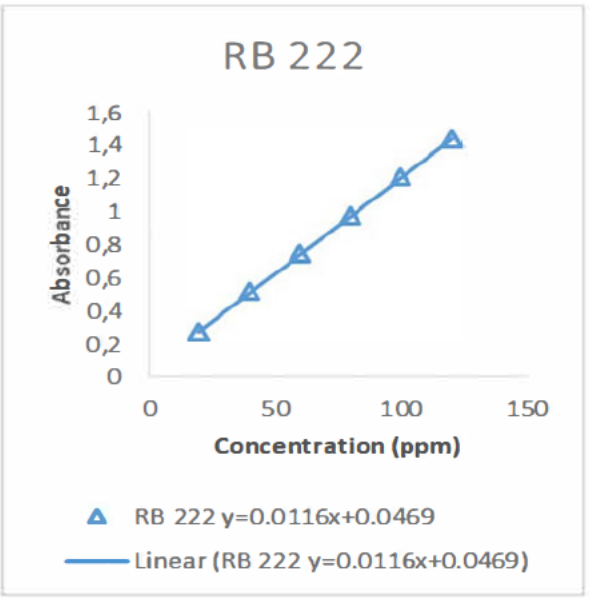

(b)

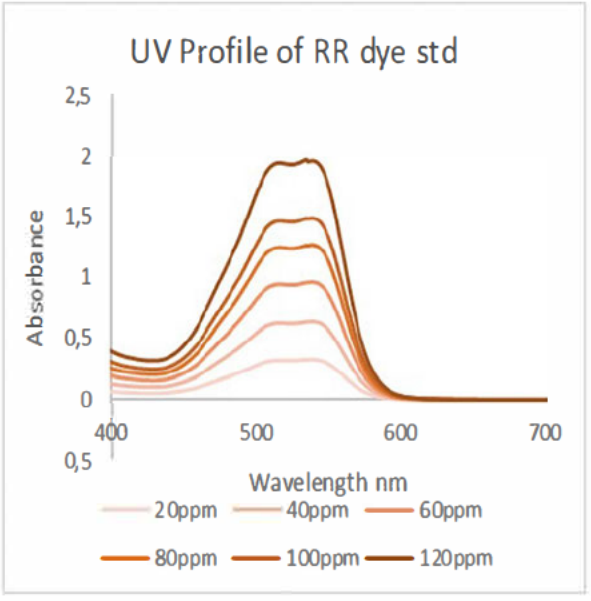

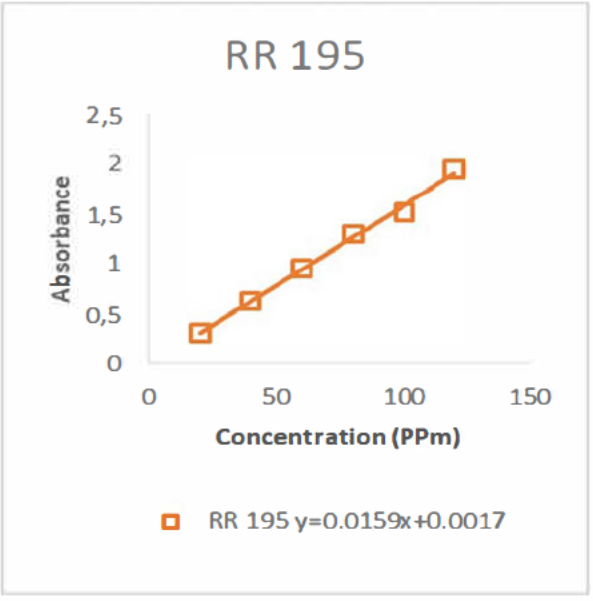

(c)

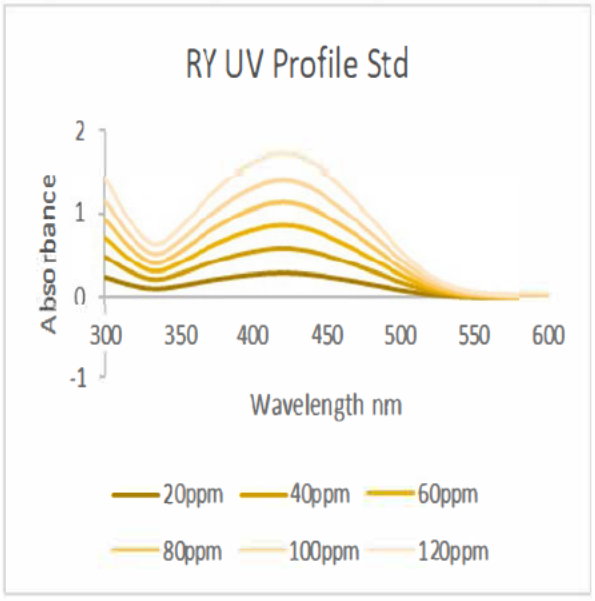

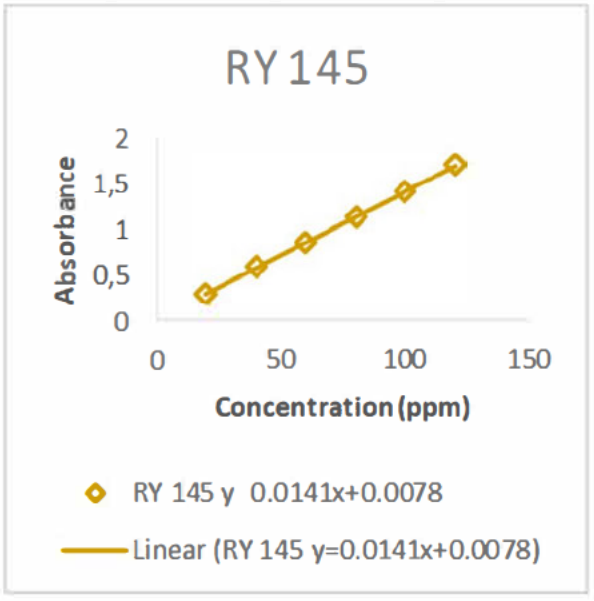

(d)

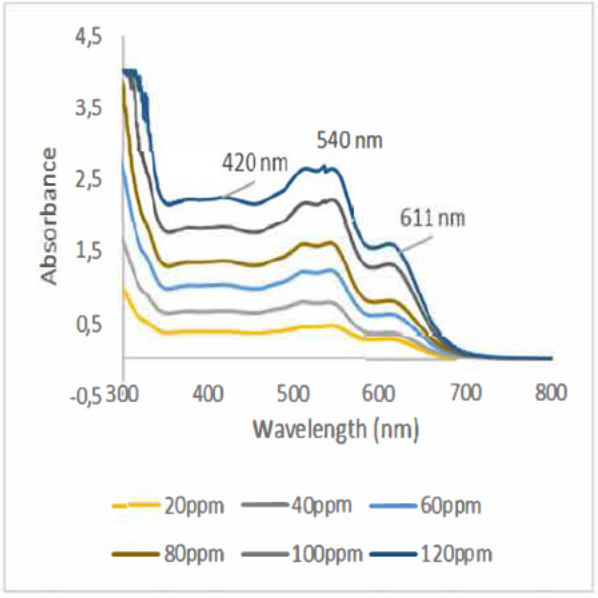

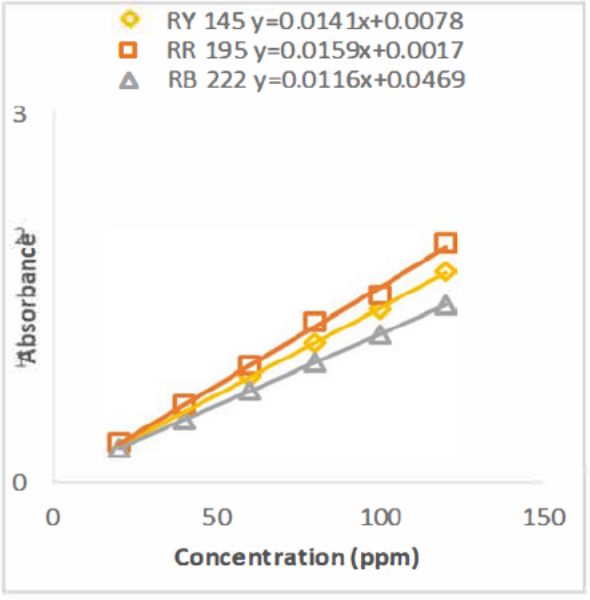

Appendix 14 UV spectra and calibration curve for dyes: (a) Reactive Blue 222 (b) Reactive Red 195 (c) Reactive Yellow 145 (d) dye mixture

Appendix 15

(a)

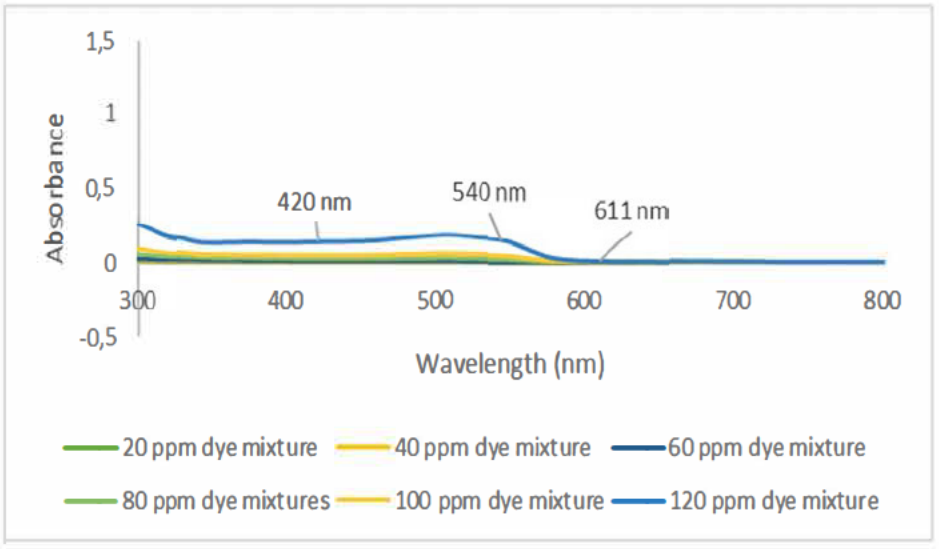

(b)

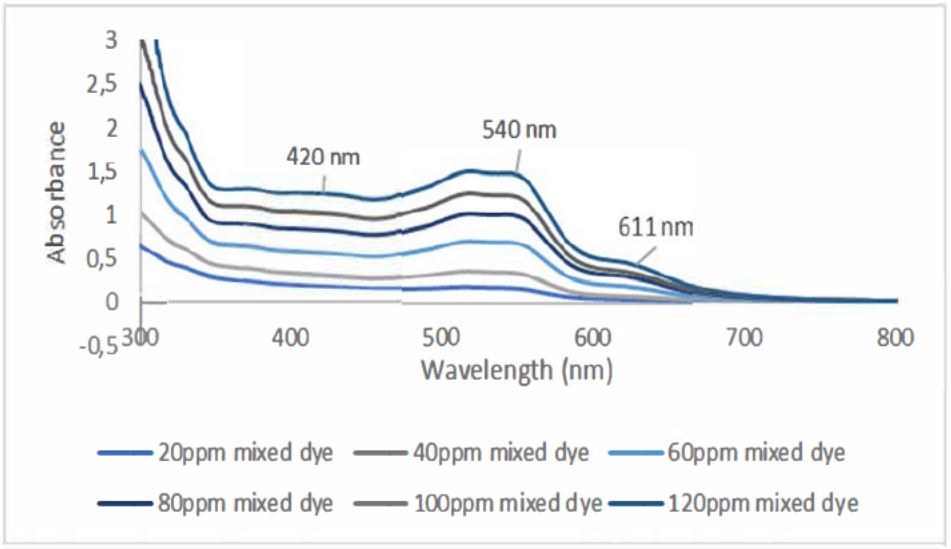

(c)

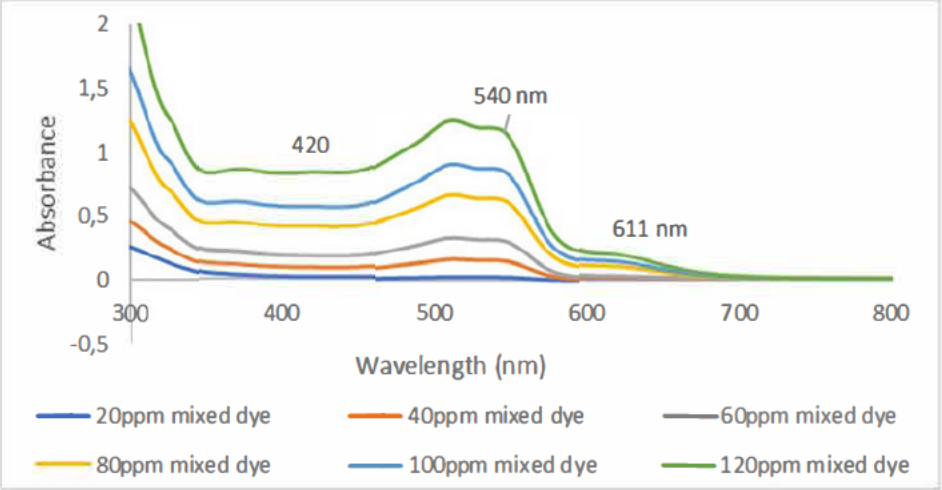

(d)

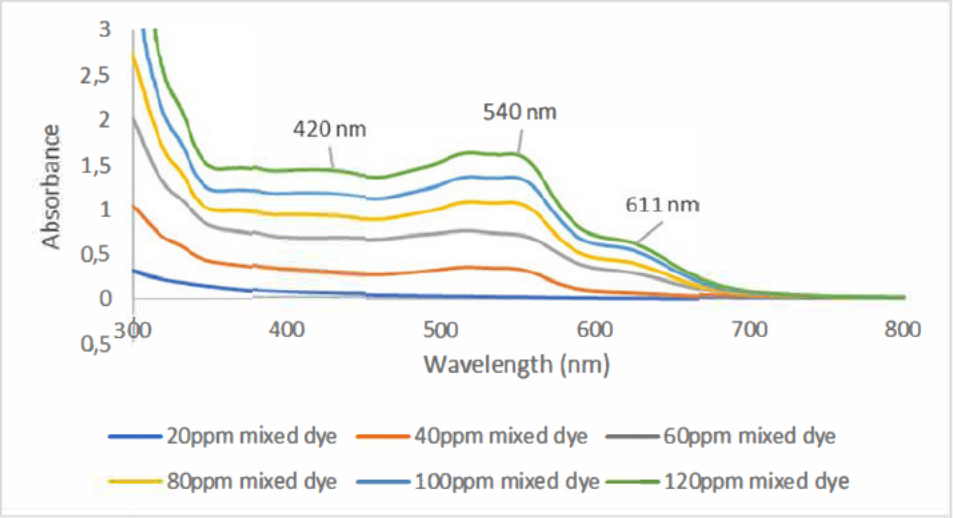

Appendix 15 UV profiles illustrating dye removal capacity using four different activated carbons after adsorption of dye standard mixtures (a) H_3PO_4 (b) KOH (c) H_2SO_4 (d) NaOH

Appendix 16

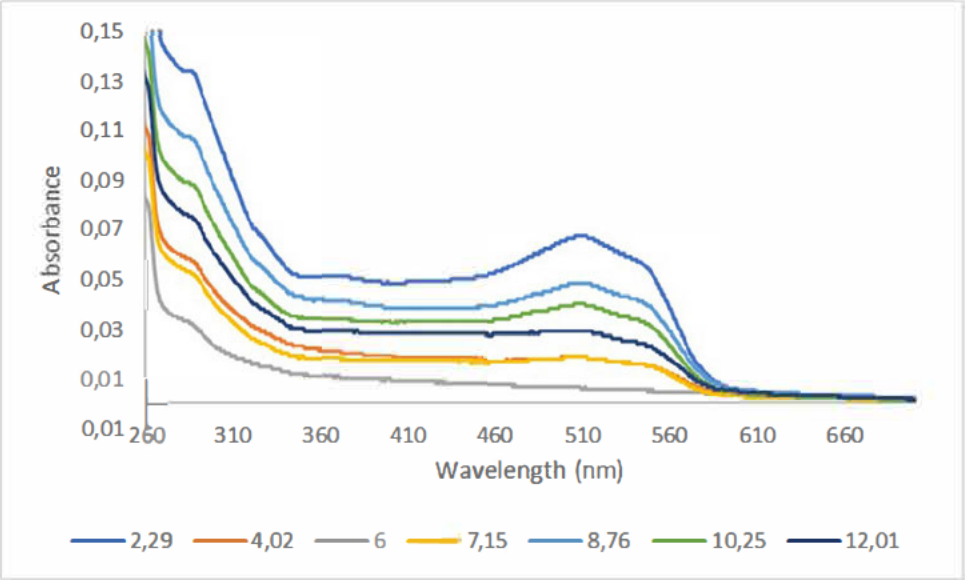

Appendix 16 UV spectrum of a 100 ppm dye standard mixture after adsorption at different pH mediums

Appendix 17

$$\text{Molar mass of NaOH} = 23.00 + 16.00 + 1.008 = 40.008\frac{\text{g}}{\text{mol}}$$

$$\begin{aligned}\text{No of moles} &= \text{C} \times \text{V} \\ &= 1.0\frac{\text{mol}}{\text{L}} \times 0.25\ \text{L} \\ &= 0.25\ \text{mol}\end{aligned}$$

$$\begin{aligned}\text{Mass of NaOH required} &= \text{Mm} \times \text{n} \\ &= 40.008\frac{\text{g}}{\text{mol}} \times 0.25\ \text{mol} \\ &= 10.002\text{g}\end{aligned}$$